Physiologically based Modelling of Cerebral Autoregulation



Yufan Wang

St Edmund Hall

Supervisor: Professor Stephen J Payne

University of Oxford

A thesis submitted for the degree of

Doctor of Philosophy

Trinity Term, 2024

Physiologically based Modelling of Cerebral Autoregulation

The human brain requires sufficient and continuous blood supply to maintain healthy function. Cerebral autoregulation (CA), a highly complex mechanism, plays a crucial role in achieving this function. Increasing evidence confirms the close association between cerebral haemodynamic abnormalities and the occurrence of cerebrovascular diseases, brain dysfunction, and cognitive impairment. To complement clinical trials and improve clinical outcomes, researchers use mathematical models to understand disease progression and test the feasibility of new therapies. However, existing cerebral autoregulation models are predominantly purely mathematical, making it challenging to relate simulation results to clinically measured parameters. Therefore, there is a need to develop CA models based on physiological mechanisms to enhance our understanding of brain physiology and diseases, and to facilitate the clinical translation of cerebral autoregulation.

In this study, we first conducted a data-driven analysis of arterial blood pressure (ABP) and cerebral blood flow (CBF) under different physiological and pathological conditions, providing the latest insights into the human cerebral pressure-flow relationship and serving as a reference for developing new mathematical models. Subsequently, we proposed the first physiologically-based mathematical model capable of simulating both activation and autoregulatory responses. To ensure a solid physiological foundation, a single vessel model was first constructed, which was then scaled up to a whole-brain vasculature model using the analogy between cerebral vasculature and electrical circuits. This model not only replicated typical autoregulation curves but also the BOLD response. This CA model was subsequently coupled with a multi-compartment porous Finite Element model, successfully incorporates autoregulation mechanisms into the computational modelling of brain oedema and osmotherapy. The improved model demonstrated closer alignment with clinical data, particularly enhancing consistency in managing intracranial pressure during the rebound phase following osmotherapy. Overall, the combined approach adopted in this study offers crucial insights into the physiological pathways of cerebral autoregulation.

Acknowledgements

During my pursuit of a doctoral degree, this thesis would not have been possible without the support of many over the past four years, and for that, I am deeply grateful.

First and foremost, I would like to express my heartfelt gratitude to my supervisor, Stephen Payne. His inspiration, guidance, and support laid a solid foundation for me to delve into the exciting field of cerebral blood flow and metabolism. I am particularly thankful for his patience in answering countless questions and providing excellent guidance throughout the research process and thesis writing. He afforded me the freedom to explore topics of genuine interest and wholeheartedly supported my decisions. As an outstanding supervisor, he has been an invaluable source of inspiration in my quest for personal growth and understanding life's purpose.

I wish to thank all members of the Cerebral Haemodynamics Group, especially Dr. Xi Chen, with whom I collaborated on the computational modelling of cerebral oedema and osmotherapy research. I am also grateful to Eleanor Stride and Jeroen Bergmann for their profound and constructive feedback during the Transfer of Status and Confirmation of DPhil status.

I would like to thank all my friends, particularly Han Wang, for providing invaluable interdisciplinary research insights. Lastly, I extend my deepest appreciation to my parents for their unwavering support.

Finally, I wish to sincerely thank myself for never giving up. Regardless of the smooth or challenging paths that lie ahead in life, I recognize that I have become my strongest pillar. This thesis is dedicated to myself.

List of Abbreviations

20-HETE	20-hydroxyeicosatetraenoic acid
AA	arachidonic acid
ABP	arterial blood pressure
AD	Alzheimer's disease
ADP	adenosine diphosphate
ARI	autoregulation index
ASL	arterial spin labelling
ATP	adenosine triphosphate
BBB	blood-brain barrier
BK	big potassium
BOLD	blood oxygen level dependent
BP	blood pressure
BRS	baroreceptor sensitivity
CA	cerebral autoregulation
Ca^{2+}	calcium
CARNet	cerebral autoregulation research network
CBF	cerebral blood flow
CBFv	cerebral blood flow velocity
CBV	cerebral blood volume

cGMP . . . cyclic guanosine monophosphate

$CMRO_2$ . . cerebral metabolic rate of oxygen

CO_2 . . . . carbon dioxide

CPP . . . . cerebral perfusion pressure

CT . . . . . computed tomography

CVR . . . . cerebrovascular reactivity

dCA . . . . dynamic cerebral autoregulation

EC . . . . . endothelial cell

ECS . . . . extracellular space

EET . . . . epoxyeicosatrienoic acids

eNOS . . . . endothelial nitric oxide synthase

fMRI . . . . functional magnetic resonance imaging

GABA . . . glutamate and γ-aminobutyric acid

HbR . . . . deoxyhaemoglobin

ICH . . . . intracranial haemorrhage

ICP . . . . . intracranial pressure

IP_3 . . . . . inositol triphosphate

K . . . . . potassium

Kir (KIR) . inward-rectifying potassium

LBNP . . . low body negative pressure

LLA . . . . lower limit of autoregulation

MABP(MAP) mean arterial blood pressure

MCAv . . . middle cerebral artery velocity

MCI . . . . mild cognitive impairment

mGluR . . . metabotropic glutamate receptors

MLCK . . . myosin light-chain kinase

MLCP . . . myosin light-chain phosphatase

MRI . . . . magnetic resonance imaging

Mx . . . . . mean flow index

Na . . . . . sodium

NIRS . . . . near infrared spectroscopy

NMDAR . . n-methyl-d-aspartate receptors

nNOS . . . neuronal nitric oxide synthase

NO . . . . . nitric oxide

NOS . . . . nitric oxide synthase

NVC . . . . neurovascular coupling

NVU . . . . neurovascular unit

OEF . . . . oxygen extraction factor

$PaCO_2$ . . . partial pressure of carbon dioxide

PET . . . . positron emission tomography

PGs . . . . prostaglandins

Ptrans . . . transmural pressure

PVS . . . . perivascular spaces

rCBF . . . . reginal cerebral blood flow

SACs . . . . stretch-activated channels

SAH . . . . subarachnoid haemorrhage

sCA . . . . static cerebral autoregulation

sGC . . . . soluble guanylyl cyclase

SMC . . . . smooth muscle cell

SPECT . . single photon emission computed tomography

SR . . . . . sarcoplasmic reticulum

TCD . . . . transcranial doppler

TFA . . . . transfer function analysis

TOx . . . . tissue oxygen reactivity index

TRPV4 . . transient receptor potential vanilloid-related 4

ULA . . . . upper limit of autoregulation

VCI . . . . vascular cognitive impairment

VOCCs . . . voltage-gated calcium channels

Contents

List of Abbreviations **v**

List of Figures **xiii**

List of Tables **xx**

1 Introduction **1**

1.1 Motivation 1

1.2 The value of mathematical modelling 3

1.3 Aims 5

1.4 Outline 6

2 Literature Review **7**

2.1 Physiology 7

2.1.1 Blood Vessels 8

2.1.2 Cells 9

2.2 Blood flow regulation 13

2.2.1 Haemodynamics 14

2.2.2 Cerebral autoregulation 16

2.2.3 Neurovascular coupling 19

2.3 Measurement Techniques 22

2.3.1 Development of CBF Measurements 22
2.3.2 Transcranial Doppler 24
2.3.3 Magnetic Resonance Imaging 25
2.3.4 ABP Measurements 26
2.3.5 Quantification of CA 27
2.4 Mathematical models 29
2.4.1 Lumped compartment models 30
2.4.2 Biochemical feedback models 32
2.4.3 Neurovascular coupling models 37
2.4.4 fMRI BOLD response model 39
2.5 Clinical conditions 40
2.5.1 Ageing 41
2.5.2 Chronic hypertension 41
2.5.3 Stroke 42
2.5.4 Alzheimer's disease 46
2.6 Conclusion 48

3 Static autoregulation in humans **49**

3.1 Introduction 50
3.2 Methods 53
3.2.1 Exclusion criteria 54
3.2.2 Inclusion criteria 55
3.2.3 Pathological conditions 58
3.2.4 Analysis of data 59
3.3 Results 60
3.3.1 normal physiological conditions 60

3.3.2 Pathological conditions 72
3.4 Discussion 79
3.4.1 Directional sensitivity of cerebral autoregulation 79
3.4.2 The impact of disease on CA 81
3.4.3 Limitations 82
3.4.4 Future research on static cerebral autoregulation assessment 85
3.5 Conclusion 86

4 A physiological-based mathematical model of cerebral vasculature 90

4.1 Introduction 91
4.2 A Model of Vascular Regulation 92
4.2.1 NVC Model 92
4.2.2 CA Model 95
4.2.3 Fitting and analysis 102
4.3 Whole brain vasculature model 107
4.3.1 Integration of arteriole model into existing whole-brain model 107
4.3.2 Fitting and analysis 110
4.4 Discussion 110
4.4.1 The role of the SR in the SMC 110
4.4.2 The role of stretch channels in the myogenic response 112
4.4.3 Impact of the Shear Stress Response on the SMC Membrane Voltage 113
4.4.4 The role of NO in autoregulation and NVC 114
4.5 Sensitivity Analysis 115
4.5.1 Methods 116
4.5.2 Results 118

4.6 Conclusions 119

5 Integrated model of cerebral oedema and osmotherapy 122

5.1 Introduction 123

5.2 Methods 125

5.2.1 Perfusion Model 125

5.2.2 Oedema and Osmotherapy Model 127

5.2.3 Model Coupling 129

5.3 Results 132

5.3.1 Model Validation 132

5.3.2 Sensitivity analysis of physiological parameters 134

5.4 Discussions 136

5.4.1 Limitations 137

5.5 Conclusions 138

6 Conclusions 139

6.1 Summary of Results 139

6.2 Future Work 141

6.2.1 Unified quantitative techniques for cerebral autoregulation analysis 141

6.2.2 Detailed capillary network models 141

6.2.3 Incorporation of physiological and pathological variations . . 142

6.2.4 Consideration of brain regions 142

References 143

List of Figures

2.1 Typical cross-section of structure of wall of (a) artery (schematic); (b) vein (schematic). Reproduced without changes from OpenStax College. 9

2.2 The relation of glial cells, neuron, capillary and extracellular space as seen in light and electron microscopy [12]. 11

2.3 (a) Schematic of the structure of a smooth muscle cell; (b) Schematic of the process of cross-bridge cycling: myosin cross bridge attaches to actin filament, then the myosin head bends as the actin filament moves while adenosine diphosphate (ADP) and phosphate are released, before new ATP molecule attaches to myosin head causing it to detach. TM: tropomyosin; T: troponin; C: calcium-binding protein. 12

2.4 Schematic representation of factors contributing to the regulation of blood flow, in approximate order of decreasing sensitivity. Figure adapted and modified from [26, 27]. 14

2.5 Simplified schematic of CBF regulatory mechanisms. ABP and IC contribute to CPP, which drives blood flow through the vasculature. The vasculature responds to various regulatory inputs, including sympathetic, myogenic, and metabolic responses, modulated by levels of carbon dioxide (CO_2) and oxygen. Metabolic demand and sympathetic nerve activity influence CBF adjustments, while CBV and CSF dynamics contribute to venous blood outflow. Reproduced without modification from [26]. 15

2.6 Simplified schematic of the Lassen curve with associated radial changes. The blue line represents cerebral blood flow, including the lower (LLA) and upper limits (ULA) of cerebral autoregulation. Grey circles indicate relative artery diameters under varying pressure conditions. Adapted from [30]. 17

2.7 Biphasic response of the cerebral vasculature to a reduction in ABP. The black line represents the response without autoregulation, where vessel compliance alone leads to a decrease in vessel radius, causing increased resistance and reduced blood flow. The red line shows the response with autoregulation, where the active myogenic response counterbalances the passive phase by inducing vasodilation to restore blood flow[27]. 18

2.8 Simplified schematic indicating main drivers in the myogenic response as proposed by [32]. Pink circles indicate increases in cytoplasmic calcium. 19

2.9 Summary of the prominent NVC and autoregulation pathways. Figure adapted and modified from [27]. In neurons, synaptically released glutamate acts on n-methyl-d-aspartate receptors (NMDAR) to raise intracellular calcium, causing nNOS to release NO, which activates the generation of cGMP to cause vasodilation. In astrocytes, glutamate raises calcium by activating the metabotropic glutamate receptors, generating arachidonic acid from phospholipase A2. The AA metabolite: EETs dilate vessels through the potassium pathway, whereas 20-HETE (in the SMC) constricts vessels. 21

2.10 Schematic of cerebral autoregulation model proposed by [73]. q, cerebral blood flow; P_a, arterial pressure; P_c, capillary pressure; P_v, cerebral venous pressure; P_{ic}, intracranial pressure; P_{vs}, venous sinus pressure. Compliance and resistance elements are defined as follows: C_{ai}, intracranial arterial compliance; R_{ai}, intracranial arterial resistance; R_{pv}, resistance of the proximal venous vascular bed; R_{vs}, resistance of the distal venous vascular bed, including the lateral lacunae and dural sinuses; C_{vi}, intracranial venous compliance; R_f, resistance to cerebrospinal fluid formation; C_{tiss}, cerebral tissue compliance; I_i, rate of saline infusion; R_o, resistance to CSF outflow; R_{ve}, resistance of the extracranial venous pathway; C_{ve}, extracranial venous compliance; and P_{cv}, central venous pressure. This model illustrates the interaction between arterial, capillary, venous, and cerebrospinal fluid compartments. 31

2.11 Schematic of model of relationship between main variables in control of cerebral blood flow [27]. The myogenic model (yellow box) controls vessel constriction and dilation via the vascular smooth muscle cell model and calcium kinetics, enabling active myogenic responses. The mechanical model (green box) addresses vessel wall stress and thickness, adjusting to pressure changes and affecting vessel compliance. The vasodilating metabolites model (red box) involves the endothelium model and transport mechanisms, which respond to metabolic signals, such as nitric oxide, from neuronal activity to mediate vasodilation. Lastly, the flow model (blue box) calculates flow rate q based on Poiseuille's law, vessel radius, haematocrit levels, and pressure gradient, governing overall flow dynamics. 33

2.12 Structure of kinetic model proposed by [78]. M: myosin cross-bridges; Mp: phosphorylated cross-bridges; Amp: phosphorylated and attached cross-bridges; AM: attached, non-phosphorylated cross-bridges. K_1 and K_6 are phosphorylation rate constants, K_2 and K_5 are dephosphorylation rate constants, K_3 and K_4 are rate constants for the attachment and detachment of fast cycling phosphorylated cross-bridges, K_7 is rate constant for latch-bridge detachment. . . . 34

2.13 Schematic of ion channels in model of SMC [82]. Blue labels indicate channels that connect SMC to extracellular space and endothelium, red labels indicate channels that cause internal exchange of calcium. Species in brackets indicates ions exchanged by the channel. STR: stretch, EXT: extrusion, VOCC: voltage operated calcium, IP3: inositol trisphosphate, CICR: calcium induced calcium release, UPT: uptake. 36

2.14 Schematic of the relationship between the kinetic and mechanical models [84]. 36

2.15 An overview of physiological processes of NVC. Neurotransmitters, such as glutamate (Glu), are released from the presynaptic neuron into the synaptic space, leading to the activation of the Na^+/K^+ pump and a rise in intracellular calcium (Ca^{2+}) within the astrocyte. The increase in Ca^{2+} activates the BK channel, allowing potassium ions (K^+) to enter the perivascular space. This K^+ efflux is sensed by smooth muscle cells via KIR channels, resulting in vascular responses that facilitate blood flow regulation in response to neuronal activity. 38

2.16 Schematic of physiological basis of BOLD response. A stimulus triggers synaptic activity, leading to changes in CBV, CBF, and $CMRO_2$. These physiological changes influence the concentration of deoxyhemoglobin (Deoxy-Hb) in the blood, which is captured by the BOLD signal model. Reproduced from [97]. 40

3.1 (a) Classical view of autoregulation, first proposed by Lassen [28]. It should be noted that the ULA was only demonstrated later in hypercapnic dogs in 1971 [153]. (b) A typical contemporary view of autoregulation showing a small plateau region and the directional sensitivity of cerebral autoregulation [159]. 51

3.2 Flow chart of excluding procedure. 58

3.3 Flow chart of excluding procedure under different physiological and pathological conditions. 59

3.4 Relationship between %MAP and %CBF in the Increased MAP and Decreased MAP Ranges. All individual lines represent individual experiments (not corrected for CO_2); the length of the line indicates the range of MAP of that experiment. Before CO_2 correction, the average slope (solid line) was 1.47%MAP/%CBF for the decreased MAP (n = 27), and 0.35%MAP/%CBF for increased MAP (n = 17). After CO_2 correction, the average slope (dashed line) was 1.11%MAP/%CBF for decreasing MAP (n=18) and 0.24%MAP/%CBF for increasing MAP (n=11). 65

3.5 Slope distribution of different blood pressure manipulation methods. Experiments inducing BP increase are represented by blue boxplots, while experiments inducing BP decrease are represented by orange boxplots. Non-pharm, non-pharmacological BP manipulation methods; Pharm, pharmacological BP manipulation methods; PE, phenylephrine; LBNP, lower body negative pressure. 67

3.6 First-order linear regression model for MAP and CBFv. The grey shading between these bounds reflects the 95% confidence level. . . 68

3.7 Third-order polynomial function regression model for MAP and CBFv. The grey shading between these bounds reflects the 95% confidence level. The blue shading between 80-100 mmHg reflects the autoregulatory plateau. 69

3.8 MAP, CBFv and CBF under different physiological and pathological conditions. 76

3.9 Relationship between %MAP and %CBF in the increased MAP and decreased MAP ranges under different conditions of static autoregulation. The length of the line indicates the range of MAP of that experiment. Since only one experimental data met the inclusion criteria in the ageing and AD conditions, they were not included for comparison. 77

3.10 Relationship between %MAP and %CBF in the increased MAP and decreased MAP ranges under different conditions of dynamic autoregulation. The length of the line indicates the range of MAP of that experiment. 79

3.11 Classical view and updated view of the cerebral autoregulation curve. The blue line and shaded area represent the autoregulation curve and plateau proposed by Lassen [28] and Paulson et al. [154]. The red line and shaded area represent the new autoregulation curve and plateau proposed in this study, based on the dataset from Numan et al. [68] and studies from 2013 to 2022. It should be noted that the new curve is asymmetric (with a lower slope for MAP > 100 mmHg than for MAP < 80 mmHg) and has a slight slope between the "autoregulation plateau" of MAP and CBF. 88

4.1 Schematic of the integrated model and the BOLD model. Different coloured arrows represent different ion pathways. NE: neuron, AC: astrocyte, PVS: perivascular space, ER: endoplasmic reticulum, ECS: extracellular space, degra: degradation. Figure adapted and modified from Mathias et al. [95] 93

4.2 Comparison of the model arteriole radius responses (flow-red lines; no flow-blue lines) and arteriole radius experimental data from Kuo et al. (1991) [35] (black lines) across a range of transmural pressures. 103

4.3 The resulting arteriole radius against time in response to variations in transmural pressure and axial pressure gradient. The top panel presents the arteriole radius over time, with the black dashed line indicating experimental data from Fig.2A in Kuo et al. (1991) [35], and the red line representing model output. The middle panel illustrates the axial pressure gradient applied during the experiment, while the bottom panel illustrates the changes in transmural pressure applied during the experiment. 104

4.4 The resulting arteriole radius against time in response to variations in transmural pressure and axial pressure gradient. The top panel presents the arteriole radius over time, with the black dashed line indicating experimental data from Fig.2C in Kuo et al. (1991) [35], and the red line representing model output. The middle panel illustrates the axial pressure gradient applied during the experiment, while the bottom panel illustrates the changes in transmural pressure applied during the experiment. 106

4.5 Resulting BOLD contrast signal. Light blue shading indicates the period of stimulation. Red line represents the model output. Blue circles indicate the static stimulus while black circles indicate flicker stimulus, manually extracted from Sadaghiani et al. (2009) [249]. . 107

4.6 Schematic of the electrical equivalence model coupled with single vessel model. P_a, P_{ic} and P_v, arterial input, intracranial and venous output blood pressure, respectively. R_{la}, resistance of non-regulating arterial compartment. R_{sa} and C_a, resistance and compliance of regulating arterial compartment; R_{sv}, resistance of capillary compartment and small veins; C_v, venous compliance; R_{lv}, resistance of large veins. 108

4.7 (a) SMC membrane voltage plotted against ABP. The black line represents the data from [157] and the red line represents the model output; (b) Steady state CBF plotted against ABP. The red line displays the model response, while the black circles indicate cat data from [251] and the blue diamonds indicate rat data from [157]. . . . 111

4.8 (a) SMC calcium concentration plotted against time; (b) Resulting arteriole radius against time. Blue line shows the output without uptake ($B_{SMC} = 0$). Grey lines show outputs when B_{SMC} is equal to 20, 40, 60 and 100, from left to right respectively. Red line shows the original output from the model ($B_{SMC} = 80$). The input is a step increase in transmural pressure from 60 mmHg to 80 mmHg. . 112

4.9 (a) Steady state open probability of calcium activated potassium channels against transmural pressure (b) SMC membrane voltage against transmural pressure. (Conditions are taken from Figure 4.7) 114

4.10 Normalized NO Concentration in the SMC. Baseline is taken as the case where the neuronal NO pathway is not activated. Blue line indicates no neuronal NO production while red line indicates that neuronal NO production is activated. 115

4.11 Mean and standard deviation of elementary effects for integrated model based on fractional changes (10%, 20%) in each model parameter. 119

5.1 Flowchart demonstrating how the CA model and the Finite Element models are coupled. 130

5.2 (a) The effective osmotic pressure of hypertonic saline with clinical data points. The clinical data obtained from 22 osmotherapy episodes are presented as mean ±SE (right). (b) The validation curve of the ICP under different conditions, including clinical data, simulation results with autoregulation, and simulation results without autoregulation. 133

5.3 The impact of autoregulatory capacity on the effectiveness of osmotherapy. 134

5.4 The evolution of ICP in osmotherapy under varying physiological parameters. (a) Varying the reflection coefficient of the original plasma composition. (b) Varying the storage factor of the interstitial fluid. (c) Varying the hydraulic conductivity of interstitial fluid in the interstitial space. (d) Varying the hydraulic permeability of the capillary wall. The reference curve corresponds to the validation case shown in Figure 5.2. 136

List of Tables

3.1 Summary of experimental methods and protocols for blood pressure changes. NS-15: Normal Saline-15, LPS: Lipopolysaccharide, SNP: Sodium Nitroprusside, ATP: Adenosine Triphosphate, NMMA: NG-monomethyl-L-arginine, HUT: Head-Up Tilt, HDT: Head-Down Tilt, LBNP: Lower Body Negative Pressure, LBPP: Lower Body Positive Pressure. 57

3.2 Summary of the included studies on SCA. Mean age is averaged value or range. Slopes presented in % MAP/% CBF and mmHg MAP/% CBF. TCD, transcranial Doppler ultrasound. PET, positron emission tomography. HUT, head-up tilt. LBNP, lower body negative pressure. LBPP, lower body positive pressure. SNP, Sodium nitroprusside. ATP, Adenosine triphosphate, MCAv: middle cerebral artery velocity. 62

3.3 Static autoregulation experiments under different physiological and pathological conditions. Slopes presented in % MAP/% CBF and mmHg MAP/% CBF. TCD, transcranial Doppler. HUT, head-up tilt. PET, positron emission tomography. 73

3.4 Dynamic autoregulation experiments under different physiological and pathological conditions. Slopes presented in % MAP/% CBF and mmHg MAP/% CBF. TD-rCBF, thermal diffusion-regional CBF. 74

3.5 Description statistics of slopes (%CBF/%MABP) under different physiological and pathological conditions on dynamic autoregulation. N indicates number of experiments. The p-value is the difference in slope compared to healthy subjects and <0.05 was considered statistically significant. 76

3.6 Description statistics of slopes (%CBF/%MABP) under different physiological and pathological conditions on dynamic autoregulation. N indicates number of experiments. The p-value is the difference in slope compared to healthy subjects and <0.05 was considered statistically significant. 78

4.1 Bounds placed on variables during optimization and used to define the limits of the parameter space for additive sensitivity analysis. . 118

5.1 Boundary conditions for the perfusion model. 127

5.2 Boundary conditions for the oedema and osmotherapy model. . . . 129

5.3 Ranges and values of E_{Mean} of parameter values in the sensitivity analysis tests. 135

1 Introduction

1.1 Motivation

With the increasing global ageing population, cerebrovascular diseases such as stroke and dementia have become very substantial and growing clinical challenges. Stroke is most commonly caused by a blockage of a supply vessel to the brain, or by a rupture of a blood vessel, resulting in a pooling of blood in the brain and a rise in intracranial pressure (ICP). Stroke causes hypoxia, irreversible brain damage, and loss of function, and is one of the leading causes of death and disability worldwide. Data from the Stroke Association show that there are more than 100,000 strokes each year in the UK and approximately 17 million new stroke patients over the world [1]. Cognitive impairment (dementia) caused by neurodegeneration is another global health concern. There are approximately 50 million dementia patients worldwide in 2020, and this number is expected to increase to 152 million by 2050. Dementia affects individuals, their families, and the economy, with estimated global costs of about US$1 trillion annually [2]. Studying cerebral blood flow can help us better understand the pathological and physiological mechanisms of these diseases, explore new biomarkers to improve risk prediction, and improve the accuracy and

effectiveness of diagnosis and treatment.

The healthy function of the brain depends on the continuous blood flow carrying oxygen and metabolites. The mechanisms that maintain CBF at a nearly constant level, despite significant changes in ABP, are collectively referred to as cerebral autoregulation. This process is highly complex, involving numerous variables such as changes in blood pressure. A series of recent studies have shown that CA is closely related to a range of brain diseases, including stroke, dementia, vascular stenosis, and various other brain diseases, as well as mental health disorders such as anxiety and depression [3]. The assessment of CA function may become a new target for the treatment and primary and secondary prevention of cerebrovascular diseases. With increasing clinical attention to brain disorders, the importance of CA has received increasing attention and emphasis. However, the regulation mechanisms of CA, the detection technology and measurement parameters of CA are extremely complex, which limit the clinical application and research of CA.

It is thus not surprisingly that the causal relationship between impaired cerebral autoregulation and various brain disorders has not been fully established. Some studies have found CA abnormalities even in patients with early cognitive impairment, indicating that CA damage is a long process that may precede other pathological processes [4]. As CA is a highly complex system and many physiological variables are involved in maintaining cerebral blood flow, data obtained directly through brain imaging techniques such as transcranial Doppler (TCD) ultrasound cannot provide all the information needed to evaluate CA. Evaluation of CA focuses on the response of cerebral blood flow to changes in arterial blood pressure, and requires the use of a quantitative mathematical model to extract the necessary information to evaluate the effectiveness of the cerebral autoregulation mechanisms in healthy or diseased states.

In-depth investigation of CA using mathematical models to complement clinical trials can help us explore the causal relationship between various pathological mech-

anisms (such as cerebrovascular reactivity, endothelial dysfunction, neurovascular dysfunction) and brain functional abnormalities. However, our understanding of the role of the human cerebrovascular system in tissue health remains poorly understood, which limits the current application of cerebrovascular models. Therefore, it is necessary to develop new physiology-based models of CBF regulation to improve our understanding of the pathogenesis and development of cerebrovascular diseases. Furthermore, evaluating CA can also help to develop appropriate clinical diagnostic and treatment strategies, as well as in post-treatment evaluation, to reduce the incidence, recurrence, disability, and mortality of cerebrovascular diseases such as stroke.

1.2 The value of mathematical modelling

To improve clinical efficacy for patients with cerebrovascular diseases, there is a need for novel treatment technologies and strategies. Most new treatments and interventions are developed, optimized, and carefully evaluated through preclinical experiments and clinical trials before they are allowed to be used and commercialized. However, these clinical trials can be very expensive and time-consuming. In addition, it is often difficult to determine the reasons for the failure of new interventions. These limitations have prompted researchers to use mathematical models to help develop and test new treatment methods and biomedical products. In the ideal scenario where a completely accurate mathematical reconstruction of a biological system is available, speculative clinical investigations to discover new treatments or lengthy clinical trials to evaluate efficacy and safety would become more tightly focused with higher success rates than at present.

The human brain is a highly complex and dynamic system involving numerous interacting components, including neurons, astrocytes, blood vessels, and various molecular and cellular processes. Mathematical models can provide quantitative descriptions of these components and their interactions and have therefore rapidly developed in the past decade to help us understand the behaviour of the brain at

different levels of organization. New brain models have been developed in a variety of topics in physiology, pathology, fluid mechanics, solid mechanics, and biomedical applications, spanning from the cellular scale of individual neurons [5, 6] to the microvascular scale [7], and to the whole brain scale of large-scale networks [8, 9].

The importance and necessity of using mathematical models to explore CA also lies in the fact that mathematical models can serve as an important tool to provide detailed information that is difficult to directly measure in clinical practice. For example, mathematical models can be used to investigate the time response of different CBF regulation mechanisms and the ability to regulate blood flow under different changes in blood pressure. This information is crucial for evaluating the effectiveness of CA and its correlation with cerebrovascular diseases. Since mathematical models can investigate the role of the vasculature at different length scales and the relation between metabolic demand of the tissue and blood flow, they can be used as a complement to gain insight into the content that imaging techniques cannot describe due to the small scale of oxygen diffusion.

Additionally, mathematical models can integrate data from different imaging modalities and provide a unified framework for interpreting and analysing these data. By combining empirical data with theoretical models, we can gain a deeper understanding of the underlying mechanisms and causal relationships of brain function and dysfunction. Mathematical models can also simulate and predict the effects of different interventions on brain function, which is essential for developing effective treatment strategies for various brain disorders. Given the high complexity of the human brain and the great variability of the characteristics of its physiological mechanisms, developing clinically insightful mathematical models is crucial for advancing our understanding of the brain and developing new tools for diagnosis and treatment of brain disorders.

It should be noted, however, that all physiological models share a common limitation: how to balance the simplicity of the model with the complexity of reality. A very

simple model may be easily related to data, but can only provide limited insight into the actual process; a very complex model may provide a wealth of details about the underlying mechanisms, but can be difficult to validate and to achieve quantitative agreement with data.

1.3 Aims

The overall aim of this thesis is to deepen the understanding of cerebral autoregulation mechanisms and to develop integrative models that link physiological responses with clinical applications, supporting diagnostic and therapeutic advancements for cerebrovascular diseases.

To achieve this aim, the following specific objectives were established:

- To quantify the static pressure-flow relationship of cerebral blood flow under normal physiological and pathological conditions using a data-driven approach, and to examine the existence and extent of the cerebral autoregulation plateau.
- To develop a physiologically-based mathematical model of cerebral autoregulation responsive to multiple regulatory stimuli: This involves combining a high-precision single-vessel model with a lumped compartment model to investigate confounding effects between myogenic mechanisms and neurovascular coupling.
- To apply the integrated autoregulation model to cerebral oedema and osmotherapy: The developed model is further incorporated into a multi-compartment porous finite element model of cerebral oedema and osmotherapy, to simulate the evolution of intracranial pressure over time in cerebral oedema patients following osmotherapy, evaluating how autoregulatory mechanisms influence clinical treatment outcomes.

1.4 Outline

Using experimental and computational techniques, we aim to provide new insights into the regulation of cerebral blood flow. A brief outline of the contents is presented here with the aim of serving as a broad overview of the research questions that were answered and of how they relate to the aim.

Chapter 2 provides a comprehensive literature review of the latest developments in research on cerebral autoregulation, including its physiological basis, measurement techniques, mathematical models, and clinical applications, providing background knowledge for the subsequent chapters.

Chapter 3 utilizes a data-driven approach to quantify and update the human static cerebral pressure-flow relationship under various physiological and pathological conditions.

Chapter 4 details the process of model construction, including the derivation of the model's equations. A detailed, physiological based single-vessel model is first constructed, which successfully replicates the BOLD signal. Then, the model is coupled with a high-order lumped compartment model to achieve replication of autoregulation. The effectiveness of the model is validated through multiple experimental data. Sensitivity analysis is conducted to identify crucial parameters and physiological pathways that significantly impact blood flow regulation.

Chapter 5 validates the clinical application potential of the autoregulation model from Chapter 4 through its integration with the multi-compartment porous finite element model of cerebral oedema and osmotherapy. The enhanced model aligns more closely with clinical data, providing better simulation of the rebound evolution of ICP following saline infusion. Sensitivity analysis investigates the critical importance of physiological parameters on the efficacy of osmotherapy.

Chapter 6 summarizes the main conclusions and limitations of the study, proposing potential directions for future research.

2

Literature Review

In this chapter, we will first introduce the structure of the cerebrovascular system and the physiological basis of cerebral blood flow regulation. Then we will review specific mathematical models and measurement techniques applied to CA assessment, and finally discusses the role of CA under different physiological and pathological conditions.

2.1 Physiology

The human brain is possibly the most metabolically active and complex organs in the body. Although the brain occupies only 2% of body weight, it consumes 20% of the body's metabolism and 14% of blood flow [10]. Given its strong dependence on nutrient supply, the brain is equipped with a complex vascular network that continuously perfuses blood and removes waste products from the tissue. Control of cerebral blood flow can be achieved simply by adjusting the diameter of individual vessels in response to changes in supply and demand. Vascular diameter is determined by vascular tone and is regulated by both local and global stimuli. This section begins with the structure of the cerebral vascular system and

its haemodynamics, then introduces the concept of cerebral autoregulation and its complex regulatory mechanisms.

2.1.1 Blood Vessels

The high energy demand of the brain requires an adaptable vascular network to provide a continuous blood supply. The cerebral vasculature is a highly complex, structurally heterogeneous, interconnected network of blood vessels that plays a vital role in supplying blood and nutrients, primarily oxygen and glucose, to brain cells.

Blood vessel walls comprise three layers: the tunica externa, the tunica media, and the tunica intima (from outer to inner). The tunica externa is mainly composed of elastin and collagen, as well as nerves and small blood vessels, which serve as the nutrient supply for cells in the wall. The tunica media predominantly comprises smooth muscle cells, whilst the tunica intima is primarily made up of endothelial cells. The three layers have different structures which determine how they perform different roles in function: the inner layer primarily acts as a sensor for wall shear stress, the middle layer acts to control vessel tone, and the outer layer acts as a structural support and connects the blood vessel to the surrounding tissue.

The proportions of these layers depend on the type of blood vessels, as shown in Figure 2.1. Arterioles have thick, elastic walls with substantial layers of smooth muscle cells to control blood flow at high pressure. Veins have thin, slightly elastic walls and valves that allow them to work at low pressure and to ensure that the blood returns to the heart. Capillaries have the thinnest walls with no smooth muscle cells since they act at low pressure to supply nutrients through the wall to the surrounding tissue.

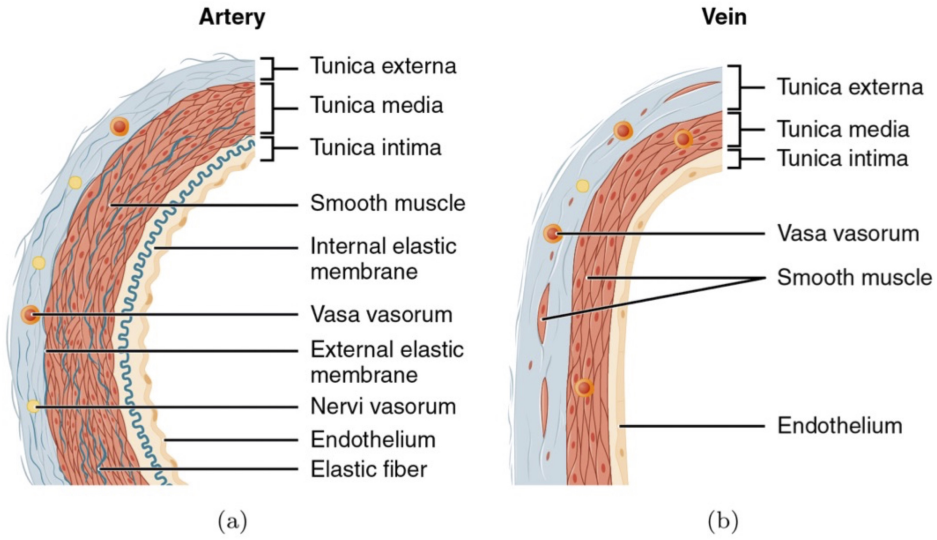


Figure 2.1: Typical cross-section of structure of wall of (a) artery (schematic); (b) vein (schematic). Reproduced without changes from OpenStax College.

2.1.2 Cells

Neurons

A neuron is the basic structural and functional unit of the nervous system, mainly composed of cell body and synapse. The cell body contains the nucleus and other intracellular organelles shared by non-neuronal cells. The synapses are responsible for the transmitting of information between neurons, including axons and dendrites: axons can make connections with other neurons due to their long shape, whereas dendrites are branches that act as receiving stations for excitation or inhibition. There are two types of signals in neurons: electrical and chemical signals, which constitute between them the basis of intracellular communication in the central nervous system.

Electrical signals directly conduct potential changes in neurons by generating action potentials. Neurons can respond to two types of stimuli: excitatory and inhibitory, which lead to an increase and a decrease in membrane potential, respectively. The combined effects of these stimuli can change the switching states of sodium and potassium channels in the cell membrane, thereby forming ionic current flow and depolarizing the cell membrane. When the depolarization makes membrane

potential higher than a certain threshold, an action potential is initiated that can propagate over long distances. Although the amplitude of the action potential is fixed, different intensities of the stimuli will produce different frequencies of the action potential, so as to convey information.

The chemical signal is used to transmit information between cells. There is a synaptic cleft between the presynaptic axon and postsynaptic cell, which is too wide to be traversed by currents. Instead, chemically mediated synaptic transmission relies on the release of neurotransmitters, such as acetylcholine or glutamate, to interact with receptors (i.e., specific protein molecules) embedded in the cell membranes, resulting in electrical changes in the target cell. The transmitters can excite or inhibit the next cell, depending on the types of receptors. However, electrical transmission can occur between some cells linked by special junctions. This close connection allows action potentials to spread directly from cell to cell without a chemical transmitter. Since ion exchange plays an important role in both electrical and chemical signalling, a tight control of the local ionic environment governed by blood flow is crucial.

Glial cells

Glial cells are non-neuronal cells in the central and peripheral nervous systems. Although they do not produce action potentials, they can maintain homeostasis and provide support and protection for neurons [11]. Neurons and glial cells are separated from each other by extracellular spaces. The main classes of neuroglial cells are astrocytes, oligodendrocytes, microglia, and ependymal cells. Astrocytes directly contact capillaries and neurons and thus will be the focus of this section. Electron micrograph images of brain tissue show that neurons and astrocytes are tightly packed together. The relation between astrocytes, neurons, capillaries, and extracellular space is shown in Figure 2.2.

There are a variety of ion channels and pumps in astrocyte membranes: predominantly potassium conductance, voltage-activated sodium and calcium channels, chloride channels, ion pumps for transport of sodium (Na^+) and potassium (K^+) as

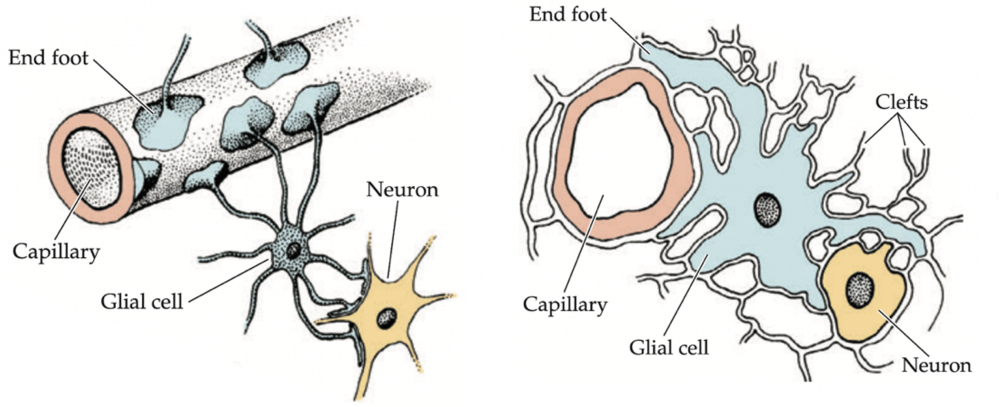


Figure 2.2: The relation of glial cells, neuron, capillary and extracellular space as seen in light and electron microscopy [12].

well as of bicarbonate and protons, transporters for glutamate and γ-aminobutyric acid as well as glycine, and receptors for transmitters [12–18].

One of the well-established functions of astrocytes is to regulate the potassium concentration in intercellular clefts and thus to maintain the external chemical environment of neurons. Potassium released from active axons depolarizes the astrocyte and enters it, altering the membrane potential and causing current flow as well as the outward movement of potassium through potassium channels elsewhere in the astrocyte. Apart from the potassium efflux, transmitters such as glutamate, glutamate and γ-aminobutyric acid (GABA), and glycine can also act on astrocyte membranes to produce depolarizing or hyperpolarizing responses [12, 17, 18]. This uptake of potassium and transmitters is termed spatial buffering [19].

The functional role of astrocytes in cerebral blood flow is now being studied intensively. Paulson and Newman (1987) [20] suggested that the endfeet of depolarized astrocytes activated by neuronal activity can act on capillaries to cause localized vasodilation. Although the mechanism by which astrocytes increase blood flow remains controversial (i.e., whether it is adenosine triphosphate (ATP), potassium or calcium waves that acts on capillary endothelial cells), evidence has confirmed the suggestion that astrocytes play a role in regulating blood circulation and thereby providing the extra supply of oxygen and glucose to active neurons [21,

22]. In addition, astrocytes can regulate blood flow by producing substances such as arachidonic acid, whose metabolites are vasoactive [23].

Smooth muscle cell

The vascular smooth muscle cells (SMC) play the dominant role in controlling blood flow since the changes in vessel radius are primarily determined by the vascular tone of the SMC. The SMC contains molecules of myosin and actin, which form parallel, overlapping thick (myosin) and thin (actin) filaments, as shown in Figure 2.3. The contraction is achieved when these filaments slide past each other, resulting in a shortening of the muscle and thus an increase in vessel tone. The molecular basis for this sliding movement is termed cross-bridge cycling. This interaction between myosin and actin results from phosphorylation, activated by an enzyme called myosin light-chain kinase, which is in turn activated by a complex formed from calcium and the calcium-binding protein calmodulin. The formation of this complex is initiated by the release of calcium ions. Therefore, it is the level of intracellular calcium that mainly controls the cross-bridge cycling and formation and hence changes in vessel compliance.

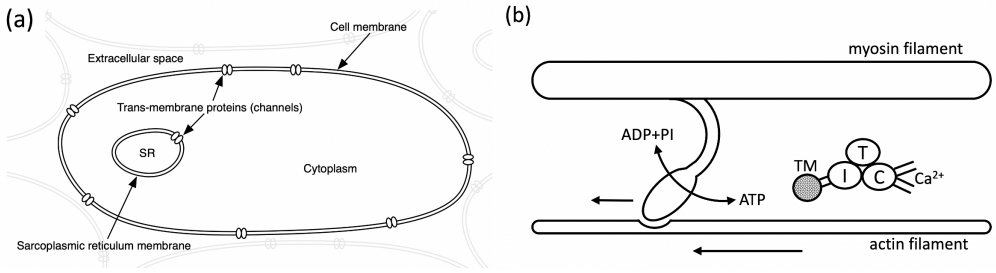


Figure 2.3: (a) Schematic of the structure of a smooth muscle cell; (b) Schematic of the process of cross-bridge cycling: myosin cross bridge attaches to actin filament, then the myosin head bends as the actin filament moves while adenosine diphosphate (ADP) and phosphate are released, before new ATP molecule attaches to myosin head causing it to detach. TM: tropomyosin; T: troponin; C: calcium-binding protein.

The SMC has a similar structure to other cells, contained by a membrane made from two layers of lipid molecules containing a phosphorus atom. Certain species need transmembrane proteins embedded in the membrane to cross the membrane and enter or leave the cell. These protein channels have various forms: some need

energy to operate, some must be activated by ion exchange or binding with specific species, and some are activated by changes in membrane potential (i.e., the potential difference generated by different concentrations of charged species on either side of the membrane). It is these channels that allow the regulation of intracellular ion concentrations, which in turn allows the cell to change its behaviour or to influence other cells.

The volume enclosed by the cell membrane is termed the lumen, which is mainly filled with cytoplasm. There are various structures and molecules contained in the cytoplasm, depending on the type of cell. One such structure is the sarcoplasmic reticulum (SR) which plays an important role in buffering the concentration of calcium. This sub-compartment is surrounded by its own membrane, which is very similar to the cell membrane in structure, and it also has transmembrane proteins that regulate the passage of certain species across the membrane. The calcium concentration in SR is much higher than that in the cytoplasm [24], which enables a high degree of control of the intracellular calcium.

2.2 Blood flow regulation

The brain mainly relies on aerobic metabolism of glucose as its energy source, with almost no energy reserves. Therefore, brain tissue is highly sensitive to ischaemic and hypoxic damage, making the brain one of the most strictly regulated organs in the body. CBF responds to a number of non-independent stimuli, which can be roughly grouped into four categories: metabolic, autoregulatory, neurogenic, chemical and sympathetic [25]. There are large differences in the sensitivity to these factors, with a high sensitivity to changes in arterial blood gas levels of carbon dioxide ($PaCO_2$), followed by chemical and systemic responses, and low sensitivity to changes in ABP, as shown in Figure 2.4 These mechanisms also have very different response times. Given that $PaCO_2$ and ABP are essentially set by the wider systemic circulation, these two stimuli can be regarded as global in nature. The remaining stimuli can be considered local in nature. It should be noted that

this is an arbitrary distinction and that there are many interactions between these mechanisms.

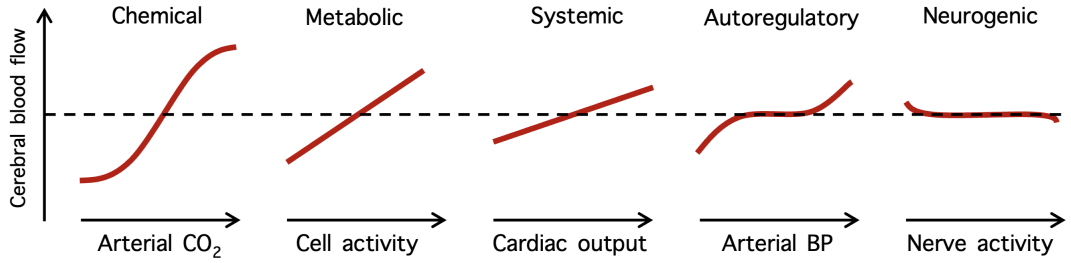


Figure 2.4: Schematic representation of factors contributing to the regulation of blood flow, in approximate order of decreasing sensitivity. Figure adapted and modified from [26, 27].

A highly simplified schematic of CBF regulatory mechanisms is shown in Figure 2.5. Cerebral perfusion pressure (CPP), the difference between arterial blood pressure and intracranial pressure, is the driving force that controls CBF. There is a strong correlation between CBF and cerebral blood volume (CBV). CBV and cerebrospinal fluid in turn determine the levels of ICP through dynamic changes in intracranial compliance, providing the first feedback mechanism. In addition, the amount of perfusion is regulated by the resistance of the cerebral vasculature through various mechanisms that can be roughly divided into the sympathetic response, the myogenic response, and the metabolic response. It is worth noting that different feedback pathways themselves involve a complex system, and there are many interactions between them. Any change in one variable can affect all aspects of cerebral vascular behaviour. It is precisely because different mechanisms do not operate in isolation that CBF regulation becomes a robust system, ensuring precise control of CBF and preventing potential brain dysfunction.

2.2.1 Haemodynamics

The brain is particularly sensitive to hypoxia (i.e., lack of oxygen) and hence the supply of blood to the brain must be critically controlled. Although the cerebral vascular system is highly complex, the cerebral blood flow in a steady state can be

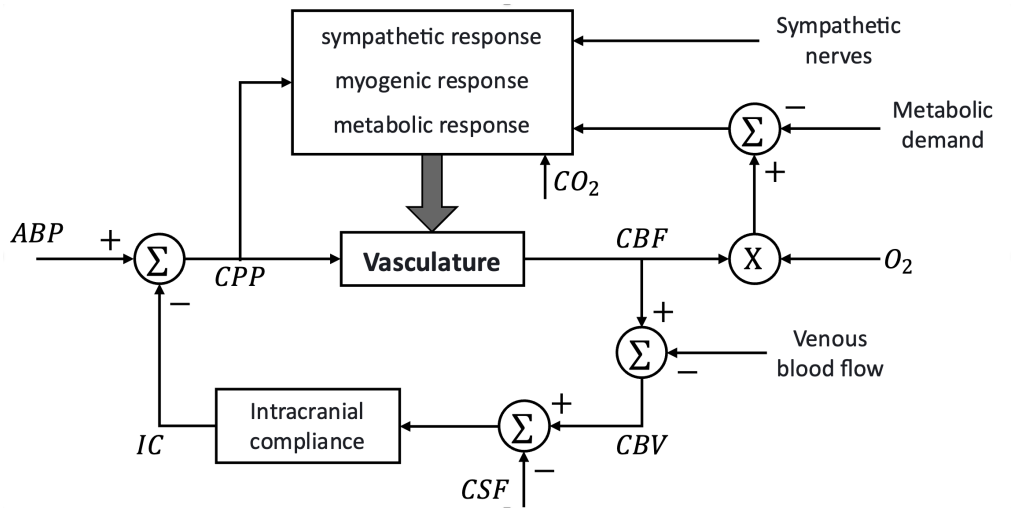


Figure 2.5: Simplified schematic of CBF regulatory mechanisms. ABP and IC contribute to CPP, which drives blood flow through the vasculature. The vasculature responds to various regulatory inputs, including sympathetic, myogenic, and metabolic responses, modulated by levels of carbon dioxide (CO_2) and oxygen. Metabolic demand and sympathetic nerve activity influence CBF adjustments, while CBV and CSF dynamics contribute to venous blood outflow. Reproduced without modification from [26].

simply represented by:

$$Q = \frac{\Delta P}{R} \tag{2.1}$$

where Q denotes CBF, ΔP denotes pressure difference (arterial to venous) and R denotes vascular resistance. Thus, CBF will decrease as the pressure difference decreases, unless the resistance to blood flow also decreases. In response to various stimuli, the brain can regulate the supply of oxygen and glucose via CBF by altering blood vessel tone, resulting in a change to the effective resistance to flow. Since pressure and flow can be linearly related, the resistances of series and parallel blood vessels can be combined in the same way as resistors in an electric circuit, forming the basis of the electrical equivalent model of CBF. The influence of blood flow inertia and vascular wall compliance is considered by modelling them as inductors and capacitors, respectively. This will be described in more detail in the next section on lumped-parameter models.

For axisymmetric steady flow, the resistance is normally assumed to be governed by the Poiseuille equation with appropriate boundary conditions (i.e., the pressure

is uniform over the cross-section area, zero velocity at the vessel wall):

$$R = \frac{8\mu L}{\pi r^4} \tag{2.2}$$

where R is the resistance of the vessel, μ is the viscosity of the fluid, L and r are the length and radius of the vessel respectively. ΔP is the difference in fluid pressure between the ends of the vessel, and Q is the volumetric flow rate through the vessel. Although blood vessel diameter, length, and haematocrit all affect vascular resistance, the latter two are essentially constant unless adaptive changes occur on a very long time scale. Therefore, blood flow can be simply regulated by changing the diameter of blood vessels. The radius and resistance have an inverse fourth power mathematical relationship, which means that even relatively small changes in this radius can lead to substantial changes to resistance and hence to flow. This does provide a very fine degree of control, especially when different generations of blood vessels react in different ways, enabling both global and local flow to be very tightly controlled. By altering the radius, autoregulatory system can prevent fluctuations in blood pressure from causing fluctuations in blood flow, avoiding brain damage caused by the lack, or excess, of oxygen in the brain tissue.

2.2.2 Cerebral autoregulation

The mechanisms that maintain CBF at a near-constant level despite large changes in ABP are collectively known as cerebral autoregulation. The concept of CA was first proposed by Lassen in his review paper in 1959 [28]. He extracted the measurement values of mean arterial blood pressure (MABP) and CBF from 11 different studies and plotted the cerebral pressure-flow curve (Lassen curve). As shown in Figure 2.6, a plateau region exists between the lower limit of autoregulation and the upper limit of autoregulation, where a change of ABP will not significantly affect CBF. In this region, autoregulation mechanisms ensure that the brain has a stable and adequate supply of nutrients through nearly constant blood flow, so as to maintain normal functions. However, it should be noted that Lassen's method has been criticized by a number of authors since the selected data points are so few that the sample

are not representative, and the validation of the Lassen curve is always done with animal data. In addition, the concept of the plateau remains controversial in the literature [29].

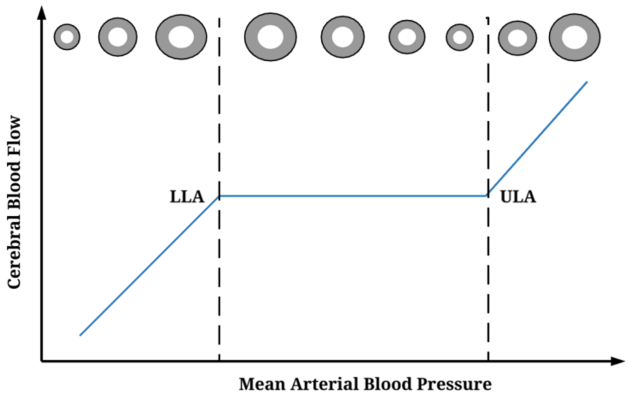


Figure 2.6: Simplified schematic of the Lassen curve with associated radial changes. The blue line represents cerebral blood flow, including the lower (LLA) and upper limits (ULA) of cerebral autoregulation. Grey circles indicate relative artery diameters under varying pressure conditions. Adapted from [30].

The myogenic response, which reflects the corresponding changes in blood vessels in response to changes in ABP, is governed by both CPP and the level of carbon dioxide in the bloodstream. Due to the compliance of the vascular wall, a decrease in ABP leads to a decrease in vessel diameter, resulting in an increase in resistance and a reduction in flow. This is termed the passive response, which is a result of decreased driving pressure and accompanying increased resistance. In healthy autoregulation, this passive response is counterbalanced by the larger active response, which acts to dilate the vessel when the pressure drops. Since these mechanisms have different response times and the active response takes a longer time to occur, the autoregulation response is thus biphasic. Figure 2.7 shows the initial increase in resistance and significant decrease in blood flow in response to a drop in driving pressure. After this, the autoregulation mechanisms begin to operate and act to reduce resistance, thereby restoring CBF to close to its original value.

The myogenic response, dominated by SMC, is widely regarded as the primary vasoconstriction mechanism in autoregulation in response to elevated blood pressure.

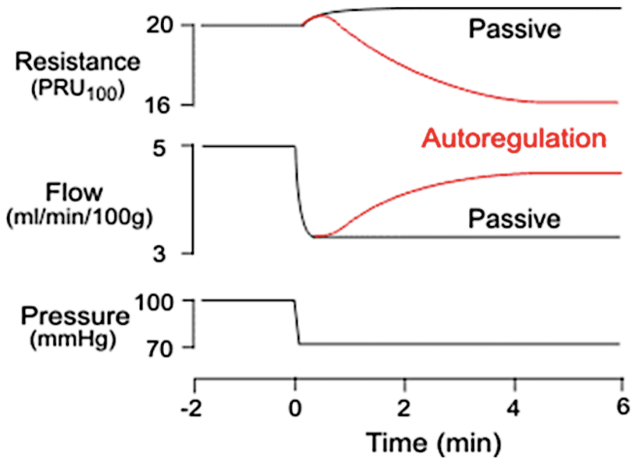


Figure 2.7: Biphasic response of the cerebral vasculature to a reduction in ABP. The black line represents the response without autoregulation, where vessel compliance alone leads to a decrease in vessel radius, causing increased resistance and reduced blood flow. The red line shows the response with autoregulation, where the active myogenic response counterbalances the passive phase by inducing vasodilation to restore blood flow[27].

Since it is intracellular calcium that largely governs the phosphorylation of myosin cross-bridges, changes in membrane potential are crucial to this contraction and dilation. Since potassium ions are the primary controller of the membrane potential, these are thus also very important. There are many K^+ channels within the cell membrane, of which the two most important are the inward-rectifying K^+ channel and the ATP-dependent K^+ channel.

The electro-mechanical coupling and the pharmaco-mechanical coupling are two ways to elevate intracellular calcium in SMC, thereby driving the myogenic response [27]. In the electro-mechanical coupling, elevated transmural pressure activates stretch-activated channels and causes depolarization [31]. The influx of calcium through the voltage-gated calcium channels (VOCCs) is observed to increase significantly with depolarization. The resulting increased intracellular calcium further leads to a release of calcium from the internal stores of the SMC, thereby causing vasoconstriction [32], as shown in Figure 2.8. In the pharmaco-mechanical coupling, neurotransmitters open the receptor-operated calcium channel in the membrane and induce the formation of inositol triphosphate (IP3). IP3 then opens related channels in the SR and releases stored calcium, causing the vessel to contract.

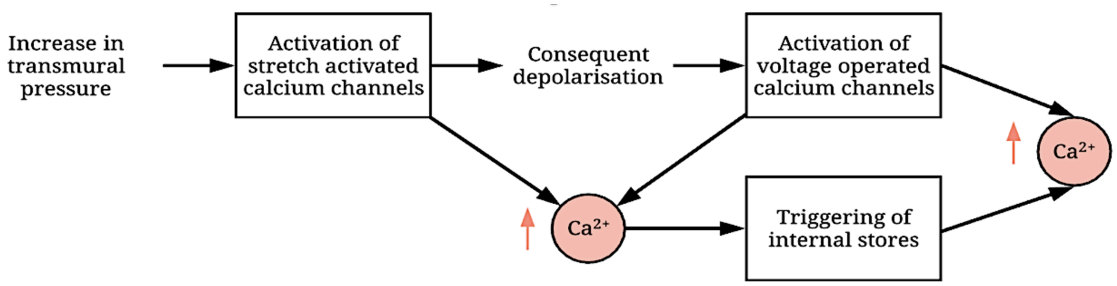


Figure 2.8: Simplified schematic indicating main drivers in the myogenic response as proposed by [32]. Pink circles indicate increases in cytoplasmic calcium.

The shear stress response driven by nitric oxide (NO) is one of the most important vasodilation mechanisms to balance vasoconstriction. Inhibition of endothelial nitric oxide synthase (eNOS) causes significant vasoconstriction and a subsequent increase in blood pressure [33]. Falcone et al. (1991) [34] and Kuo et al. (1991a) [35] both found that flow-induced vasodilation was endothelium-dependent. These experiments all confirm the important role of vascular endothelial NO synthesis in regulating CBF. In response to the shear stress, endothelium cells produce NO through eNOS, before NO diffuses into the SMC and participates in the production of cyclic guanosine monophosphate (cGMP). cGMP can not only reduce intracellular calcium concentration through various mechanisms, but directly stimulate myosin light-chain phosphatase. This enzyme dephosphorylates myosin heads to inhibit phosphorylation, resulting in a reduction in smooth muscle tone. Interestingly, this pathway shows great similarity with the NO dynamics in neurovascular coupling (NVC), where NO produced in another cell freely diffuses into the SMC before eliciting a vasodilatory response. However, the shear stress response has been shown to saturate at low flow levels, meaning that the myogenic response can be viewed as the driving force in dynamic cerebral responses to changes in ABP [35].

2.2.3 Neurovascular coupling

Neurovascular coupling describes the close interactions between neuronal activity and CBF that maintain the local balance between supply and demand of oxygen and glucose both in time and space [36]. Since brain tissue can store only minimal quantities of oxygen and glucose, the additional supply through vasodilation of

the arterioles, driven by the neurovascular unit is of great importance. Neurons, astrocytes, vascular smooth muscle cells and the endothelium that make up the neurovascular unit (NVU) all play a role in vasodilation caused by increased synaptic activity.

The potassium and NO signalling pathways, as well as the metabolism of arachidonic acid (AA), are three of the dominant NVC mechanisms, as shown in Figure 2.9. The potassium pathway is initiated by neuronal activity, which releases potassium and glutamate into the synaptic cleft. Astrocytes then siphon potassium into the cytoplasm through Na/K pumps, resulting in membrane depolarization and an increase in intracellular calcium. The increased calcium leads to the opening of big potassium (BK) channels in astrocytic end-feet, releasing potassium into the perivascular space [37]. The rise in perivascular potassium concentration leads to a further efflux of potassium through the inward-rectifying potassium (Kir) channels from the SMC into the perivascular spaces (PVS), hyperpolarizing the SMC membrane and closing the VOCCs, preventing an influx of calcium. The decrease in calcium concentration relaxes the SMC via actin-myosin cross bridge formation, dilating the vessel, which results in increased blood flow [34].

The metabolites of AA produced and released by astrocytes also contribute to this process within our current understanding of NVC mechanisms. The released glutamate from neurons activates metabotropic glutamate receptors (mGluRs) on the astrocyte membrane and increases cytoplasmic calcium concentration. Phospholipase A2 is then activated to promote AA production from membrane phospholipids, which in turn leads to the production of AA metabolites, including prostaglandins (PGs), epoxyeicosatrienoic acids (EETs), and 20-hydroxyeicosatetraenoic acid (20-HETE). These have different effects: EETs induce vasodilation, 20-HETE causes vasoconstriction and PGs can elicit either response [21, 38–40]. However, although many experimental studies have investigated these metabolites, few attempts have been made to model them, which limits their inclusion in this study.

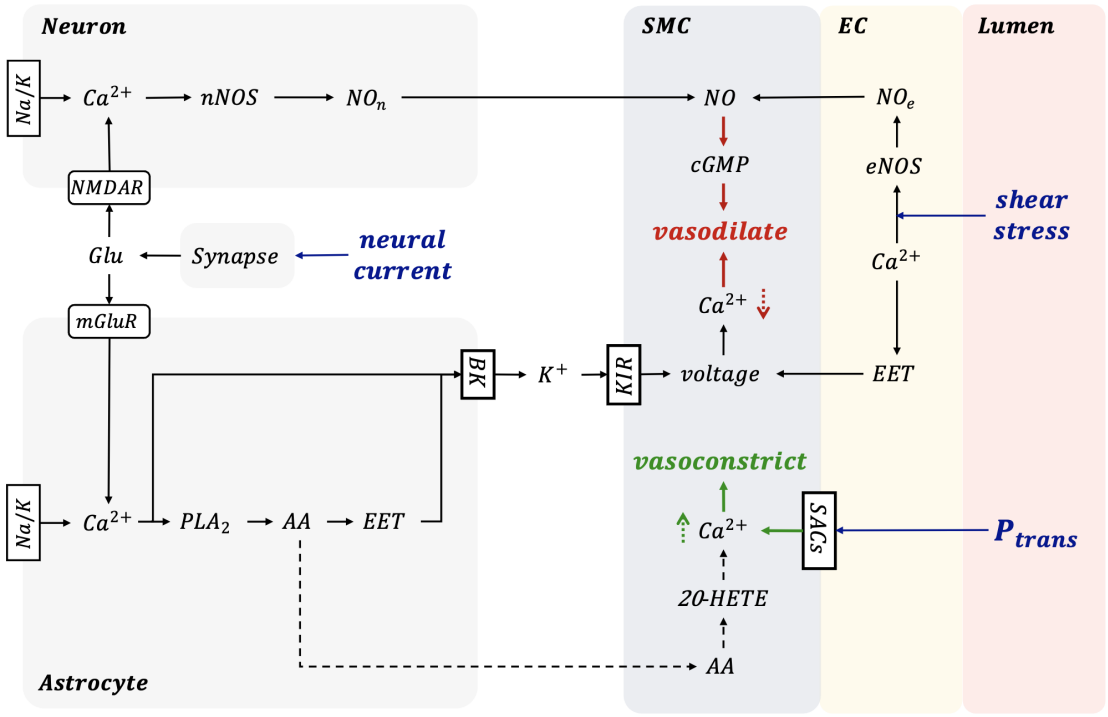


Figure 2.9: Summary of the prominent NVC and autoregulation pathways. Figure adapted and modified from [27]. In neurons, synaptically released glutamate acts on n-methyl-d-aspartate receptors (NMDAR) to raise intracellular calcium, causing nNOS to release NO, which activates the generation of cGMP to cause vasodilation. In astrocytes, glutamate raises calcium by activating the metabotropic glutamate receptors, generating arachidonic acid from phospholipase A2. The AA metabolite: EETs dilate vessels through the potassium pathway, whereas 20-HETE (in the SMC) constricts vessels.

As well as the above pathways, the effects of the NO on NVC have been widely discussed recently. Kitaura et al. (2007) [41] have confirmed the role of NO as a vasodilator during NVC. Glutamate released by synapses acts on NMDAR, causing neuronal nitric oxide synthase (nNOS) to catalyse the production of NO from L-arginine. NO then diffuses from the neuron to the SMC and inducing vasodilation through an intermediary molecule called cGMP [42]. In addition to directly mediating the generation of cGMP to dilate vessels, NO can also interact with AA pathways by inhibiting the enzymes that synthesise 20-HETE and EETs, thereby regulating blood flow [43].

Although neural activity plays an important role in controlling CBF, the understanding of neural control of autoregulation is still limited. A recent review pointed out eight reasons for the poor understanding of NVC [44]: redundancy, heterogeneous

distribution of sympathetic innervation, blood-brain barrier (BBB) permeability, species divergence, duration and intensity of sympathetic stimulation, asymmetry and influence of perfusion pressure, regional differences in cerebral autoregulation, and metabolic restraint.

2.3 Measurement Techniques

We now move to examine the techniques that have been developed to measure CBF and metabolism, as these measurements provide the foundation both for model development and for clinical decision-making. The first work in this field can be traced back to the 1940s, and significant progress has been made in the accuracy and reproducibility of clinical measurement techniques over the following decades, resulting in a wealth of experimental data.

2.3.1 Development of CBF Measurements

Accurate quantification of blood pressure and CBF is the key for assessing CA. Brian imaging techniques can be divided into externally-based measurements and internally-based measurements. The former, which are based on surface probes or detectors, interrogate the cerebral vasculature from outside and thus have the advantage of high temporal solution, portability and low cost compared with the latter. However, those measurements that directly image the entire brain from within can provide more information and have substantial value in validating mathematical models due to their high spatial solution. Since few techniques can directly measure CBF, it is important to link them to proposed mathematical models in order to interpret the obtained results.

The first landmark in measuring CBF was the nitrous oxide method proposed by Kety and Schmidt in 1948 [10], which relied on the Fick principle (simple conservation of mass of the tracer). After inhaling nitrous oxide, the difference between the measured NO concentrations in arterial and venous blood over a period of time was inversely proportional to CBF. This method reported the CBF of normal

young males to be 54±12 ml/(100g · min). Although the principle was very simple, this method has formed the foundation for almost all subsequent measurements of cerebral perfusion.

The next stage in cerebral perfusion measurement was the development of methods that could reconstruct a full 3D image of perfusion. In the 1970s, computed tomography scans appeared, which used multiple images from different angles to reconstruct a full 3D image, generating 3D xenon-enhanced computed tomography (CT) perfusion maps that could display continuous brain sequences [45]. One of the challenges in the application of Xe-CT is the low energy of the gamma rays, which limits its spatial resolution. The development of new tracers led to the introduction of single-photon emission computed tomography [46]. The basis of its application is to inject a radioactive isotope that emits gamma rays into the subject's bloodstream, similar to Xe-CT, and to reconstruct multiple brain sequences through tomographic scanning. Then a response model similar to the Kety-Schmidt model is used to calculate the regional CBF. Similar methods also include positron emission tomography. By injecting a tracer usually made from a biological substance, it can be used to provide tomographic images of quantitative parameters describing various aspects of brain haemodynamics, including regional CBF, regional CBV, and regional oxygen extraction fraction [47].

A quantitative comparison between non-invasive measurement modalities for CBF can be found in Wintermark et al.'s (2005) review [47]. They illustrate the different criteria that help distinguish between them, including different tracers (diffusible or non-diffusible, endogenous or exogenous) and different technical requirements. Generally, the best technique should be chosen based on the required information, temporal and spatial resolution for different research and clinical applications. However, it is worth noting that since the advent of Transcranial Doppler, image-based techniques have been less widely used in CA studies, as discussed in the next section.

2.3.2 Transcranial Doppler

In recent years, transcranial Doppler ultrasound has become a necessary tool for quantifying dynamic CA due to its high temporal resolution. In 1982, TCD was first performed in humans by Aaslid et al. [48]. While the widespread use of TCD has brought some degree of consistency among different studies, some participants may have poor acoustic windows, which can make it difficult to obtain a good quality signal. Additionally, the biggest challenge of TCD application is that it is only a measure of CBFv rather than CBF. The assumption of using cerebral blood flow velocity (CBFv) as a direct surrogate of CBF relies on the assumption that the cross-sectional area of the vessel being insonated remains constant (changes in blood vessel diameter can be ignored).

However, it is technically challenging to measure the relatively small changes in intracranial blood vessel diameter, and thus the hypothesis of constant blood vessel diameter has been debated. Several scholars have studied the changes in the diameter of cerebral arteries when ABP, $PaCO_2$, and arterial oxygen partial pressure changes [49–53], but existing data cannot yet reach a definitive conclusion. Some studies have also explored the response of blood vessel diameter to drug stimulation, but the results have been inconsistent [54, 55]. Therefore, to reliably evaluate CA using TCD, drug-induced stimulation should be combined with other stimulus methods to gain more detailed information.

Reehal et al. (2021) evaluated the dynamic CA in the middle cerebral artery, anterior cerebral artery, and posterior cerebral artery of 40 healthy volunteers using TCD [56]. They found that the time delay of CA could be consistent across different regions, and the haemodynamic regulation of the posterior circulation seemed to be tighter. However, the relatively lower CBFv in the posterior cerebral artery may affect the gain. This study suggests that discriminating dynamic CA between cerebrovascular territories is feasible with TCD, which may help to quantify the extent and regional features of brain damage in different diseases. TCD has also been proven to be useful for studying neurovascular coupling [57]. With the development

of technology, the dynamic changes in vessel diameter can be better quantified. Therefore, it is expected that TCD will have higher accuracy and reproducibility in the future.

2.3.3 Magnetic Resonance Imaging

In order to overcome the disadvantage of poor spatial coverage using surface-based measurements, many internally-based techniques capable of imaging the whole brain have been developed. Magnetic resonance imaging (MRI) is one of the most popular and widely used techniques to measure CBF since it has the advantage of no ionizing radiation, excellent spatial resolution down to less than 1 mm and very good soft tissue contrast [27]. With these advantages, the blood oxygen level dependent (BOLD) functional MRI response has become the central non-invasive technique for imaging activation response. The BOLD signal relies on the different magnetization properties of oxyhaemoglobin and deoxyhaemoglobin. During activation, the increased activity of the neurons demands extra oxygen. In response to the increased metabolism, CBF is observed to overcompensate, resulting in venous blood becoming more oxygenated. This is reflected by an increase in the cerebral metabolic rate of oxygen ($CMRO_2$) and a decrease in deoxyhaemoglobin. As deoxyhaemoglobin is paramagnetic, the increased signal in response to mental activation can thus be measured by the BOLD fMRI. This was first measured by Ogawa et al. (1990) in rats and by Ogawa et al. (1992) in humans [58, 59].

Given that MRI can directly measure CBF with high spatial resolution, there is growing interest in using MRI to assess CA in recent years [60, 61]. However, currently there is no device that can accurately record continuous blood pressure during an MRI scan, which is the biggest challenge in using MRI to evaluate CA. Although lower spatial resolution was used to achieve higher temporal resolution, Horsfield et al. successfully demonstrated that the spatial heterogeneity of CA can be quantified using MRI [61].

2.3.4 ABP Measurements

The second parameter that must be measured in evaluating CA is arterial blood pressure, which can be measured by invasive and non-invasive methods. Invasive methods involve inserting a catheter into the artery and connecting it to a pressure sensor. This technique is considered the "gold standard" but can only be used under specific conditions. Therefore, non-invasive methods are more widely used, although their effectiveness and accuracy have to be considered carefully.

The most widely used non-invasive continuous blood pressure device in CA research is photo-plethysmography (Finapres), which has been in use for over 30 years. It is based on the "unloading" technique of the blood vessels, which involves applying pressure to the peripheral artery (usually the finger) and maintaining constant arterial blood volume by matching the applied pressure with the arterial blood pressure. The resulting ABP is a continuous measurement curve with high temporal resolution. However, since the measurement site is far from the brain, it is necessary to assume that the peripheral arterial pressure and the cerebral arterial pressure are equal.

Studies have evaluated the impact of different ABP measurement methods on CA. Sammons et al. (2007) found good consistency in the automatic regulation index (ARI) values obtained, although there were some biases, such as higher ARI values based on Finapres compared to invasive methods [62]. Subsequently, Peterson et al. (2014) compared CA parameters (phase difference, gain, coherence, and correlation coefficient) measured by invasive and non-invasive techniques and found similar results, although pre-correction of the measurements was necessary [63]. Both studies indicate that non-invasive blood pressure measurement techniques can be a reliable method for evaluating CA, with significant technological and clinical advantages.

2.3.5 Quantification of CA

CA assessments include static and dynamic cerebral autoregulation. Static cerebral autoregulation (sCA) refers to the change in ABP and CBF measured when a single variable reaches a steady state. This concept can be used for experimental manipulation of blood pressure to evaluate CA, or to assess the adaptive response of CA to chronic, sustained increases in blood pressure in pathological conditions such as chronic hypertension. Dynamic cerebral autoregulation (dCA) refers to the rapid autoregulatory response to changes in blood pressure (such as postural changes), i.e., the changes in CBF in response to real-time fluctuations in blood pressure. There is still controversy regarding the correlation and difference between sCA and dCA [64].

There are two types of CA experiments: the first type relies on the spontaneous fluctuations of ABP and CBF and evaluates the relationship between the two over time, while the second type evaluates CBF/CBFv response by inducing changes in ABP. The former method is more comfortable for subjects but requires a longer duration to obtain accurate CA data, while the latter method is less time-consuming (and mostly simple to perform), but not all subjects can tolerate it, especially those with serious illnesses.

The most common methods of inducing blood pressure changes include thigh cuff test, lower body negative pressure test, head-up/head-down tilt, handgrip test, Valsalva manoeuvre, sit-to-stand test, squat-stand test, and transient hyperaemia test [65]. Repeated sit-to-stand test increases the power spectral density of blood pressure and blood flow, thus improving consistency [66]. Sorond et al. (2009) also showed that the sit-to-stand test was better tolerated than the thigh cuff test, with less ARI variability between different tests for the same subject [67]. Panerai et al. (2001) [65] conducted a meta-analysis of the results obtained by different testing methods, comparing the thigh cuff test, lower body negative pressure test, cold pressor test, handgrip test, and Valsalva maneuver at rest. They found that although the amplitude of pulse and step responses was significantly affected by

the type of movement, the ARI value was not related to the type of operation [65]. They also found that there was no evidence that different levels of sympathetic nerve activity could be reflected in the autoregulatory response in different testing methods.

Although there are numerous methods to induce changes in blood pressure, the range of blood pressure that can be altered is extremely limited. Therefore, few attempts have been made to characterise the cerebral pressure-flow relationship over a wide range of MAP. In the most comprehensive study to date, Numan et al. [68] reviewed 459 studies on static autoregulation through PubMed and Scopus searches. After an exclusion procedure, 49 experiments were included and divided into groups of decreasing MAP and increasing MAP. The mean sensitivities to changes in MAP were found to be 0.82 ± 0.77 %/% for decreased MAP and 0.21 ± 0.47 %/% for increased MAP, which were altered to 0.64 ± 1.16 %/% and 0.39 ± 0.30 %/% respectively when changes in $PaCO_2$ were corrected for. It is worth noting that this type of analysis is still population-based, and it is difficult to separate individual subject responses from these results, as the summation of many different autoregulation curves may not necessarily result in an 'average' autoregulation curve. Therefore, the behaviour of static autoregulation still remains incompletely understood.

Some researchers believe that the accuracy and repeatability of the spontaneous blood pressure fluctuation method are lower than that of the physiological stimulation method [69]. However, Tzeng et al. (2012) [70] studied the relationship among spontaneous transfer function metrics and the rate of regulation index and ARI derived from thigh-cuff test and squat-to-stand test [70]. They found that the CA metrics were generally unrelated or showed weak to moderate correlations. Moreover, they pointed out that the spontaneous fluctuation method is considered to be more physiologically ideal as it reduces interference of autonomic nervous or cognitive processes that may affect the intrinsic mechanisms of dCA caused by

blood pressure manipulation. In conclusion, there is currently no gold standard for testing method.

CA assessment involves various detection techniques and measurement indicators. Perhaps differences in methodology, data collection time, algorithms, and other factors have led to conflicting research results. Therefore, in recent years, researchers have made many efforts to promote the standardization of CA research. In 2016, the international Cerebral Autoregulation Research Network (CARNet) published the first white paper on transfer function analysis of dCA [71], which provided detailed specifications for the analysis of spontaneous blood pressure fluctuations in terms of examination procedures, parameter settings, data collection standards, recording duration, and reporting content. This has made the measurement of CA more stable, reliable, and comparable, laying the foundation for the reproducibility and homogeneity of dCA research and providing technical support for multi-centre clinical studies. In 2020, CARNet launched the international individual patient data meta-analysis (IPD-MA) project [72], which aims to investigate the extent, severity, and temporal characteristics of dCA injury in patients with ischaemic stroke, as well as the relationship between dCA parameters and clinical outcomes, neuroimaging, and baseline demographics. The goal is to establish a risk prediction and prognosis model for ischaemic stroke using large, standardized datasets provided by multiple centres. These contribute to ensuring the reliability and reproducibility of CA research and provide more robust scientific evidence to support clinical practice.

2.4 Mathematical models

As we have learned from the previous sections, the regulation of CBF is a highly complex system, with many physiological variables involved in maintaining adequate cerebral perfusion. The complexity of CA allows us to model the ABP and CBF/CBFv relationship through different methods. CA mathematical models have been well developed over the last thirty years and have provided considerable insight into the processes that govern autoregulation. Considering that there are

multiple regulatory mechanisms operating at different timescales and length scales within the vascular system, it is unsurprising that the scales of interest for CBF models vary significantly from relatively large-scale lumped compartment models to highly accurate mechanical and biochemical models.

2.4.1 Lumped compartment models

The cerebrovascular system can be simplified into two compartments, the arterial and venous compartments, with the arterial compartment driven by ABP and the blood flowing from the arteries to the veins and out under venous pressure. Integrating different vascular compartments using circuit elements such as resistors, inductors, and capacitors into an equivalent circuit of the cerebrovascular system can effectively simulate the compensation of the brain's active response to passive response, achieving the modelling of CA. Generally, the model should include at least three parts: using resistors to simulate the pressure drop along the vessel caused by blood viscosity; using inductors to simulate the inertia of blood; and using capacitors to simulate the compliance of the vessel system to store blood.

It should be noted that using current transmission to simulate blood flow is not precise, and these models only roughly simulate the behaviour of actual cerebral autoregulation. In reality, each vascular compartment contains many blood vessels of different levels. In most cases, lumped cerebral compartment models adopt a high-level approach with a relatively small number of model parameters to simplify the brain into two or three compartments. This can reduce the complexity of modelling and simulate the physiological basis of necessary parameters, such as arterial compliance. The construction of any physiological model requires a balance between simplicity and accuracy, and the equivalent circuit model of the brain is no exception.

The first model to simulate the entire cerebral circulation based on the concept of equivalent circuits was proposed by Ursino (1988) [73], as shown in Figure 2.10. The biggest innovation of this model was to consider autoregulation and

to increase the number of arterial compartments, providing a solid foundation for almost all subsequent compartment models of CA. Numerous experimental simulations confirmed the good effectiveness of the model. Ursino et al. (1995) used this model to simulate the intracranial pressure dynamics in patients with acute brain injury, and the results showed that intracranial pressure was influenced by changes in cerebrospinal fluid, CBF and CBV [74]. Subsequently, Ursino and Lodi (1997) proposed a highly simplified model, combining two feedback compartments into one, simplified into a fluid-based feedback mechanism with a single gain and time constant [75]. This simplified model had only about 12 parameters, but its behaviour performance was very similar to that of the complex model.

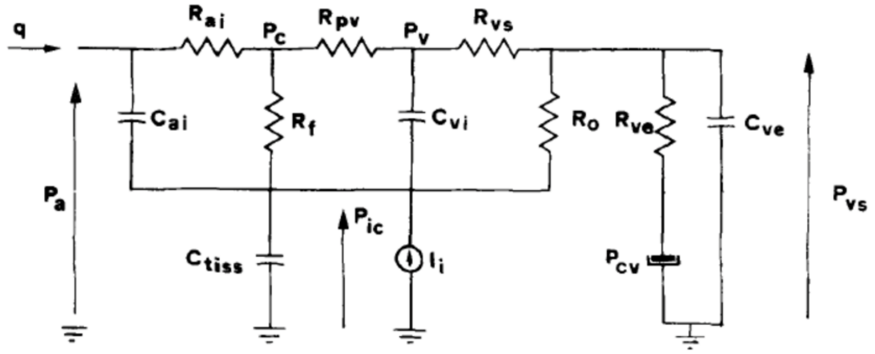


Figure 2.10: Schematic of cerebral autoregulation model proposed by [73]. q, cerebral blood flow; P_a, arterial pressure; P_c, capillary pressure; P_v, cerebral venous pressure; P_{ic}, intracranial pressure; P_{vs}, venous sinus pressure. Compliance and resistance elements are defined as follows: C_{ai}, intracranial arterial compliance; R_{ai}, intracranial arterial resistance; R_{pv}, resistance of the proximal venous vascular bed; R_{vs}, resistance of the distal venous vascular bed, including the lateral lacunae and dural sinuses; C_{vi}, intracranial venous compliance; R_f, resistance to cerebrospinal fluid formation; C_{tiss}, cerebral tissue compliance; I_i, rate of saline infusion; R_o, resistance to CSF outflow; R_{ve}, resistance of the extracranial venous pathway; C_{ve}, extracranial venous compliance; and P_{cv}, central venous pressure. This model illustrates the interaction between arterial, capillary, venous, and cerebrospinal fluid compartments.

Ursino et al. (2000) further extended the two arterial compartment model to cover CO_2 reactivity, and the results were verified in animal experiments[8]. Payne (2006) constructed another model of autoregulation, which was validated against a wide source of CBF experimental data. Three feedback functions were coupled together to vary the compliance and hence the resistance of the small arteries [9].

It should be noted that the third feedback component to model neural activation allowed the model to produce valid output responses to neural stimuli, rather than just responding to changes in ABP and arterial CO_2 concentration. Payne et al. (2009) further extended this model to include haemoglobin transport and hence to reproduce near infrared spectroscopy (NIRS) signals [76]. Spronck et al. (2012) also used a similar methodology to that of Ursino (1988), but with the crucial difference that the autoregulatory mechanisms were divided into the constitutive myogenic and shear stress elements [77]. Thus, this model contained four feedback mechanisms, based on myogenic, shear stress, neurogenic and metabolic regulation, which was fitted to experimental data with good results.

These models provide evidence that an electrical equivalent circuit of cerebral vasculature can respond to both local and global stimuli. The form of the feedback functions and the resulting changes they elicit in the equivalent resistance of the lumped arterioles provide important information about the magnitude and dynamics of a response to a particular stimulus. In addition, it is necessary to include different feedback mechanisms explicitly so as to assign physiological meaning to different components.

2.4.2 Biochemical feedback models

While lumped compartment models present a relatively large-scale view of the cerebral vasculature, biochemical feedback models aim to replicate the cellular processes associated with the regulation of CBF. The advantage of this is that by using biochemical principles, any output behaviour observed in response to stimuli has a physiological basis, allowing the validation of biochemical hypotheses related to individual vessel experimental data. However, many of these models are quite complex since they must contain the detailed physiological pathways controlling the SMC in order to replicate typical experimental results measured by brain imaging techniques (such as the BOLD response).

Biochemical and mechanical mechanisms along with a number of physical laws together govern the relationship between pressure and radius for a single blood vessel, as shown in Figure 2.11 [27]. The complexity of this system means that this literature review is limited to models that are closely relevant to our investigation: the electrochemistry of the smooth muscle cell, models of the interaction between chemical concentrations and smooth muscle contraction (kinetic model), and models of the mechanics of smooth muscle (mechanical model).

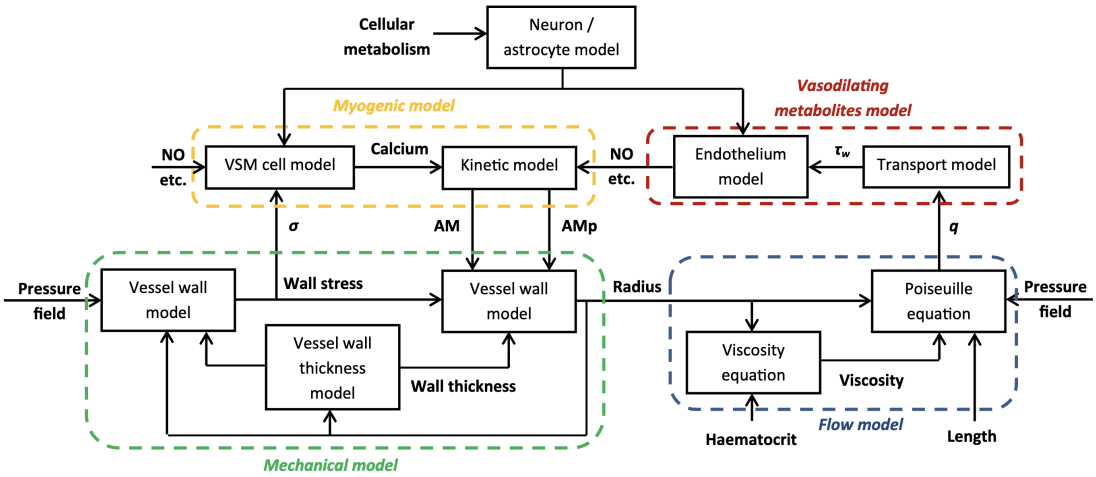


Figure 2.11: Schematic of model of relationship between main variables in control of cerebral blood flow [27]. The myogenic model (yellow box) controls vessel constriction and dilation via the vascular smooth muscle cell model and calcium kinetics, enabling active myogenic responses. The mechanical model (green box) addresses vessel wall stress and thickness, adjusting to pressure changes and affecting vessel compliance. The vasodilating metabolites model (red box) involves the endothelium model and transport mechanisms, which respond to metabolic signals, such as nitric oxide, from neuronal activity to mediate vasodilation. Lastly, the flow model (blue box) calculates flow rate q based on Poiseuille's law, vessel radius, haematocrit levels, and pressure gradient, governing overall flow dynamics.

Hai and Murphy (1988) [78] first proposed a 4-state kinetic model describing the attachment and phosphorylation of myosin cross-bridge with seven rate constants governing transitions between the four states, as shown in Figure 2.12. This model provides the molecular basis for smooth muscle contraction and thus lays the foundation for nearly all following models of the vessel wall.

Given the importance of the calcium concentrations in SMC, it is vital to understand

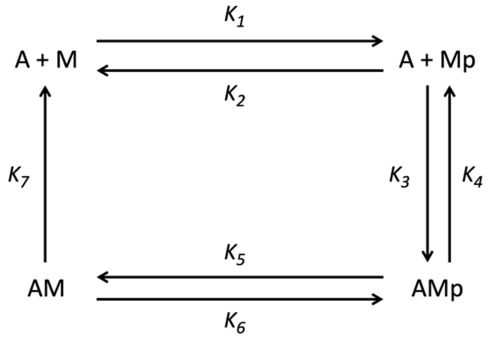


Figure 2.12: Structure of kinetic model proposed by [78]. M: myosin cross-bridges; Mp: phosphorylated cross-bridges; Amp: phosphorylated and attached cross-bridges; AM: attached, non-phosphorylated cross-bridges. K_1 and K_6 are phosphorylation rate constants, K_2 and K_5 are dephosphorylation rate constants, K_3 and K_4 are rate constants for the attachment and detachment of fast cycling phosphorylated cross-bridges, K_7 is rate constant for latch-bridge detachment.

the physiological pathways that govern calcium changes in detail. Yang et al. (2003) [79] created a lumped-parameter Hodgkin-Huxley model capable of modelling the calcium dynamics in SMC and the consequent kinetic and mechanical model responses, which ultimately determine the vessel tone. The coupling of the electrochemical model with a fluid compartment model (including cytoplasm, extracellular space and SR) allowed the tracking of all ionic currents across the membrane and hence the membrane potential. This model also contains a mechanical model that takes the states of the kinetic model as inputs and translates them into the length of the SMC. Although this near-complete model of the SMC has been validated against experimental data, it failed to include any NO dynamics, which prevents analysis of the shear stress mechanism. Furthermore, the myogenic response in Yang's model was driven by stress rather than stretch, which has not been subsequently confirmed by experimental data.

The model of Banaji et al. (2005) [80] took a more detailed approach than Yang, incorporating the SMC model with NO dynamics as well as the response to complex stimuli (such as vascular CO_2 levels). In addition, Banaji succeeded in integrating the single vessel model into a compartmental model of the whole cerebral vasculature, allowing an accurate Lassen curve to be produced. The compartmental model was adapted from Ursino (1988), but the two feedback equations were replaced by a

more detailed biochemical model, relating the activation factors directly to the level of myosin light-chain phosphorylation in each compartment. While the detailed approach of Banaji allowed the underlying physiology to be analysed, the model is highly complex, making it difficult to fit experimental data. In order to solve this problem and correctly interpret the information that can be extracted from measurements (for example, NIRS signals), Banaji et al. (2008) [81] later constructed a much simpler model, making it possible to reproduce several experimental data sets while simulating responses to physiologically and clinically important stimuli.

Koenigsberger et al. (2006) [82] proposed one of the most comprehensive models to describe the SMC calcium dynamics based on the work of Parthimos et al. (1999) [83]. The model is centred around four variables: cytoplasmic calcium concentration, SR calcium concentration, cell membrane potential and the open state probability of calcium-activated potassium channels. Figure 2.13 displays the included channels that contribute to setting these states of the model. Although some channels are not directly involved in the exchange of calcium, they can alter the membrane voltage by changing the potassium, chloride, and sodium ion concentrations within the cell, thereby indirectly affecting the intracellular concentration and the SMC contractile mechanism.

Another integrated model proposed by Catherall (2015) not only investigated the role of NO in the autoregulatory response, but also accurately replicated the available experimental data [84]. In a similar manner to Banaji, the single vessel model containing the myogenic and shear stress response was integrated as part of the whole brain vasculature. The mechanical model of Catherall (2015), based on the work of Stålhand et al. (2008) [85] and Yang et al. (2003) [79], represents the total wall tension in SMC as the sum of passive and active components. The passive component used to counter the disturbance of the vessel radius is usually given by an exponential term, whereas the active component driven by the output of the kinetic model is usually given by a Gaussian function. Both of these components are functions of vessel radius, thus completing the feedback loop. Although the

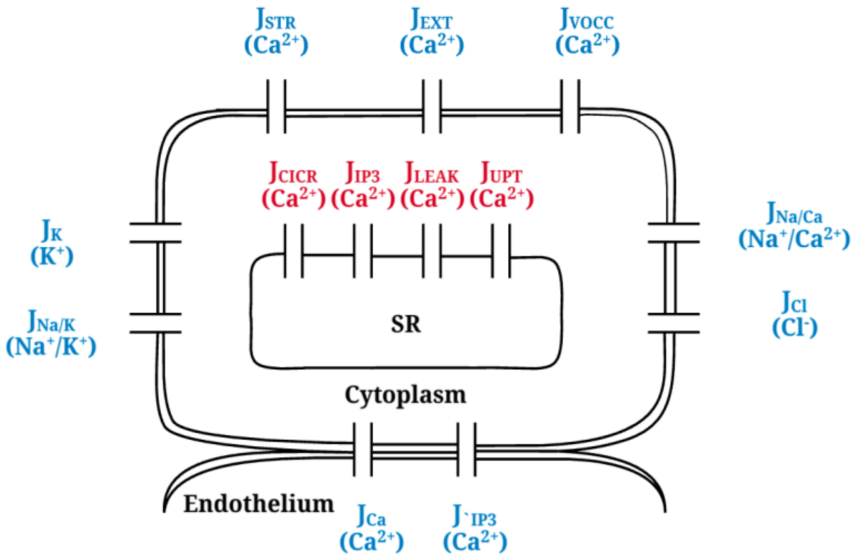


Figure 2.13: Schematic of ion channels in model of SMC [82]. Blue labels indicate channels that connect SMC to extracellular space and endothelium, red labels indicate channels that cause internal exchange of calcium. Species in brackets indicates ions exchanged by the channel. STR: stretch, EXT: extrusion, VOCC: voltage operated calcium, IP3: inositol trisphosphate, CICR: calcium induced calcium release, UPT: uptake.

physiological pathways to control CBF are complicated, the inputs to the kinetic and mechanical models in SMC are far simpler. The critical quantities for altering the vessel radius are the SMC concentrations of calcium and cGMP, as shown in Figure 2.14, which again emphasizes the central role of the smooth muscle cell in regulating cerebral blood flow. Despite the fact that Catherall proposed possibly the simplest form of the mechanical model to mimic the biochemical behaviour, the model suffered from the simplistic treatment of the NO and calcium dynamics in the SMC, thus lacking a detailed physiological basis.

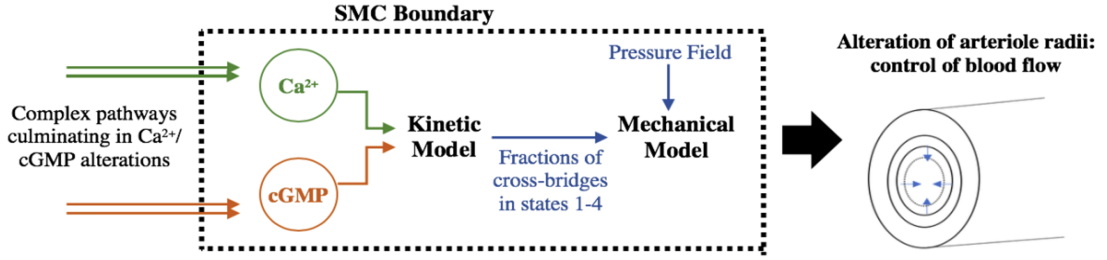


Figure 2.14: Schematic of the relationship between the kinetic and mechanical models [84].

These two types of cerebral autoregulation models have their own advantages and disadvantages: the lumped compartment models are relatively easy to fit to limited experimental data, but their results are hard to interpret due to the lack of physiological basis; the biochemical feedback models contain more physiological information, but they are significantly more complicated. Therefore, a combined approach is often adopted, where an equivalent circuit is still used but the compliance and resistance associated with the arterioles are derived from a single vessel model. In this way, the feedback system can still be modelled while the active control mechanisms have an underlying physiological basis by relating the effective resistance to the radius of the artery through the analogy between Poiseuille's equation and Ohm's law.

2.4.3 Neurovascular coupling models

In parallel with the development of models of autoregulation, there have been a number of models that attempt to model the response to activation. Farr and David (2011) proposed one of the earliest mathematical models of a complete NVU to simulate neuronal activity [86], as shown in Figure 2.15. The glutamate efflux into the synaptic space allowed the inclusion of astrocytic calcium. This model also considered the production of EETs in the astrocyte and the release of potassium into the perivascular space via the calcium mediated BK channels and Kir channels. However, the rate of change of perivascular potassium was found to be too slow to induce vessel dilation.

Dormanns et al. (2015) [87] then constructed a more complete mathematical model to investigate the astrocytic mediated perivascular potassium and the SMC calcium pathways in NVC, based on the work of [37, 86, 88]. The model consists of seven compartments: the neuron, synaptic cleft, astrocyte, perivascular space, SMC, endothelium and the lumen, which were assembled using a lumped compartment approach. They successfully related a neuronal input to the resulting vasodilation/contraction and indicated that the astrocytic calcium pathway is not the only pathway mediating the NVC. Since NO plays a crucial role in the control

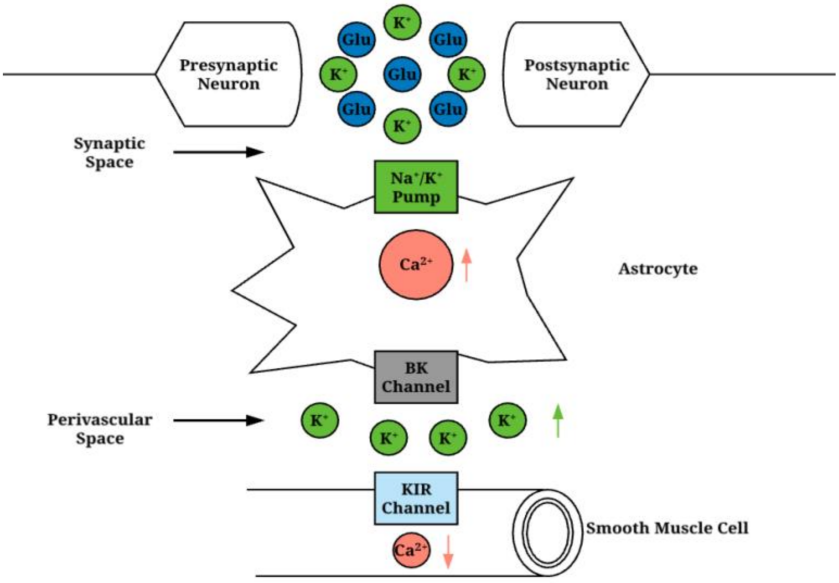


Figure 2.15: An overview of physiological processes of NVC. Neurotransmitters, such as glutamate (Glu), are released from the presynaptic neuron into the synaptic space, leading to the activation of the Na^+/K^+ pump and a rise in intracellular calcium (Ca^{2+}) within the astrocyte. The increase in Ca^{2+} activates the BK channel, allowing potassium ions (K^+) to enter the perivascular space. This K^+ efflux is sensed by smooth muscle cells via KIR channels, resulting in vascular responses that facilitate blood flow regulation in response to neuronal activity.

of CBF, Dormanns et al. (2016) [89] further extended their model to include the dynamics of NO and investigated the governing source of vasodilating NO in the SMC, based on the work of [90, 91]. They found that the vasodilation caused by NO could be enhanced during neuronal activation. The endothelial NO is the governing source of vasodilating NO in the steady state, whereas neuronal NO has a significant vasodilatory role during neuronal activation.

Although experimental data have shown that astrocytic calcium contributes to the response to neuronal activation, the mechanism remains unclear [92]. Kenny et al. (2018a) [93] thus extended Dormanns's model to include the glutamate-induced astrocytic calcium pathway with EET signalling and the stretch dependent transient receptor potential vanilloid-related 4 (TRPV4) calcium channel on the astrocytic endfeet to study the influence of astrocytic calcium in mediating NVC vasodilation. However, in contrast with experimental results, the increase in astrocytic calcium itself is unable to induce vasodilation or constriction, but plays a role in the NVC

potassium pathway through opening BK channels and hence enhances vasodilation. Kenny et al. (2018b) [94] further proposed a more physiologically correct model to contain the extracellular potassium diffusion, which allows for direct communication between adjacent NVUs. This macro scale NVC model with an added extracellular space (ECS) compartment allows the investigation of synchronized cellular behaviour such as vasomotion and paves the way for simulating results such as BOLD signalling [95].

2.4.4 fMRI BOLD response model

Since there is no external tracer and BOLD imaging can be performed on standard MRI machines, resulting in high spatial and temporal resolution, most experimental data for the NVC response are measured in humans using BOLD fMRI. Many models have thus been developed for replicating and interpreting the BOLD response. The principle of BOLD imaging is that when neural activity increases, the proportion of local CBF increase is greater than its metabolic rate, which leads to the washout of deoxyhaemoglobin. Since deoxyhaemoglobin is paramagnetic, this concentration changes can thus be detected using MRI [58]. The Balloon Model of Buxton et al. (1998) [96] is one of the earliest and most influential models and has proved to be the foundation for many other models of the response to activation. Figure 2.16 gives an illustration of the typical BOLD response and the relationship between the stimulus and the resulting changes in flow and metabolism. The BOLD signal is calculated based on two contributing elements: changes in venous CBV and deoxyhaemoglobin. CBV is driven by CBF and deoxyhaemoglobin is driven by the balance between CBV, CBF and $CMRO_2$, which are all driven by neural stimulus.

Mathias et al. (2018) [95] successfully incorporated a BOLD signal model into a full Hodgkin Huxley model of the neuron based on the work of [98]. The detailed properties of the model provide the physiological basis for a rise in synaptic potassium and glutamate following neuronal activity and enabled the model to capture the oxygen consumption of the neuronal sodium/potassium pump as well as the cerebral metabolic rate of oxygen, thus producing typical BOLD contrast

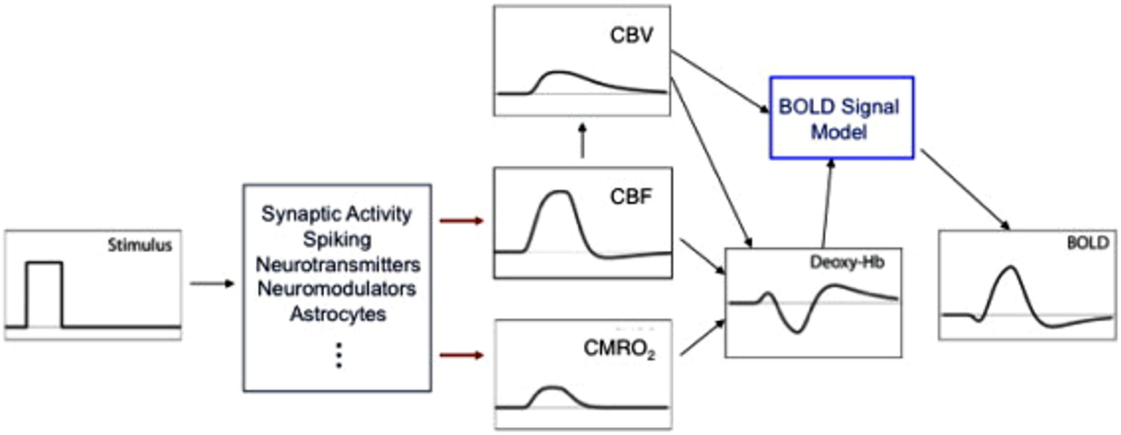


Figure 2.16: Schematic of physiological basis of BOLD response. A stimulus triggers synaptic activity, leading to changes in CBV, CBF, and $CMRO_2$. These physiological changes influence the concentration of deoxyhemoglobin (Deoxy-Hb) in the blood, which is captured by the BOLD signal model. Reproduced from [97].

signals. However, since BOLD imaging is an indirect measurement of metabolism, its underlying physiology remains poorly understood. The possible physiological origins of the initial dip and undershoot in typical BOLD responses are controversial, highlighting the uncertainty behind the relationship between neural stimulus and the model outputs. It should also be noted that CA models based on global CBF regulation share many similarities with BOLD response models based on local CBF regulation. Despite their close relationship, there has been little research linking them or using data from one model to validate the other.

2.5 Clinical conditions

The key driver for studying CA is to understand how it is involved in physiological and pathological processes. Whether there is clinical value in assessing CA in patients, and how to incorporate these measurement indicators into treatment decisions for specific patient groups are pressing questions. Therefore, recent research has extensively explored the clinical pathophysiology of CA, giving us a better understanding of CA under normal physiological and pathological conditions. However, it should be noted that CA assessment in a clinical context is only a detection indicator, not a treatment target. That is, assessing whether CA is

impaired in different pathological conditions, rather than directly treating it. CA remains an underlying symptom of disease or physiological dysfunction that cannot be corrected directly.

2.5.1 Ageing

The impact of ageing on cerebral autoregulation have been studied across different age groups. While ageing leads to a decrease in baseline CBFv, it is generally believed that both static and dynamic autoregulation capacity are not affected by normal ageing, even in subjects >75 years of age [99–103]. Carey et al. (2000) [99] first studied CA in resting-state elderly participants using ARI and found that CA is not affected by physiological ageing, despite reduced CBFv and baroreceptor sensitivity in older adults. Yam et al. (2005) also confirmed this using correlation coefficients [103]. A review of eight studies on dCA in healthy elderly subjects (aged 50 to 75 years), found that dCA was preserved in healthy aged people during induced decreases and spontaneous oscillations in blood pressure (BP) in the low frequency range, independent of the method of assessment [102].

However, recent research has led to some controversy regarding the impact of ageing on CA. Some studies have demonstrated that cerebral autoregulation becomes less effective with ageing, making the brain more vulnerable to changes in blood pressure. In a study assessing dCA over a ten-year period in the same subject group, a drop in autoregulation strength was observed [104]. Another study spanning the whole adult life span also found an increase in autoregulatory gain with age [105]. In addition, gender differences in CA function have been observed in elderly subjects [106]. However, due to the large individual variability in CA in healthy older adults, these do not necessarily imply impaired dCA in elderly subjects.

2.5.2 Chronic hypertension

Patients with chronic hypertension retained the ability to maintain CBF in response to acute changes in perfusion pressure, in line with previous studies [107, 108]. How the slower and progressively decreasing blood pressure induced by antihypertensive

treatment would affect CBF is also important for clinical application. In 3 studies with 114 hypertensive patients, including young, middle-aged, and old individuals, autoregulation was evaluated before and after BP-lowering treatment [109–111]. Despite different measurements modalities (TCD, Xenon-133 or MRI arterial spin labeling), all studies have demonstrated that pharmacological treatment to lower blood pressure has no effect on dynamic and static autoregulation, i.e. both dynamic and static autoregulation remain normal before and after antihypertensive treatment. It should be noted that limitations of all the studies on hypertension are that no patients over 80 years of age were included, and participants may have comorbidities such as cerebral small vessel disease, diabetes, depression and cognitive impairment.

Arterial stiffness, reduced vascular compliance and endothelial dysfunction caused by chronic hypertension can also lead to impaired cerebrovascular reactivity (CVR) and NVC [36, 112]. Impaired CVR and NVC may contribute to the development of cerebral ischaemia, cognitive decline and other neurological disorders. Studies have demonstrated that antihypertensive therapy can improve CVR in response to hypercapnia and hypoxia. Additionally, long-term blood pressure control may help prevent or delay the onset of cognitive impairment and dementia associated with hypertension-induced cerebral small vessel disease. Although the preservation of autoregulation in hypertensive patients and the increases in CBF confirm the benefits of antihypertensive therapy, it is important to note that the benefits of lowering blood pressure may vary from depending on the individual, and treatment should be tailored to each patient's specific needs and medical history. Regular monitoring is essential for managing hypertension and optimizing health outcomes.

2.5.3 Stroke

BP control plays a key role in the management of acute ischaemic and haemorrhagic stroke in order to prevent secondary injury due to extreme hypoperfusion or hyperperfusion [113]. The assessment of autoregulation can provide clinical guidance on BP control, hence a substantial literature has emerged in this area using different protocols and techniques. Some of the earliest studies into autoregulation following

stroke were performed in the 1970s. The impairment of autoregulation following acute to subacute stages of stroke (ischaemic or haemorrhagic) was generally agreed in most studies [113]. However, some studies have shown that patients with mild stroke maintain intact autoregulatory function [114]. Furthermore, even in patients with moderate to severe stroke, autoregulation is not impaired at all time points [115]. These findings suggest that extent of impairment of autoregulation post-stroke depends on stroke severity and its temporal evolution. In addition to these two factors, individual heterogeneity due to stroke phenotype, etiology, subtype, location, comorbidities, and early intervention can also influence the outcome of studies on autoregulation.

Ischaemic stroke

Autoregulation is impaired in patients with ischaemic stroke, with significant associations to disease severity and poor clinical outcomes. Aries et al. (2010) [113] reviewed 23 studies using TCD to investigate CA in patients with ischaemic stroke. Despite the limitations of different studies, the conclusion was consistent that the impairment of autoregulation in ischaemic stroke was observed in both hemispheres. Since small vessel stroke occurs in the context of cerebral microangiopathy, it induces a more global pattern of CA impairment, whereas large vessel stroke mostly results in focal CA impairment [116].

Impaired CA indices are associated with unfavourable outcomes and neurological complications. Most studies of autoregulation in ischaemic stroke have performed assessments in the acute (<48 h) and subacute phases (<14 days after ictus) [113, 115], with a much smaller number of studies performing measurements several weeks or months after stroke onset [117–119]. These studies assessing the evolution of autoregulation parameters in ischaemic stroke, have shown a deterioration of autoregulation metrics in the first 2 week after ictus, with return to normal values between 1 and 3 months later. Although the temporal profile of the autoregulatory impairment following ischaemic stroke suggests a trend towards improvement over

time, severe disturbances in autoregulation have also been observed in chronic stroke. The time course of CA impairment after ischaemic stroke warrants further study as it may have implications for guiding clinical prognosis and blood pressure management, preventing secondary injury and improving clinical outcomes.

Both vascular reactivity and neurovascular coupling have been shown to be affected in patients with ischaemic stroke [119]. Ischaemic stroke affects chronically regional perfusion and CO_2 vasoreactivity in main vascular territories. Vasodilation responses to hypercapnia were markedly reduced, but vasoconstriction responses to hypocapnia were preserved or even exaggerated [120]. Furthermore, in studies using BOLD-fMRI, impaired cerebral vascular responses to neural activation have been found, often coupled to a reduction in CO_2 reactivity [121–123]. Although BOLD-fMRI seems to be more sensitive to the neurovascular disturbance induced by stroke, the basic mechanisms of the BOLD response in the ischaemic brain have not been completely elucidated and BOLD-fMRI findings need to be interpreted with caution [124].

Haemorrhagic stroke

The reason for the small number of experiments quantitatively studying the autoregulatory capacity of haemorrhagic stroke may be that static autoregulatory measures require mechanical manoeuvres or pharmacological induced blood pressure changes, which can be dangerous in critically ill subarachnoid haemorrhage (SAH) patients. Although early studies of static CA in patients with SAH were contradictory, more recent studies have shown that dynamic CA, regardless of the methodology, is impaired in SAH [125, 126]. Recent studies have further demonstrated that the degree of CA impairment is tightly correlated with clinical severity and persists for days after SAH. CA impairment can be present bilaterally or only in the symptomatic (vasospasm or delayed cerebral ischaemia) hemisphere [127]. The temporal evolution of the autoregulation effectiveness in haemorrhagic stroke shows a similar pattern to that of ischaemic stroke. The autoregulatory capacity is impaired and decreases

in the first 2 weeks after ictus and recovers to normal values within a month [128, 129].

The clinical importance of autoregulation studies in patients with haemorrhagic stroke is that they can be used to identify patients at high or low risk of delayed ischaemic complications and unfavourable clinical outcomes after SAH. Studies using different CA indices (including mean flow index (Mx), pressure reactivity index, ARI and tissue oxygen reactivity index (Tox), etc.) have reported that CA impairment may be predictive of vasospasm and Delayed Cerebral Ischaemia in SAH patients [128, 130, 131].

Real-time monitoring of cerebral haemodynamic status during the acute phase of a stroke is very helpful for evaluating individual therapeutics and improving outcomes. Therefore, further consideration should be given to incorporate autoregulatory assessment as part of routine protocols for the management of patients with stroke. Considering that the temporal evolution of autoregulation after ischaemic and haemorrhagic stroke showed a similar pattern, i.e., it tends to be impaired within 2 weeks after stroke onset and recovers after 1 to 3 months, it can be expected that the greatest clinical benefit could be achieved by blood pressure management during the most critical period, that is between 1 and 3 weeks after onset.

However, it should be noted that the highly heterogeneous nature of the population and the response of brain tissue over many different time scales are both key parameters in assessing autoregulatory dysfunction. Systemic interventions intended to increase blood flow within ischaemic regions can paradoxically reduce perfusion in that region and/or others [132, 133]. It is very likely that many of the seemingly contradictory findings in the earlier literature are due to these heterogeneities. It should also be noted that the responses after ischaemic and haemorrhagic stroke are different, meaning that the management of ABP post-stroke needs careful consideration. This drives the need to rapidly stratify the different stroke subtypes and incorporate physiological information (e.g., patient age, previous blood pressure,

cardiac history, and other factors) in the acute care of stroke patients in order to individualize hemodynamic management and improve clinical outcomes.

2.5.4 Alzheimer's disease

In contrast to the large body of work that has been devoted to the study of baseline BP and CBF in Alzheimer's disease (AD), studies that investigated cerebral autoregulation specifically in clinical AD has only recently become available and is somewhat inconclusive. Zhang et al. (2020) [134] conducted sCA studies on 42 patients with mild cognitive impairment in the early stage of AD and found that sCA was impaired. Zhou et al. (2019) [135] evaluated the CA of 31 AD patients using TCD and found that changes in CBFv induced by the supine-to-stand test was significantly lower than that of the normal control group, indicating decreased autoregulatory ability in response to transient blood pressure changes. However, Heus et al. (2018) [136] obtained the opposite conclusion. They used transfer function analysis (TFA) to study dCA and baroreflex sensitivity in 90 AD patients with different stages (including 27 with mild cognitive impairment (MCI) and 53 with dementia). They found no significant differences in dCA and baroreceptor sensitivity (BRS) compared to the controls, either at rest or during the sit-to-stand test, suggesting preserved dCA at different stages of AD. In other studies investigating CBF fluctuations in response to blood pressure changes in AD patients, 5 reported preserved autoregulation [137–141] while 2 reported impaired autoregulation [142, 143]. In the future, more studies on cerebral haemodynamic at different stages of AD are needed to determine the relationship between CA and the occurrence and progression of AD.

A growing number of experiments report impairment of mechanisms associated with autoregulation in AD. Functionally relevant potassium channel activity in cerebral endothelial and smooth muscle cells is impaired in Alzheimer's disease [144]. Patients with mild cognitive impairment and AD showed reduced wall shear stress and increased vascular pathology, compared to normal controls. The level of wall shear stress associated with the degree of cognitive decline may indicate the involvement

of vascular disease in the development of AD. However, the lack of techniques with high spatial and temporal resolution to measure the diameter of cerebral arteries makes it challenging to study shear stress patterns in intracranial arteries. Therefore, it is difficult at this stage to conclude a causal relationship between CBF-regulated endothelial mechanisms and cerebrovascular disease. In addition, the vasoconstrictor reflex becomes excessive in Alzheimer's disease, disrupting a key homeostatic mechanism of cerebral circulation and making CBF more dependent on MABP.

The global changes in CBF, CO_2 reactivity, and NVC in AD have been studied much more extensively than autoregulation. Subjects with early stage probable AD exhibit impaired cerebrovascular responses to hypercapnia measured with TCD, compared with cognitively normal controls [142]. Impaired cerebrovascular reactivity is also associated with an increased risk of development of AD from MCI and an increased risk of cognitive decline in AD. In addition to changes in cerebrovascular reactivity, there is increasing evidence that neurovascular dysfunction plays a key role not only in the pathobiology of vascular cognitive impairment (VCI) but also in Alzheimer disease, which may also already be present in the preclinical stage. Neurovascular dysfunction increases the brain's susceptibility to injury by altering regulation of the cerebral blood supply, disrupting BBB function, and reducing the trophic support and repair potential of the injured brain [145]. By using BOLD-fMRI, Kisler et al. (2017) [146] observed that individuals with underlying or early stage of AD have diminished local CBF responses in cognitively demanding tasks. Moreover, this study also showed that resting-state neural connectivity in brain regions prone to atrophy in AD (e.g., hippocampus, medial prefrontal and cingulate cortex) are disrupted.

There is an increased awareness of the importance of cerebrovascular dysregulation in the development of AD. It has been shown that increased cerebrovascular resistance index and reduced CBF predict the onset of AD even earlier than traditional biomarkers (e.g., cerebrospinal fluid β-amyloid, cerebral hypometabolism, or brain

atrophy) [147, 148]. These steady-state haemodynamic changes may therefore be used as early biomarkers of dementia and a predictor of dementia progression. In addition, studies have shown that therapies to improve cerebral perfusion through anti-hypertensive treatment can improve cognitive function in AD, further suggesting that monitoring BP and treating arterial hypotension are essential. In the absence of mechanism-based therapies to treat vascular and neurodegenerative dementia, approaches aimed at maintaining cerebrovascular health by controlling vascular risk factors are anticipated to be extremely valuable.

2.6 Conclusion

In this chapter, we have provided a comprehensive review of the physiological basis, measurement techniques, mathematical models, and clinical applications of the brain. We started with the anatomy and geometric structure of the brain, and then moved on to the global and local CBF regulation mechanisms. While mathematical models have successfully reproduced many aspects of arterial behaviour, a physiologically-based model that successfully integrates CA with NVC has yet to be developed. Since NVC and autoregulation can respond to different stimuli through many similar pathways, building a comprehensive model that can simultaneously study both activation and autoregulatory responses would be valuable. In addition, although CA assessment plays an important role in the diagnosis and prognosis of cerebrovascular diseases, its clinical application has not been widely promoted. The main reasons include unclear mechanisms of action, imperfect examination methods, and unclear intervention measures. To address these pressing problems, we will use mathematical models to conduct in-depth research on the physiological mechanisms of CA, to promote the clinical translation of CA and make it a new target for acute treatment and prevention of cerebrovascular disease.

3

Static autoregulation in humans

The work related to healthy subjects in this chapter has been published in [149]. Static autoregulation in humans. Journal of Cerebral Blood Flow & Metabolism. 2023;0(0). doi:10.1177/0271678X231210430

The classic view of cerebral autoregulation, that CBF remains constant over a wide range of ABP, has been cited and described in numerous publications and textbooks since it was introduced by Lassen [28]. However, increasing evidence has challenged the existence of this wide cerebral autoregulation plateau [29, 49, 150, 151]. To provide an updated understanding of the static cerebral pressure-flow relationship, and to provide experimental data support for the mathematical model in subsequent sections, we conducted a comprehensive literature research and used a data-driven approach to more rigorously quantify the characteristics of the autoregulation curve. This data-driven approach provides a quantitative method of

analysing static autoregulation that can be easily updated as more experimental data become available.

3.1 Introduction

The brain is one of the most tightly regulated organs in the human body. Healthy CBF and metabolism are essential for the proper functioning of the human brain. CBF regulation is closely related to changes in arterial blood pressure. As early as the 1930s, studies demonstrated in animal models that cerebral blood vessels dilate or constrict in response to reduced or enhanced arterial blood pressure [152]. In 1959, Niels Lassen first constructed the relationship between MAP and CBF using data taken from 11 studies [28]. Based on this analysis, it was proposed that there is a plateau region above the LLA, where CBF remains essentially constant across a relatively wide range of MAP (approximately 60-150 mmHg, Figure 3.1(a)). Due to the fact that Lassen's original publication did not include data at higher blood pressure values, the concept of the ULA was later proposed and validated [153–155]. This physiological relationship was termed static CA. Subsequent studies in animals, non-human primates, and humans have replicated Lassen's curve and confirmed the substantial autoregulatory capacity of the cerebral circulation [155–158]. Prior to this, CBF was assumed to vary passively with perfusion pressure.

Despite the fact that Lassen's autoregulation curve continues to be cited and described in numerous publications and textbooks, increasing evidence has challenged the existence of this wide cerebral autoregulation plateau [29, 49, 150, 151]. In 1983, Heistad and Kontos pointed out that the original study [28] had incorrectly plotted several points in the figure and that some of the experimental data were invalid due to incorrect experimental design [160]. When these erroneous experimental data were corrected, the autoregulation plateau disappeared. Additionally, recent evidence suggests that in healthy humans, the range of MAP within which CBF is maintained constant is much smaller than originally proposed (only $\pm 10\% \Delta$MAP) [29]. Furthermore, due to differences in baseline blood pressure, the upper and

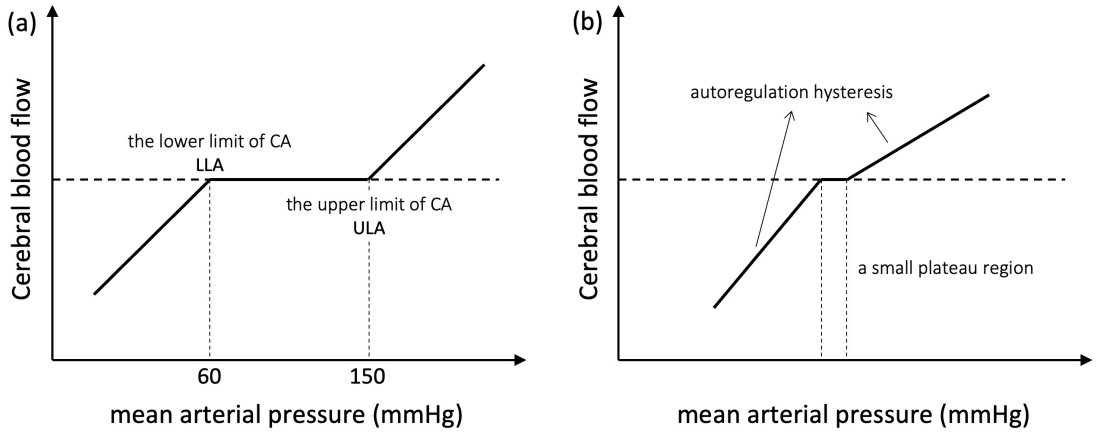


Figure 3.1: (a) Classical view of autoregulation, first proposed by Lassen [28]. It should be noted that the ULA was only demonstrated later in hypercapnic dogs in 1971 [153]. (b) A typical contemporary view of autoregulation showing a small plateau region and the directional sensitivity of cerebral autoregulation [159].

lower limits of autoregulation, as well as the plateau region, also vary significantly among individuals. One study captured MAP/CBF relationships individually from 10 hypertensive patients and found that the extent of autoregulatory range varied between patients [155]. Therefore, it remains unknown whether the group-averaged autoregulatory curve would apply to all individuals [3].

Assessment of CA requires simultaneous measurements of CBF and BP. Over the past 20 years, there has been significant development in the study of the human cerebral pressure-flow relationship, with the introduction of CBF quantification techniques that provide high temporal resolution. The use of non-invasive techniques such as transcranial Doppler ultrasound and digital arterial volume clamp (such as Finapres) to continuously measure CBF velocity and MAP allowed the dynamic relationship between these two variables to be quantified. CA measurement methods are thus generally divided into two categories: static and dynamic CA [161]. Static CA is the autoregulatory response to steady-state changes in ABP or ICP (when mean blood pressure changes to a new level and remains stable for several minutes or hours), providing information on the CPP range in which CA is active [152]. The dynamic CA refers to the instantaneous change in CBF in response to rapid changes in MAP (in a time scale of seconds). Although sCA and dCA operate on

different time scales, the CBF regulatory mechanisms involved in these two types of CA may be the same or have some common basis. The differences and similarities between them have been reported in many studies [64, 162].

However, few attempts have been made to characterize the cerebral pressure-flow relationship over a wide range of MAP due to the lack of methods to alter blood pressure effectively. In the most comprehensive study to date, Numan et al. [68] reviewed 459 studies on static autoregulation through PubMed and Scopus searches. After an exclusion procedure, 49 experiments were included and divided into groups of decreasing MAP (n = 23) and increasing MAP (n = 26). The mean sensitivities to changes in MAP were found to be $0.82 \pm 0.77\%/\%$ for decreased MAP and $0.21 \pm 0.47\%/\%$ for increased MAP, which were altered to $0.64 \pm 1.16\%/\%$ and $0.39 \pm 0.30\%/\%$ respectively when changes in $PaCO_2$ were corrected for. Their findings suggested that the efficacy of regulating CBF seemed to differ depending on the direction of blood pressure changes, with a more effective capacity to maintain stable CBF during acute (transient) periods of hypertension compared to hypotension. This directional sensitivity of CBF response to MAP will cause the slope of the autoregulation curve to be greater below the LLA than above the ULA, as shown in Figure 3.1(b). However, the mechanisms governing this are not entirely understood.

It is worth noting that most of the convincing evidence for this asymmetry is based on studies of dCA [163–166]. While Numan et al. [68] also observed directional sensitivity in sCA, several studies included in the review used blood pressure manipulation drugs (such as Dexmedetomidine and Sevoflurane), as well as included some dCA experiments (such as supine-to-stand and cold pressor test), leading to potential confounding factors such as medication effects, autonomic activation, and differences in $PaCO_2$. Thus, the presence of autoregulatory asymmetry in sCA needs to be reconsidered. In addition, in this study, they only considered linear changes in CBF, and did not consider the range of the autoregulatory plateau. They also did not consider the effects of sex or age on the results, largely due to the size

of the dataset. With more sCA experimental datasets becoming available, a more detailed analysis can be performed to better understand the directional sensitivity, which may provide better guidance for clinical arterial pressure management.

Therefore, to provide an updated understanding of the static relationship between MAP and CBF, and to characterize the autoregulation curve more rigorously, we conducted a comprehensive literature review and data-driven analysis of static cerebral autoregulation. Firstly, we re-examined the experiments on sCA in Numan et al. [68] and excluded experiments that might involve dCA, and updated more experiments from 2013 to 2023, to explore the relative changes in cerebral pressure-flow response in healthy humans more rigorously. Based on these results, we will investigate the directional sensitivity of sCA and whether this asymmetry persists after CO_2 correction, by exploring the CBF response to MAP increases and decreases separately. Secondly, we developed an autoregulation curve in humans using regression analysis in absolute CBF units to quantitatively determine the LLA, ULA and CA plateau. Finally, the effects of sex and age on the cerebral pressure-flow relationship are also investigated.

3.2 Methods

In the original analysis by Numan et al. [68], a total of 459 studies published before 2012 were obtained through a PubMed search. 40 studies (49 experiments) were included after exclusion criteria, with 23 experiments lowering MAP and 26 experiments raising MAP. In this updated and expanded review, we re-examined the 459 studies published before 2012. Additionally, we used PubMed, Scopus, and Springer to search for studies with 'arterial pressure', 'cerebral blood flow' and 'healthy subjects' published between January 2013 and September 2022. Non-human studies and non-English studies were excluded, and the selected population was limited to healthy subjects aged 18 to 65. The updated search resulted in the review of an additional 946 studies. As we were also interested in the relationship between absolute CBF and MAP, studies reporting baseline MAP and CBF values in healthy

subjects were included in our analysis. Due to the fact that Numan et al.'s [68] study included some dCA experiments, we applied more stringent controls and updates to the exclusion criteria. Based on this, we re-examined the 40 studies already selected by Numan et al. [68] and screened the additional 946 studies to ensure that all experiments included in this analysis strictly followed the sCA assessment. All experimental data used in subsequent analyses were directly adopted from the included literature if explicitly stated in the text or presented in tables. Otherwise, data were manually extracted when displayed in figures.

3.2.1 Exclusion criteria

Parallel changes in other critical variables such as CO_2, brain activation and sympathetic tone may also be present when manipulating blood pressure. Exclusion procedures were tightly controlled to attenuate and eliminate the adverse effects of these variables on CBF and thereby more accurately determine the cerebral pressure-flow relationship. Multiple experiments have shown that hypocapnia or hypercapnia can affect the range of autoregulation as well as the LLA and ULA [167]. Studies have also shown that middle cerebral artery diameter can be altered in severe hypercapnia (+15 mmHg) resulting in non-negligible errors in CBF measurements, but not in mild hypercapnia (+7.5 mmHg) [168, 169]. Therefore, experimental procedures known to affect the $PaCO_2$ levels (e.g., hyperventilation, exercise, altitude, and heat stress) and/or experiments with changes in $PaCO_2$ of more than 7.5 mmHg were excluded. In addition, experiments involving cognitive and functional tasks were excluded because blood flow to specific brain regions may be increased through neurovascular coupling. Furthermore, studies that involved dynamic changes in MAP and CBF (e.g., squat-stand manoeuvres, handgrip test or Valsalva manoeuvre), and/or CBF and MAP recordings less than 2 minutes after BP manipulation were excluded as they do not reflect a steady-state scenario. Only stable steady-state levels of MAP and CBF were included to evaluate the static CA.

3.2.2 Inclusion criteria

The methods for inducing BP changes can basically be divided into pharmacological-induced and postural manoeuvres-induced, but the optimal protocol for studying sCA remains undetermined and the advantages/disadvantages of different methods are still under debate. Postural manoeuvres, mainly achieved through tilting or changes in circulatory blood volume in the study of sCA, have the advantages of being non-invasive and more consistent with physiological conditions, but have limitations such as limited amplitude of BP changes and difficulty in controlling the magnitude and stability of induced changes. Using pharmacological agents to manipulate BP can better control the stability and duration of BP changes. Drugs such as phenylephrine for inducing hypertension or nitroprusside for inducing hypotension have been widely used in experiments evaluating sCA. However, pharmacological methods have limitations due to their invasive nature, and many drugs can activate the autonomic nervous system, potentially interfering with the changes in CBF produced.

To exclude the influence of normal MAP fluctuations on CBF and ensure a reasonable stimulus to activate autoregulation mechanisms, the minimum change in MAP (ΔMAP) was set to $\pm 5\%$ from baseline. Studies should include baseline measurements of CBF and MAP, as well as at least one stable step change in MAP to calculate the relative change slope. Experiments inducing BP changes by postural manoeuvres required stable recording of MAP and CBF/CBFv for at least 5 minutes to ensure that BP changes reached a stable state. Pharmacological agents used to induce BP changes have been confirmed not to have a direct effect on cerebral vasculature. Detailed descriptions of all blood pressure manipulation methods can be found in Table 3.1.

As shown in Figure 3.2, after exclusion criteria were applied, a total of 143 studies were included. Multiple experiments within a single study were considered separately, resulting in a total of 148 experiments. Of the 148 experiments, 104 only included baseline CBF and MAP values to explore the relationship between absolute CBF

and MAP. 39 studies (44 experiments) with MAP changes (27 experiments with MAP decrease and 17 experiments with MAP increase) were included to investigate the relationship between relative CBF and MAP.

Table 3.1: Summary of experimental methods and protocols for blood pressure changes. NS-15: Normal Saline-15, LPS: Lipopolysaccharide, SNP: Sodium Nitroprusside, ATP: Adenosine Triphosphate, NMMA: NG-monomethyl-L-arginine, HUT: Head-Up Tilt, HDT: Head-Down Tilt, LBNP: Lower Body Negative Pressure, LBPP: Lower Body Positive Pressure.

Methods	BP change	Description and Experimental Protocol	Record time	Number of studies
NS-15 infusion	decrease	15 ml · kg–1 of normal saline was administered. The ABP and CBFv waveforms were averaged for each 6-min measurement.	6 min	1
LPS injection	decrease	Purified lipopolysaccharide was administered as an intravenous bolus injection at a dose of 2 ng/kg body weight in 1 min. BP and CBFv were recorded continuously, starting 2 h before administration of LPS until 8 h after LPS administration.	1 hour	1
Phenylephrine	increase	An intravenous bolus injection of 150 μg Phenylephrine was administered with continuous recording. Data were recorded throughout a 10-min supine period.	10 min	10
SNP	decrease	An intravenous bolus injection of 100 μg sodium nitroprusside was administered with continuous recording. Data were recorded throughout a 10-min supine period.	10 min	5
ATP	decrease	The injection rate of ATP was 0.16 mg/kg/min which is a common dose used for myocardial perfusion studies. ATP injection was started 3 min before the start of emission scan and continued for 5 min. Emission scan was performed for 10 min.	10 min	1
NMMA	decrease	In a double-blind, placebo-controlled, cross-over design, each subject was randomised to receive either A: placebo (5% dextrose) or L-NMMA (B: 0.3 mg/kg, C: 1 mg/kg, D: 3 mg/kg) intravenously over 5 min on four different days separated by at least 1 week. CBFv and MAP were recorded every 5 min until 60 min after start of the L-NMMA/placebo infusion.	2 hours	2
Propofol	decrease	Drugs were administered after recording baseline data for 6 minutes after at least 30 minutes of rest. Propofol was infused at an dose of 2.0 mg/kg/h for 5 minutes. Drug administration data were recorded for 6 minutes.	6 min	1
Tilt	decrease	Each participant performed an orthostatic tilt test which involved resting for 5 min in the supineposition followed by 5 min in upright tilt at an angle of 70°.	5 min	2
HUT	decrease	The protocol consisted of 10 min of recording at rest in supine position followed by head-up tilt test. HUT was performed in a controlled environment, with subjects laying on the tilt table supported by two belts at the level of thigh and waist and with both feet touching the footrest of the table. The tilt table inclination was 60°. The maximum duration of the HUT session was 40 min.	5 min	6
HDT	increase	MAP and CBFv were obtained in the upright sitting posture during the 0.5h before head–down tilt. The subjects were then positioned horizontal supine on a gurney for 5 min and then transferred to 6° HDT on a tilted bed where they remained for the next 24h.	5 min	1
LBNP	decrease	The lower body negative pressure protocol began with a 5-min baseline period (0-mmHg LBNP) followed by a 5-min period with chamber pressures set at 15, 30, 45, and 60 mmHg. Continuous, non-invasive blood pressure and hemodynamic measurements were collected before and during the progressively stepwise LBNP protocol. MAP remained relatively constant during LBNP.	5 min	10
LBPP	increase	Participants lay supine in a custom-made LBPP box, sealed distal to the iliac crest. Following instrumentation and 20 min of supine rest, baseline values of all measures were recorded. All LBPP stages were 5 min in duration.	5 min	3
Cold stress	decrease	Cold stress test was achieved by the water-perfused suit. The total time of the trial was 60 min, consisting of three consecutive stages: baseline normothermic conditions (10 min with 33 °C water through the suit), mild cold stress (20 min with 25 °C water), and post-cold recovery (30 min with 33 °C water). Hemodynamic measurements were conducted continuously throughout the trial.	10 min	1
Gravity	increase	Exposure to each level of gravity was performed using a tilt chair or a centrifuge. Baseline data were collected for 6 min after 15 min of quiet rest in the centrifuge chair, following which the centrifugation was begun. Data collection at each level of hypergravity was performed for 6 min from 15 min after exposure.	6 min	1

DRAFT Printed on November 15, 2024

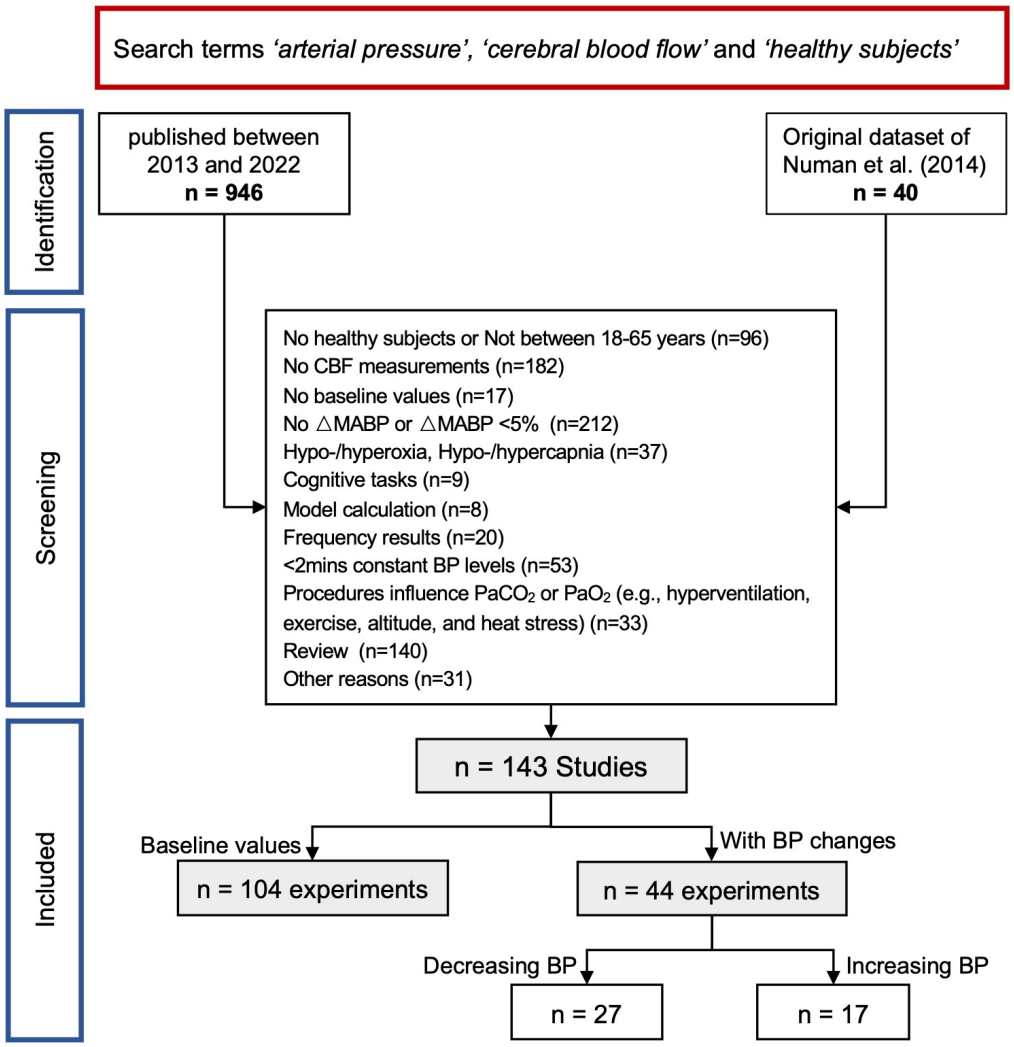


Figure 3.2: Flow chart of excluding procedure.

3.2.3 Pathological conditions

To explore the effect of different diseases on the cerebral pressure-flow relationship, we modified the search criteria on PubMed, Scopus, and Springer to search for studies with 'arterial pressure', 'cerebral blood flow' and 'cerebrovascular pathology' [e.g., ageing, hypertension, ischaemic stroke, haemorrhagic stroke and Alzheimer's disease] published between 1971 and 2022. Non-human experiments and non-English language studies were excluded. To eliminate the "physiological noise" caused by other CBF regulatory mechanisms, we replicated all the exclusion procedures mentioned in the previous section. However, it should be noted that there is limited research focusing specifically on changes in CA under pathological conditions. To

provide more information on the effects of diseases on CA, we also included studies that investigated dynamic CA under pathological conditions. 886 studies met the search criteria and were evaluated. As shown in Figure 3.3, 37 studies were included after the exclusion procedure.

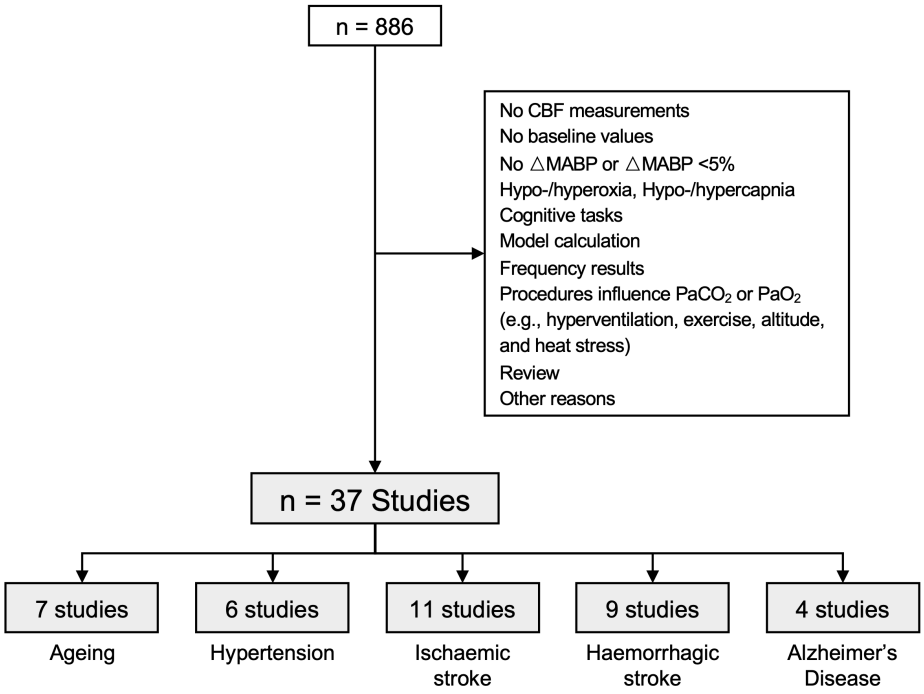


Figure 3.3: Flow chart of excluding procedure under different physiological and pathological conditions.

3.2.4 Analysis of data

Correction for CO_2

Although studies with induced hypercapnia or hypocapnia have been excluded, the effect of uncontrolled changes in $PaCO_2$ persisted in some of the included studies. To eliminate the effect of CO_2, CBF or CBFv measured in the middle cerebral artery will be recalculated for studies that report changes in $PaCO_2$. Considering the exclusion process, which limited the variation in $PaCO_2$ within 7.5mmHg for the included experiments, and the minor differences observed in the baseline $PaCO_2$ of the subjects ranging from 38-42mmHg, a simple linear correction method is justified. The correction factor used for cerebrovascular reactivity to $PaCO_2$ was 4%/mmHg

in hypercapnia and 3%/mmHg in hypocapnia [51]. Following the calculation of CO_2-corrected CBF, the CBF/MAP slope will be recalculated.

Statistical analysis

All statistical analyses were performed using SPSS (IBM SPSS Statistics Version 25.0) and presented as mean ± standard deviation. For each experiment, the relative changes in MAP and CBF from baseline was calculated. The slopes were calculated with linear regression between changes in %MAP and %CBF, and mmHg (MAP) and %CBF. The derived 'average slope line' was weighted to the number of subjects in each study. Specifically, each study slope line was multiplied by the sample size. These values were then summed and divided by the pooled sample size (total number of pooled subjects). The Shapiro-Wilk test was applied to verify the normal distribution for each variable. Differences between the slopes during increased or decreased MAP were evaluated using a Mann–Whitney U-test. We used p-values to determine if there was a statistically significant difference between the means of two groups, and used Cohen's d to measure the effect size and indicate how meaningful the relationship between variables or the difference between groups is. All p-values of <0.05 were considered statistically significant. Pearson's product-moment correlation coefficients were used to determine the correlation between the different variables. Based on our physiological understanding of autoregulation characteristics, we chose linear regression and a third-order polynomial function to fit the relationship between the absolute CBF and MAP to maximize goodness of fit. The Curve Fitting Toolbox in MATLAB was used for conducting regression analysis, while the fitting tool in SPSS was used for secondary validation.

3.3 Results

3.3.1 normal physiological conditions

From all the articles reviewed, 143 studies were included in this study. Experiments with changes in MAP (n = 44) were divided into decreasing MAP (n = 27) and

increasing MAP (n = 17) to investigate the directional sensitivity of CA. All experimental data were used to fit the autoregulation curve.

Methods for continuous arterial pressure measurement can vary among studies. Most studies recorded blood pressure non-invasively using photoplethysmography (Finapres). The Finapres device uses a finger cuff and provides an estimation of the continuous ABP waveform based on the principle of arterial volume clamping [170]. Other methods included auto-inflatable cuff (non-invasive) or intravascular catheters (invasive). Although there are various techniques for measuring CBF, over 90% studies used TCD to explore the cerebral pressure-flow response. Other methods included positron emission tomography and Kety Schmidt technique. The combination of TCD and photoplethysmography (Finapres) measurements was the primary choice for examining changes in CBF caused by BP alterations. In all included experiments, blood pressure was altered within a relatively limited extent (see Table 3.2 for details), varying only between 54 and 138 mmHg. Note that this range did not reach the upper limit of the classical autoregulation curve [154].

Table 3.2: Summary of the included studies on SCA. Mean age is averaged value or range. Slopes presented in % MAP/% CBF and mmHg MAP/% CBF. TCD, transcranial Doppler ultrasound. PET, positron emission tomography. HUT, head-up tilt. LBNP, lower body negative pressure. LBPP, lower body positive pressure. SNP, Sodium nitroprusside. ATP, Adenosine triphosphate, MCAv: middle cerebral artery velocity.

First Author	Year	BP direction	Method measure CBF(v)	Method measure BP	Method to change BP	Baseline BP (mmHg)	Baseline CBF	End BP	End CBF	Δ $PaCO_2$ (mmHg)	Correct MCAv	Number of subjects	Mean age subjects	Slopes (%/%)	Slopes (mmHg/%)	Ref.
Kurazumi	2022	increase	TCD	Radial artery	NS-15 infusion	79.0	67.3	86.0	72.1	-1.0	74.2	12	21	0.80	1.02	[171]
Pernice	2022	decrease	TCD	photoplethysmography	HUT	98.5	71.5	92.9	61.0	-	-	13	27	2.57	2.60	[172]
Bari	2022	decrease	TCD	Radial artery	HUT	99.3	47.9	68.9	37.1	0.0	37.1	13	27	0.73	0.74	[173]
Rosenberg	2021	decrease	TCD	photoplethysmography	LBNP	94.1	64.5	85.1	53.0	-6.1	63.7	52	26	1.86	1.98	[174]
Rosenberg	2021	decrease	TCD	photoplethysmography	LBNP	95.4	64.4	89.4	56.2	-3.7	63.3	19	27	2.02	2.12	[174]
Robertson	2020	decrease	TCD	volume-clamp method	Tilt	80.0	75.0	70.0	67.0	-2.0	69.9	13	21	0.85	1.07	[175]
Robertson	2020	decrease	TCD	volume-clamp method	Tilt	85.0	62.0	72.0	46.0	-3.0	50.6	14	22	1.69	1.99	[175]
Stok	2019	decrease	TCD	photoplethysmography	HUT	77.0	61.0	60.0	52.0	-4.0	58.8	22	40	0.67	0.87	[176]
Schlotman	2019	decrease	TCD	photoplethysmography	LBNP	94.0	67.7	83.0	51.5	-	-	107	29	2.04	2.18	[177]
Schlotman	2019	decrease	TCD	photoplethysmography	LBNP	92.0	75.4	81.0	60.3	-	-	85	27	1.67	1.82	[177]
Yoshida	2018	increase	TCD	photoplethysmography	LBPP	87.0	62.0	92.1	63.8	2.6	58.8	14	24	0.50	0.57	[178]
van Helmond	2018	decrease	TCD	brachial artery	LBNP	103.0	62.0	86.0	54.0	-1.0	55.9	10	32	0.78	0.76	[179]
van den Brule	2018	decrease	TCD	Radial artery	LPS injection	91.0	69.9	78.9	59.0	-	-	10	23.3	1.17	1.29	[180]
van der Scheer	2018	increase	TCD	upper-arm cuff	Cold stress	85.0	63.0	90.0	64.0	-	-	6	40	0.27	0.32	[180]
Bronzwaer	2017	decrease	TCD	photoplethysmography	LBNP	96.0	59.0	88.0	44.0	-5.0	53.2	14	56	3.05	3.18	[181]
Lund	2017	decrease	TCD	brachial artery	HUT	87.1	51.4	57.2	32.2	-	-	20	25	1.09	1.25	[182]
Bronzwaer	2017	decrease	TCD	plethysmography	HUT	95.0	70.0	76.0	60.0	-3.3	66.0	10	22	0.71	0.75	[183]
Ogawa	2016	decrease	TCD	Radial artery	Gravity	79.0	65.0	54.0	60.0	-2.0	63.8	10	23	0.24	0.31	[184]
Kay	2016	decrease	TCD	photoplethysmography	LBNP	96.5	61.4	88.1	44.1	-3.3	50.8	7	26	3.24	3.35	[185]
Rickards	2015	decrease	TCD	brachial artery	LBNP	94.0	70.0	86.0	61.5	-2.0	65.2	9	31	1.43	1.52	[186]
Perry	2014	increase	TCD	photoplethysmography	LBPP	83.7	62.0	93.0	59.7	-1.0	61.6	15	28	-0.33	-0.40	[187]
Del Pozzi	2014	increase	TCD	photoplethysmography	Phenylephrine	78.0	71.0	87.0	75.0	1.0	72.9	12	23	0.49	0.63	[188]
Shaw	2014	decrease	TCD	photoplethysmography	HUT	84.2	61.9	70.4	40.6	-2.5	45.2	15	26.3	2.10	2.49	[189]
Lewis	2014	decrease	TCD	photoplethysmography	LBNP	89.0	66.3	71.7	60.3	0.0	60.3	24	25	0.46	0.52	[190]
Perry	2013	increase	TCD	photoplethysmography	LBPP	81.0	74.0	94.0	72.0	0.0	72.0	15	26	-0.17	-0.21	[191]
Stewart	2013	increase	TCD	photoplethysmography	Phenylephrine	78.0	71.0	87.0	75.0	1.0	72.9	12	18-24	0.49	0.63	[55]

Continued on next page

DRAFT Printed on November 15, 2024

Table 3.2 Continued from previous page

First Author	Year	BP direction	Method measure CBF(v)	Method measure BP	Method to change BP	Baseline BP (mmHg)	Baseline CBF	End BP	End CBF	Δ $PaCO_2$ (mmHg)	Correct MCAv	Number of subjects	Mean age subjects	Slopes (%/%)	Slopes (mmHg/%)	Ref.
Schlader	2013	decrease	TCD	brachial artery	LBNP	89.0	59.6	71.7	45.2	-6.0	55.4	8	29	1.25	1.40	[192]
Stewart	2013	decrease	TCD	photoplethysmography	SNP	78.0	71.0	61.0	62.0	-3.0	67.8	12	18-24	0.58	0.75	[55]
Guo	2013	decrease	TCD	auto-inflatable cuff	SNP	80.7	67.8	75.6	62.7	-4.9	71.4	5	24	1.19	1.47	[193]
Chan	2011	decrease	TCD	Photoplethysmography	SNP	81.0	71.0	59.0	65.0	-	-	14	25	0.46	0.61	[194]
Chan	2011	increase	TCD	Photoplethysmography	Phenylephrine	83.0	75.0	101.0	80.0	-	-	14	25	0.30	0.37	[194]
Ogoh	2011	increase	TCD	Brachial Artery	Phenylephrine	77.0	50.0	97.0	52.0	1.5	48.9	8	26	0.15	0.20	[54]
Ogawa	2010	decrease	TCD	Radial artery	Propofol	77.0	63.0	70.0	58.0	0.0	58.0	10	22	0.87	1.13	[195]
Tzeng	2010	decrease	TCD	Photoplethysmography	SNP	84.0	70.0	63.0	58.0	-	-	10	26	0.69	0.82	[166]
Tzeng	2010	increase	TCD	Photoplethysmography	Phenylephrine	84.0	70.0	103.0	77.3	-	-	10	26	0.46	0.55	[166]
Brassard	2010	increase	TCD	Left brachial artery	Phenylephrine	84.0	66.6	108.0	70.5	0.8	68.9	9	23	0.22	0.29	[196]
Hussain	2009	decrease	PET	/	ATP	84.3	56.0	78.8	54.0	-	-	10	24	0.55	0.65	[197]
Zhang	2009	increase	TCD	Photoplethysmography	Phenylephrine	83.0	63.0	114.0	70.0	0.0	70.0	13	30	0.30	0.36	[151]
McCulloch	2005	increase	TCD	Radial artery	Phenylephrine	81.0	74.0	101.0	84.4	-	-	12	21–59	0.57	0.70	[198]
Lavi	2003	decrease	TCD	Tonometry	SNP	85.0	65.0	78.0	64.0	-	-	17	27	0.19	0.22	[199]
Hjorth Lassen	2003	increase	TCD	Sphygmomanometer	L-NMMA	80.2	71.5	95.8	73.0	0.0	73.0	6	25	0.14	0.18	[200]
McCulloch	2000	increase	TCD	Radial artery	Phenylephrine	80.0	59.9	101.0	68.9	-	-	8	22-52	0.57	0.72	[201]
Kawai	1993	increase	TCD	Sphygmomanometer	HDT	90.0	55.5	99.0	63.2	-	-	8	36	1.39	1.54	[202]
Jobes	1975	increase	Kr-uptake technique	Radial artery	Phenylephrine	88.0	38.9	120.0	49.5	0.0	49.5	8	/	0.75	0.85	[203]

DRAFT Printed on November 15, 2024

Relative CBF

For each experiment, the percent change from baseline was calculated for MAP and CBF. The slopes were calculated with linear regression between changes in %MAP and %CBF, and mmHg (MAP) and %CBF [68]. In the studies where MAP decreased, the calculated slopes were found to lie between 0.19 and 3.24%CBF/%MAP. The average slope for decreased MAP was 1.47 ± 0.71%CBF/%MAP (or 1.61 ± 0.73 %CBF/mmHg MAP). In the studies where MAP was increased, the slopes ranged between -0.33 and 1.39%CBF/%MAP with an average slope of 0.37 ± 0.38%CBF/%MAP (or 0.45 ± 0.45%CBF/mmHg MAP).

A significant difference in CBF/MAP slope was observed between increasing and decreasing MAP in both relative and absolute measures, as shown in Figure 3.4 (both $p < 0.001$; $d = 1.93$ for %CBF/%MAP comparison, and $d = 1.91$ for %CBF/mmHg MAP comparison), which is plotted in the same form as Numan et al. [68] for ease of comparison. 8 experiments in which MAP was decreased and 9 experiments in which MAP was increased had changes in MAP from baseline greater than 20%. 10 experiments in which MAP was decreased had changes in MAP between 5% and 10%, whereas 3 experiments that had increases in MAP showed a similar level of change. The remaining 9 included experiments in the decreasing MAP group and 5 remaining experiments in the increasing MAP group showed a percentage change in MAP between 10% and 20%.

CO_2 correction

18 experiments with decreasing MAP and 11 experiments with increasing MAP reported values for $PaCO_2$ (or partial pressure of end-tidal CO_2), which allowed for a post-hoc $PaCO_2$ correction for changes in CBF. After calculating the CO_2-corrected CBF, the CBF/MAP slopes were recalculated as described above. To quantify the influence of the CO_2 correction factor, the CBF/MAP slopes in these selected studies were also calculated prior to correction. Following correction, the slopes for the decreasing MAP range varied between -0.96 and 2.58 %CBF/%MAP (mean 1.11 ±

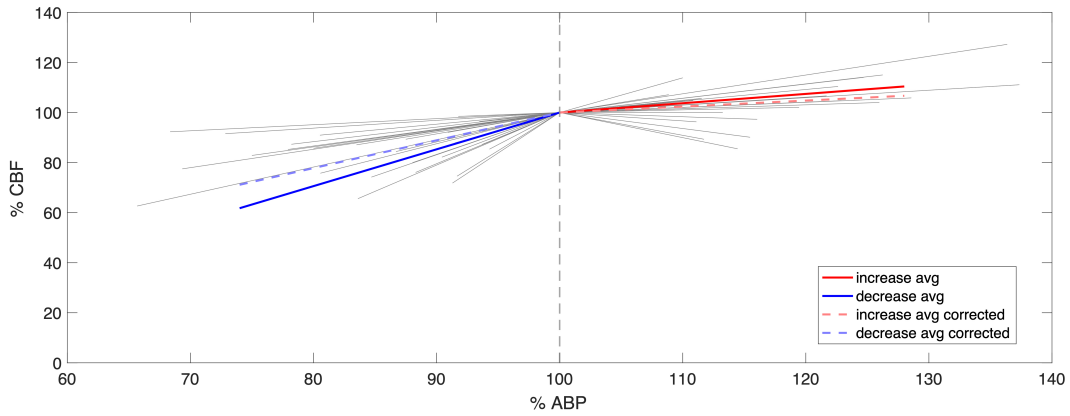


Figure 3.4: Relationship between %MAP and %CBF in the Increased MAP and Decreased MAP Ranges. All individual lines represent individual experiments (not corrected for CO_2); the length of the line indicates the range of MAP of that experiment. Before CO_2 correction, the average slope (solid line) was 1.47%MAP/%CBF for the decreased MAP (n = 27), and 0.35%MAP/%CBF for increased MAP (n = 17). After CO_2 correction, the average slope (dashed line) was 1.11%MAP/%CBF for decreasing MAP (n=18) and 0.24%MAP/%CBF for increasing MAP (n=11).

0.78%CBF/%MAP, 1.21 ± 0.65%CBF/mmHg MAP). The slopes in the increasing MAP range post correction varied between -0.41 and 1.39%CBF/%MAP (mean 0.24 ± 0.60%CBF/%MAP, 0.29 ± 0.50%CBF/mmHg MAP). Consistent with the uncorrected slope results, the corrected slopes also showed significant differences in the range of increasing and decreasing MAP ($p = 0.003$; $d = 1.25$), as shown by the dashed lines in Figure 3. In addition, the CO_2 correction had a significantly greater effect on experiments with decreasing MAP than on experiments with increasing MAP due to the different sensitivity to CO_2 in each direction.

Manipulation and measurement methods

The CBF measurement methods used in different studies were varied. Of the 44 experiments included in this analysis with MAP changes, 42 used TCD. The slope produced by measuring CBF with methods other than TCD was 0.55 %CBF/%MAP (MAP decreased) and 0.75 %CBF/%MAP (MAP increased), while the average slope measured using TCD was 1.49 ± 0.71%CBF/%MAP (MAP decreased) and 0.35 ± 0.38%CBF/%MAP (MAP increased). Since only 2 experiments used non-TCD methods to study CA, it is not yet known whether different CBF measurement

methods lead to differences in slopes.

Of the 17 experiments that increased MAP, the most frequently used experimental method to manipulate blood pressure was phenylephrine (pharmacological). 5 experiments using non-pharmacological BP manipulation methods yielded mean slopes of 0.21 ± 0.58%CBF/%MAP, while 12 experiments using pharmacological BP manipulation methods yielded mean slopes of 0.45 ± 0.20%CBF/%MAP. Significant differences were found with %CBF/%MAP between the different BP increasing manipulation methods ($p < 0.001$; $d = 0.55$). Of the 27 experiments that decreased MAP, the most frequently used experimental method to manipulate blood pressure was lower body negative pressure (LBNP, non-pharmacological). 19 experiments using non-pharmacological BP manipulation methods yielded mean slopes of 1.63 ± 0.65%CBF/%MAP, while mean slopes with pharmacological BP manipulation methods were 0.63 ± 0.32%CBF/%MAP. Significant differences were found with %CBF/%MAP between the different BP decreasing manipulation methods ($p < 0.001$; $d = 1.95$).

The statistical differences observed between pharmacological and non-pharmacological BP manipulation methods indicated that different methods have different levels of reproducibility and stability. Regardless of whether the experiment induced an increase or decrease in MAP, a tighter slope distribution was observed for pharmacological manipulation methods, indicating higher reproducibility as shown in Figure 3.5. However, studies of dCA have also shown that manoeuvres such as the sit-to-stand are biologically acceptable and reproducible for creating oscillations in blood pressure, and are thus most representative when compared to other techniques [204, 205]. This suggested that using drugs to induce BP changes has an advantage in longer time-scale sCA studies, whereas postural changes to induce BP changes are more advantageous in shorter time-scale dCA studies. It should also be noted that any pharmacological approach has the inherent limitation that the drugs may have multiple unknown effects on the cerebral vasculature. Therefore, when choosing

a BP manipulation method, it is important to evaluate and choose based on the specific research design and purpose.

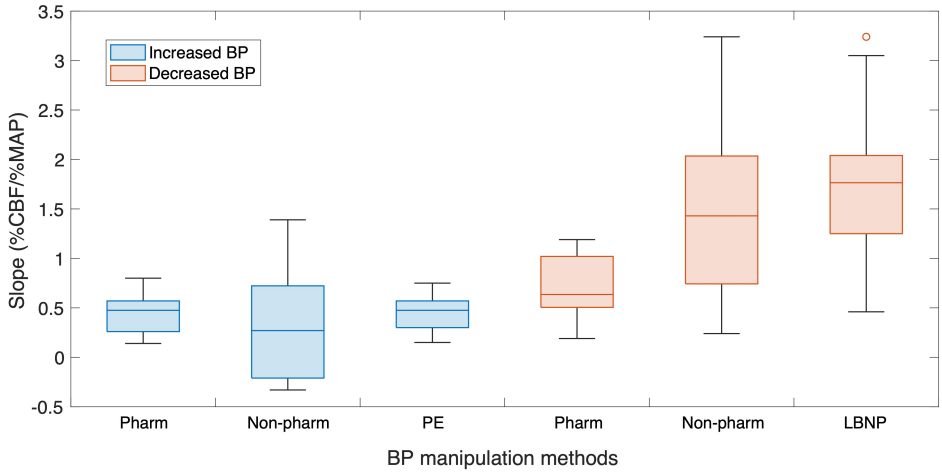


Figure 3.5: Slope distribution of different blood pressure manipulation methods. Experiments inducing BP increase are represented by blue boxplots, while experiments inducing BP decrease are represented by orange boxplots. Non-pharm, non-pharmacological BP manipulation methods; Pharm, pharmacological BP manipulation methods; PE, phenylephrine; LBNP, lower body negative pressure.

Absolute CBF

Although direct comparison of absolute CBF (or velocity) changes between measurement techniques is not possible, over 90% of all experiments included in this study used CBFv (MCAv) as an indicator of CBF measured by TCD. To obtain sufficient experimental data to fit the absolute cerebral pressure-flow relationship, we hypothesized that CBFv (MCAv) could be used as a surrogate CBF measure. The limitations of this assumption will be discussed later.

A significant positive correlation was observed between MAP and absolute CBFv ($r = 0.363$; $p < 0.001$), as shown in Figure 3.6. MAP varied between 53 and 138 mmHg but did not reach the upper limit of autoregulation proposed by Lassen.

Compared to the first-order linear model, the fit quality of the third-order polynomial function was improved (first order: $R^2 = 0.1320$ vs. third order: $R^2 = 0.1341$), although this would be expected given the additional degrees of freedom. A relatively flat 'autoregulatory plateau' was observed from the third-order polynomial model,

as shown in Figure 3.7. After differentiation of the function, we found that CBF remained essentially stable when MAP varied between 80 and 100 mmHg. To further quantify this behaviour, the correlations between MAP and CBF were recalculated over different blood pressure ranges, as indicated in Supplemental Figure S4. If the relationship between pressure and flow is purely passive, the correlation coefficients should increase monotonically or remain essentially constant. However, the correlation between blood pressure and flow was first found to increase, then to decrease and then to increase again, with the two turning points being observed at 80 and 100 mmHg, as shown by the shaded area in Supplemental Figure S4. This indicates that this range of MAP appears to act as the 'plateau' region for static cerebral autoregulation, supporting the claims that this region is a relatively small one.

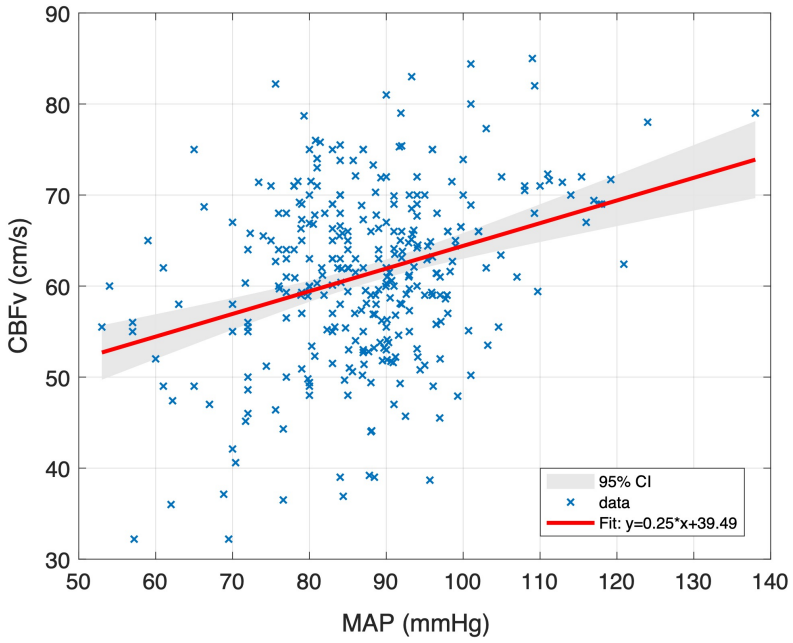


Figure 3.6: First-order linear regression model for MAP and CBFv. The grey shading between these bounds reflects the 95% confidence level.

To better understand the relationship between MAP and CBF, correlation and linear regressions were further performed according to data points below 80 mm Hg, 80 to 100 mm Hg, and above 100 mm Hg. This segmentation also ensured that sufficient experimental data were available for analysis in each blood pressure range.

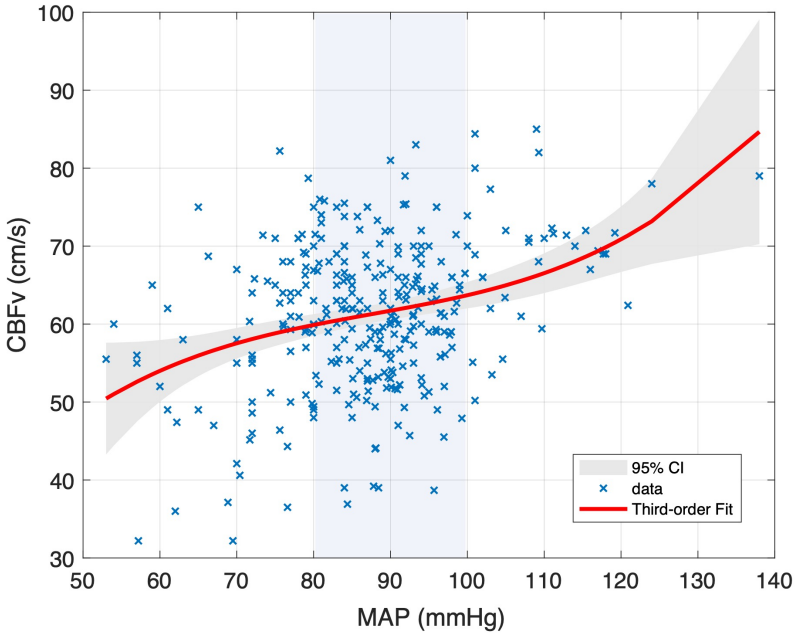


Figure 3.7: Third-order polynomial function regression model for MAP and CBFv. The grey shading between these bounds reflects the 95% confidence level. The blue shading between 80-100 mmHg reflects the autoregulatory plateau.

In the MAP range of 80 to 100 mmHg, the correlation coefficient between MAP and CBF was only 0.003 ($p = 0.952$), indicating that the CBF was largely unaffected by MAP and showed significant autoregulatory characteristics. However, it is worth noting that within this range, the linear regression analysis between MAP and CBF still demonstrated a small slope instead of a horizontal line with zero slope. For experimental data in the MAP range below 80 mmHg or above 100 mmHg, the correlation coefficients between MAP and CBF were found to be 0.359 and 0.332, respectively ($p = 0.001$, $p = 0.068$). This suggests that when MAP exceeds 100 mmHg or is lower than 80 mmHg, autoregulation mechanisms are no longer able to maintain CBF stability, and CBF will increase with increasing blood pressure. The slope of the linear regression analysis for the different blood pressure ranges showed that CBF was more sensitive to BP decrease than BP increase (0.515 for BP range below 80 mmHg; 0.301 for BP range above 100 mmHg;), which was consistent with the results of the relative analysis.

The Influence of Age

Age and biological sex remain important modifiers of cerebrovascular function in health and disease, but their impact on cerebral blood pressure and flow remains unclear. In this review, 91 experiments reported mean age for subjects and 67 experiments reported haemodynamic related data by sex, which allowed us to explore the effect of sex and age on cerebrovascular and autoregulation.

There were significant differences in baseline vascular measures between young (18–40 years old; number of subjects = 2854; mean age = 28) and older (40–65 years old; number of subjects = 1341; mean age = 50) participants. At baseline, MAP was significantly higher in older participants (young: 88.08 ± 6.72 mmHg vs. older: 90.96 ± 3.72 mmHg). MCAv was 10.2% lower in older participants (young: 63.20 ± 7.45 cm/s vs. older: 56.78 ± 6.14 cm/s).

To further explore the correlation between age and baseline blood pressure, a regression analysis was performed (see Supplemental Figure S4). The results showed that there was a statistically significant positive correlation between age and baseline MAP, i.e., as age increased, baseline MAP also increased ($r = 0.198$). The linear relationship established between the independent variable age and the dependent variable MAP at baseline was extremely statistically significant, but the goodness of fit for the regression was poor ($R^2 = 0.038$; $p = 0.009$). A statistically significant negative linear correlation was also found between baseline CBF and age (see Supplemental Figure S5), whereby baseline CBF decreased with increasing age ($r = -0.101$; $p < 0.001$). However, the goodness of fit for the regression was poor ($R^2 = 0.131$).

Both the Pearson correlation coefficient and regression analysis outputs showed there was no relationship between age and absolute and relative slopes ($r = 0.009$). No age differences were observed in the cerebral haemodynamic response to changes in pressure suggesting that ageing itself did not alter cerebral autoregulation, in good agreement with the substantial literature on the effect of ageing on dynamic CA [3, 99, 102].

The Influence of Sex

17 experiments included only male subjects and 3 experiments included only female subjects, which allowed us to examine sex differences in CBF autoregulation. There were no significant differences in the demographic and haemodynamic characteristics of study participants at baseline between biological sex categories. No sex differences were found for age (male: 26 ± 4 years vs. female: 27 ± 5 years; $p = 0.776$; $d = 0.22$). Although the results were consistent with previous studies in that female subjects had a lower mean BP and a higher CBF than males [206], no statistically significant gender differences were found (MAP: male = 88.48 ± 6.74 mmHg vs. female = 87.77 ± 6.19 mmHg; $p = 0.583$; $d = 0.11$. CBF: male = 60.11 ± 7.58 cm/s vs. female = 63.34 ± 11.14 cm/s; $p = 0.070$; $d = 0.34$). Pearson correlation coefficients also confirmed that sex was not associated with baseline MAP or CBF ($r = 0.045$; $r = -0.056$, respectively).

Since there were no experiments conducted solely on female participants to induce an increase in MAP, it is unclear whether the slope of increased BP is influenced by gender. In experiments inducing a decrease in MAP, 17 studies included only male participants while 3 studies included only female participants. In the male group, the slopes for the decreasing MAP ranged from 0.15 to 2.04 %CBF/%MAP (mean 1.29 ± 0.69 %CBF/%MAP, 1.42 ± 0.71 %CBF/mmHg MAP). In the female group, the slopes for the decreasing MAP ranged from 0.85 to 1.69%CBF/%MAP (mean 1.58 ± 0.26%CBF/%MAP, 1.75 ± 0.26%CBF/mmHg MAP). No significant difference in CBF/MAP slope was observed between female and male in both relative and absolute measures ($p = 0.382$ for %CBF/%MAP comparison, $p = 0.371$ for %CBF/mmHg MAP comparison). Therefore, the study results indicated that the cerebrovascular response to decrease in BP has no sex differences, although given the small number of studies performed in women this finding should be treated with caution at this stage.

3.3.2 Pathological conditions

37 studies meeting the inclusion criteria were summarized in Table 3.3 and Table 3.4. Multiple experiments included in a single study were separately taken into account. For each experiment, the percent change from baseline was calculated for MAP and CBF to standardize studies using different measurement approaches. The slopes were calculated with linear regression between changes in %MAP and %CBF, and mmHg (MAP) and %CBF.

Table 3.3: Static autoregulation experiments under different physiological and pathological conditions. Slopes presented in % MAP/% CBF and mmHg MAP/% CBF. TCD, transcranial Doppler. HUT, head-up tilt. PET, positron emission tomography.

Conditions	First Author	Year	Method measure CBF	Method measure BP	Method to change BP	Baseline BP (mmHg)	Baseline CBF	End BP	End CBF	Number of subjects	Mean age subjects	Slopes (%/%)	Slopes (mmHg/%)	Ref.
Ageing	Wollner	1979	133Xe-injection	Roche Arteriosonde	tilt	93.5	-	77.25	-	4	79.25	0.21	0.22	[207]
	Robertson	2014	TCD	photoplethysmography	supine to sit	101	58	76	49	12	76	0.63	0.62	[208]
	Connen	1988	133Xe inhalation	photoplethysmography	clonidine	122.67	64.54	106	55.93	21	61	0.98	0.80	[209]
	Strandgaard	1976	A-VO2 differences	arterial catheter	trimethaphan infusion and HUT	145	-	113	-	13	52	1.18	0.81	[210]
Hypertension	Novak	2010	TCD	photoplethysmography	tilt	84.1	36.4	110.0	51.8	43	64.2	1.38	1.64	[211]
	Eames	2004	TCD	photoplethysmography	bendrofluazide	105.0	44.8	101.0	42.5	18	76.1	1.38	1.31	[212]
	Georgiadis	2002	TCD	photoplethysmography	norepinephrine infusion	74.3	39.8	98.1	43.2	8	53.5	0.27	0.36	[213]
	Schwarz	2002b	TCD	photoplethysmography	tilt	90.0	61.4	82.7	57.5	18	61.2	0.78	0.87	[214]
	Schwarz	2002b	TCD	photoplethysmography	norepinephrine infusion	90.0	61.4	76.1	53.7	18	59.1	0.81	0.90	[214]
Ischaemic stroke	Ouchi	2001	PET	brachial artery catheter	supine to sitting	109.9	-	106.1	-	22	61.2	1.20	1.09	[215]
	Olsen	1983	133Xe-injection	arterial catheter	infusion of angiotensine	104.9	30.6	138.5	46.0	6	61.4	0.69	0.42	[216]
	Meyer	1973	A-VO2 differences	arterial catheter	head-up tilting	108.6	33.7	84.7	29.6	32	33.7	0.55	0.51	[118]
	Meyer	1973	A-VO2 differences	arterial catheter	head-down tilting	101.9	33.1	115.7	34.1	32	34.1	0.22	0.22	[118]
Haemorrhagic stroke	Ezra	2020	TCD	radial artery	sodium nitrite infusion	75.5	62.4	71.1	60.3	10	52.3	0.58	0.76	[217]
	Diringer	2017	PET	unknown	phenylephrine	110.8	43	136.7	44	13	60	0.42	0.37	[218]
	Gould	2013	CTP CBF	unknown	systolic BP reduction	116	39.17	100	36.88	16	39.17	0.28	0.27	[219]
	Manno	1998	TCD	photoplethysmography	phenylephrine	90	38.4	111	39.3	13	59	0.10	0.11	[220]
	Darby	1994	133Xe inhalation	unknown	dopamine	90	-	-	39.3	13	59	0.10	0.11	[132]
	Muizelaar	1986	133Xe inhalation	arterial cannula	phenylephrine	101.5	42.6	134	33.3	4	44.25	2.07	1.76	[221]
	Pickard	1980	133Xe inhalation	arterial cannula	halothane	84	43	51	22.5	10	43	1.21	1.14	[222]
AD	Simard	1971	133Xe-injection	arterial catheter	infusion of angiotensin II	42	-	-	-	8	61	0.40	-	[139]

DRAFT Printed on November 15, 2024

Table 3.4: Dynamic autoregulation experiments under different physiological and pathological conditions. Slopes presented in % MAP/% CBF and mmHg MAP/% CBF. TD-rCBF, thermal diffusion-regional CBF.

Conditions	First Author	Year	Method measure CBF(v)	Method measure BP	Method to change BP	Baseline BP (mmHg)	Baseline CBF	End BP	End CBF	Number of subjects	Mean age subjects	Slopes (%/%)	Slopes (mmHg/%)	Ref.
Ageing	Oudegeest-Sander	2013	TCD	photoplethysmography	squat to stand	96	50.5	61	39.2	20	66	0.61	0.64	[223]
	Oudegeest-Sander	2013	TCD	photoplethysmography	squat to stand	102	46	69	33.3	18	78	0.85	0.84	[223]
	Fisher	2008	TCD	photoplethysmography	moderate-intensity leg cycling	80.9	41.5	95.5	46.5	27	76	0.67	0.83	[224]
	Serrador	2005	TCD	photoplethysmography	sitting to standing	95	64	118	68	10	57	0.26	0.27	[107]
	Sorond	2005	TCD	photoplethysmography	sitting to standing	89	35	64	29	21	70	0.61	0.69	[225]
	Lipsitz	2000	TCD	photoplethysmography	sitting to standing	85	50	59	41	13	73	0.59	0.69	[101]
	Lipsitz	2000	TCD	photoplethysmography	sitting to standing	87.2	42.1	66.2	30.2	10	72	1.17	1.35	[101]
Hypertension	Serrador	2005	TCD	photoplethysmography	sitting to standing	93	32	71	29	20	72	0.40	0.43	[107]
	Serrador	2005	TCD	photoplethysmography	sitting to standing	107	37	86	33	18	74	0.55	0.51	[107]
	Traon	2002	TCD	photoplethysmography	standing up	116	34.7	90.1	30	21	48.9	0.62	-	[108]
	Lipsitz	2000	TCD	photoplethysmography	sitting to standing	87	-	90	-	10	72	0.61	0.52	[101]
Ischaemic stroke	Salinet	2014	TCD	photoplethysmography	elbow passive flexion and extension	91.9	47.5	94.1	49.7	15	62.4	1.98	2.16	[119]
	Immink	2005	TCD	photoplethysmography	spontaneous oscillations	-	-	-	-	20	61	0.79	-	[226]
	Gierthmuhlen	2011	TCD	photoplethysmography	leg-cuff test	-	-	-	-	17	54.5	0.82	-	[227]
Haemorrhage stroke	Budohosky	2013	TCD	photoplethysmography	spontaneous oscillations	100	-	125	-	66	54	0.8	0.80	[228]
	Budohosky	2013	TCD	photoplethysmography	spontaneous oscillations	100	-	75	-	66	54	1.12	1.12	[228]
	Muench	2005	TD-rCBF	radial artery	positive end-expiratory pressure	96.4	34.3	82.2	23.5	10	53	2.13	2.21	[229]
AD	Van beek	2012	TCD	photoplethysmography	sit-stand manoeuvres	87.6	37.7	104.8	43.5	15	72.3	0.79	0.90	[143]
	Van beek	2010	TCD	photoplethysmography	sit-stand manoeuvres	87.9	34.4	75.6	30.1	21	72.9	0.89	1.01	[66]
	Claassen	2009	TCD	photoplethysmography	spontaneous oscillations	98	38	59	26	9	67.9	0.79	0.81	[137]

DRAFT Printed on November 15, 2024

The fluctuations in blood pressure currently used to calculate the cerebral pressure-flow slope were induced mainly by changes in posture, e.g., from sit to stand or squat to stand, thus simulating blood pressure changes as they occur in daily life. All experiments of autoregulation in patients with chronic hypertension induced a fall in blood pressure by postural changes or drugs. The reason why no experiments were found to increase blood pressure may be because it is dangerous for hypertensive patients to re-increase their blood pressure. Experiments using vasoactive drugs to study cerebral autoregulation in AD were excluded due to the fact that these drugs (e.g. nicardipine) have a direct effect on CBF. It has been demonstrated that nicardipine reduces blood pressure without reducing CBF in patients with established cerebrovascular disease and a high probability of impaired autoregulation [230]. Therefore, the observed stability of CBF during the reduction in blood pressure in some experiments was at least partly due to direct cerebral vasodilation mediated by nicardipine. Phenylephrine and dopamine are vasoactive amines that cannot cross the blood-brain barrier. Therefore, the direct effects of phenylephrine or dopamine on the cerebral vasculature are negligible [231].

Ageing, hypertension, stroke, and dementia all had significant impacts on the arterial blood pressure and cerebral blood flow, compared with data obtained from healthy individuals in previous studies, as shown in Figure 3.8. Hypertensive patients had the highest MAP and the lowest mean CBFv, while stroke patients had the lowest CBF. The decline in global CBF has been shown by different CBF measurements, including Xenon-133, single photon emission computed tomography (SPECT), positron emission tomography (PET), TCD, extracranial ultrasound, and arterial spin labelling (ASL) MRI. The reasons for these changes are not yet clear but may be associated with several mechanisms including changes in vascular elasticity, the development of atherosclerosis, damage to small blood vessels in the brain, and alterations in the autonomic nervous system.

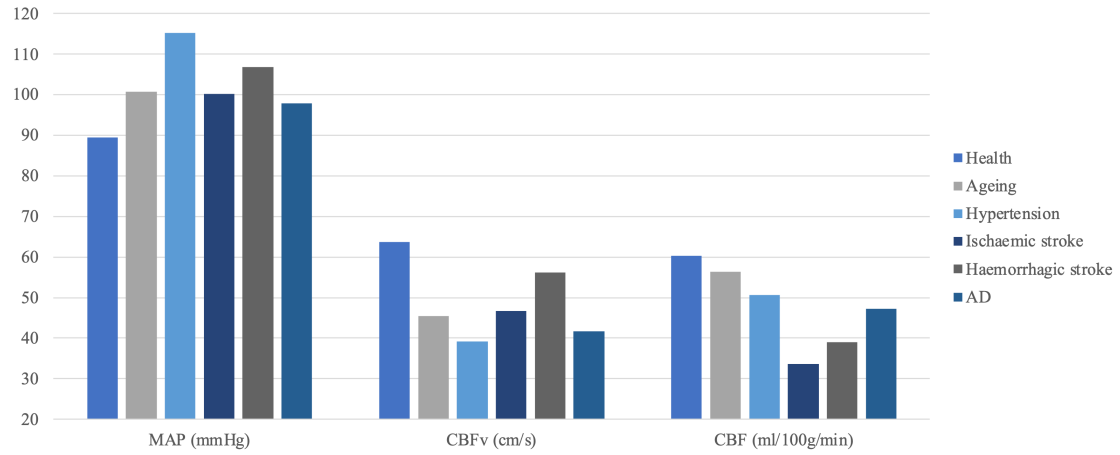


Figure 3.8: MAP, CBFv and CBF under different physiological and pathological conditions.

Static autoregulation

Details of descriptive statistics of the slopes under different physiological and pathological conditions on static autoregulation were shown in Table 3.5, while comparison was presented in Figure 3.9. Different studies used different CBF measurement methods, such as 133Xe injection, TCD and PET. Despite the use of different BP manipulations and CBF measurement techniques, no significant differences in slope were found.

Table 3.5: Description statistics of slopes (%CBF/%MABP) under different physiological and pathological conditions on dynamic autoregulation. N indicates number of experiments. The p-value is the difference in slope compared to healthy subjects and <0.05 was considered statistically significant.

Conditions	N	Decreased MAP slope	p-value	N	Increased MAP slope	p-value
Ageing	1	0.21	-	-	-	-
Chronic hypertension	3	0.95 ± 0.21	0.945	-	-	-
Ischaemic stroke	5	0.90 ± 0.31	0.486	5	0.81 ± 0.52	**0.044**
Haemorrhagic stroke	4	0.97 ± 0.29	0.641	3	0.50 ± 0.56	0.629
Alzheimer's Disease	1	0.40	-	-	-	-

Compared with healthy subjects, there were no significant differences in the static and dynamic cerebral blood flow-pressure relationships in older adults. Furthermore, the slope of dynamic autoregulation was higher than that of static autoregulation,

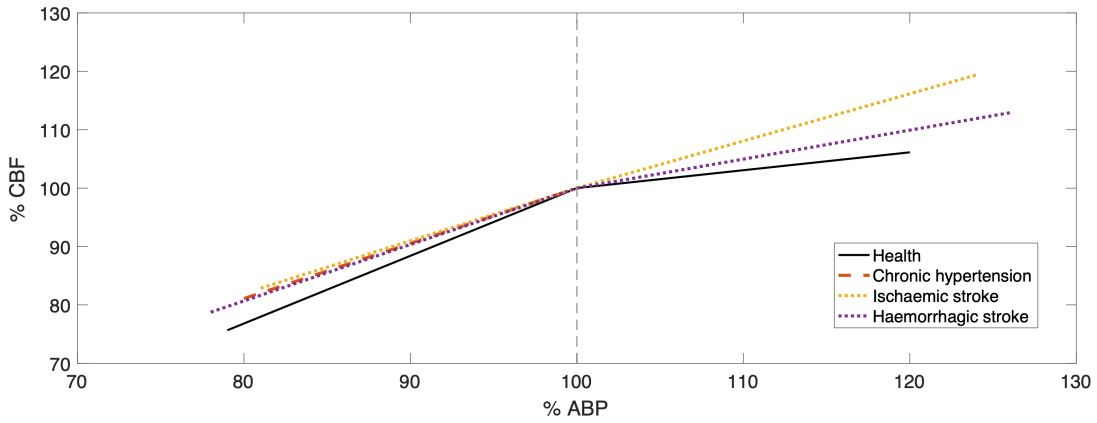


Figure 3.9: Relationship between %MAP and %CBF in the increased MAP and decreased MAP ranges under different conditions of static autoregulation. The length of the line indicates the range of MAP of that experiment. Since only one experimental data met the inclusion criteria in the ageing and AD conditions, they were not included for comparison.

indicating that older adults have a higher variability in CBF response to rapid BP changes, consistent with previous findings in healthy subjects that CBF buffering capacity was largely dependent on the rate of change in BP [232]. Additionally, in static autoregulation, stronger autoregulatory responses were observed during periods of BP elevation compared to BP reduction, which is consistent with results from studies on healthy subjects [68]. While this study confirmed the presence of age-related increases in MAP and decreases in CBF, the relative changes in CBF in response to BP change were similar compared with younger healthy subjects, suggesting preserved autoregulation with ageing.

The absence of statistically significant differences between healthy subjects and hypertensive patients indicated that patients with chronic hypertension retained the ability to maintain CBF in the face of acute changes in perfusion pressure, in line with previous studies [107, 108]. A statistically significant difference was observed between ischaemic stroke patients and healthy controls for increase MAP, suggested that the cerebral pressure-flow relationship was altered after ischaemic stroke. Although no statistical difference was observed, we found that haemorrhagic stroke patients had a steeper slope when BP increased, indicating that CBF became more sensitive to changes in blood pressure. During decreased MAP, stroke had

no significant effect on static autoregulatory capacity. In addition, the significant difference in slope observed in healthy subjects between increasing and decreasing MAP disappeared in both haemorrhagic and ischaemic stroke patients.

Dynamic autoregulation

Details of descriptive statistics of the slopes under different physiological and pathological conditions on dCA were shown in Table 3.6, while comparison was presented in Figure 3.14. A statistically significant difference was observed only between haemorrhagic stroke patients and healthy controls during decreased MAP. Our findings are consistent with most studies that the cerebral pressure-flow relationship is altered following SAH or intracranial haemorrhage (ICH), indicating impaired autoregulation. No significant effect was observed on dynamic autoregulation under other conditions. Although our results found no evidence of impaired autoregulation in AD patients, in two experiments with healthy, age-matched controls, we found that the slopes of dynamic autoregulation were significantly higher in AD patients than in controls (AD: 0.86 %CBF/%MAP vs. Control: 0.53 %CBF/%MAP). This suggested that CBF was more sensitive to changes in blood pressure, indicating reduced efficiency of CBF in regulating blood pressure fluctuations in AD. In addition, consistent with the results of dynamic autoregulation in healthy subjects, no significant differences were observed between increasing and decreasing MAP in CBF/MAP slopes in all conditions, in both relative and absolute measures.

Table 3.6: Description statistics of slopes (%CBF/%MABP) under different physiological and pathological conditions on dynamic autoregulation. N indicates number of experiments. The p-value is the difference in slope compared to healthy subjects and <0.05 was considered statistically significant.

Conditions	N	Decreased MAP slope	p-value	N	Increased MAP slope	p-value
Ageing	5	0.73 ± 0.19	0.524	2	0.56 ± 0.18	0.758
Chronic hypertension	4	0.54 ± 0.09	0.274	-	-	-
Ischaemic stroke	2	0.78 ± 0.40	0.731	2	1.30 ± 0.60	0.485
Haemorrhagic stroke	2	2.13 ± 0.13	**0.028**	1	0.80	-
Alzheimer's Disease	2	0.86	-	1	0.79	-

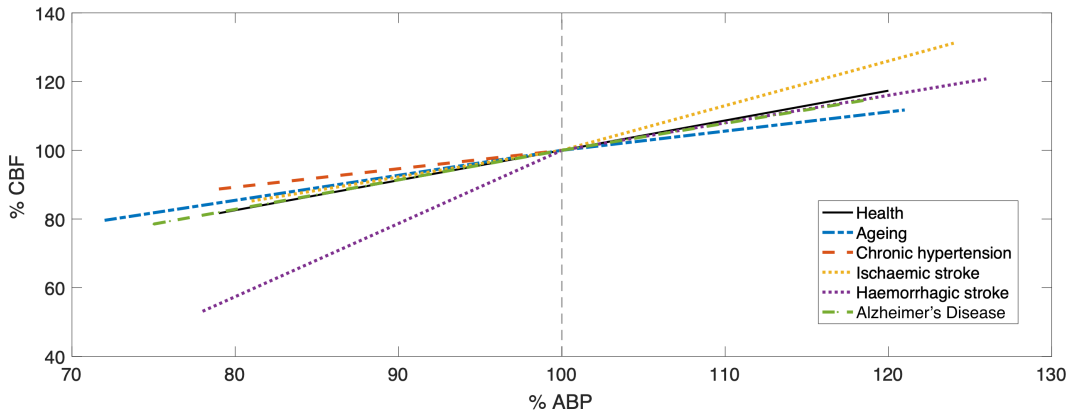


Figure 3.10: Relationship between %MAP and %CBF in the increased MAP and decreased MAP ranges under different conditions of dynamic autoregulation. The length of the line indicates the range of MAP of that experiment.

3.4 Discussion

3.4.1 Directional sensitivity of cerebral autoregulation

A stronger autoregulatory response was observed during the increase in blood pressure compared to the decrease in sCA, consistent with former studies and findings in dCA [29, 68, 164–166, 233]. However, our findings differ from those of Numan et al. [68] in that this asymmetry in autoregulation did not disappear after CO_2 correction. Compared to 2014, we have employed stricter exclusion criteria to eliminate interference from some dCA study results, thus confirming the presence of directional sensitivity in static CA. Although CBF remained more sensitive to blood pressure reduction after CO_2 correction, the CO_2 correction eliminated the significant difference in CBF response to increased and decreased MAP (the CBF to changes in ABP were found to be $1.47 \pm 0.71\%/\%$ for decreased ABP and $0.37 \pm 0.38\%/\%$ for increased ABP, which were altered to $1.11 \pm 0.78\%/\%$ and $0.24 \pm 0.60\%/\%$ after CO_2 correction). The greater effect of CO_2 correction on CBF regulation for reduced MAP may be related to the activation of metabolic pathways during hypoperfusion.

It should be noted that a positive correlation between changes in blood gas levels and the capacity of autoregulation was observed both before and after CO_2 correction.

A larger magnitude of $PaCO_2$ variations was associated with an increased slope of %CBF/%MAP. This finding suggests that different CBF regulatory mechanisms do not operate in isolation, as metabolic pathways can influence autoregulation. The interdependence of CBF regulation highlights the robustness of the cerebrovascular system in ensuring precise control of CBF, while also emphasizing the challenges in isolating and studying specific CBF regulatory mechanisms.

Several potential mechanisms have been proposed to explain the directional sensitivity of CA, including selective cerebral vasoconstriction secondary to activation of the perivascular cerebral sympathetic nerves, as well as intrinsic differences in myogenic responses to falling and rising MAP [166]. Another possible explanation might be that compensatory vasodilatation during MAP decrease may increase intracranial pressure, aggravating MAP decrease and reducing the benefit of lowered blood flow resistance [234]. Previous studies have shown that a substantial MAP change of approximately 50% from baseline is required to trigger sympathetic nervous system activation [235]. However, our research findings suggest that directional sensitivity of CA is independent of the magnitude of MAP changes, consistent with the findings of Panerai et al. [236] regarding dynamic CA. The activation of cerebral sympathetic nerve activity alone is therefore insufficient to explain this phenomenon. Directional sensitivity is more likely determined by the intrinsic properties of vascular smooth muscle cells, which serves to protect the brain from the risk of hyperperfusion during MAP increases and subsequently prevent oedema and capillary damage.

Although the physiological mechanisms of autoregulatory asymmetry remain unclear and part of the explanation is based on evidence from animal studies, the finding of autoregulatory asymmetry has clinical implications. The differential CA response between increasing and decreasing MAP in humans was initially reported in patients with traumatic brain injury [233], suggesting that directional sensitivity may be enhanced in pathological conditions. This indicates the potential for quantifying CA directional sensitivity as a clinical indicator for predicting cerebral diseases. Given

the brain heterogeneity and the significant individual variability in autoregulation, further research and clinical trials are needed to make CA assessment a reliable clinical tool.

3.4.2 The impact of disease on CA

With the increasing ageing population and the rising incidence of hypertension, stroke, and dementia, it is crucial to enhance our understanding of cerebral blood flow regulation in both health and disease. We quantitatively investigated dynamic and static autoregulation by reviewing literature on different physiological and pathological conditions and found that autoregulation was altered in stroke and AD patients compared to healthy subjects, suggesting impaired autoregulation. The more passive cerebral pressure-flow relationship in these patients indicates a decreased ability to resist changes in blood pressure, highlighting the need for real-time monitoring and blood pressure management to reduce the risk of haemorrhage.

Although experimental data are limited, and we used a simple linear regression method to calculate the relative changes in cerebral blood flow when blood pressure changes, the consistency shown by studies using different blood pressure manipulations and evaluation methods suggested that the relative changes in cerebral pressure and blood flow velocity have clinical significance in predicting disease such as stroke and Alzheimer's disease. This analysis provided a simplified approach to quantitative analysis of autoregulation that can be easily updated as more experimental data become available.

However, it should be noted that distinguishing the effects of normal ageing and disease regulation on CBF regulation is difficult due to the presence of many confounding factors. Vascular risk factors such as hypertension, diabetes, dyslipidaemia or congestive heart failure are more common in the elderly. In addition, the incidence of neurodegenerative diseases such as Alzheimer's disease, vascular dementia and mixed dementia also increases sharply with ageing [237]. As these diseases remain asymptomatic in their early stages and thus are difficult

to identify clinically, some studies may have unknowingly included older subjects with reduced CBF caused by neurodegenerative diseases. It is necessary to conduct further experiments that can disentangle age-related vascular risk factors from normal ageing to gain a better understanding of the mechanisms underlying various cerebrovascular disorders.

Overall, an in-depth investigation of changes in cerebral autoregulation under various physiological and pathological conditions has the potential to enhance the prevention and treatment of CBF dysregulation and related brain disorders. This can be achieved by providing real-time information to clinicians about the patient's cerebral autoregulation status and informing targeted interventions to achieve optimal CBF. However, due to the substantial heterogeneity in patient conditions and autoregulation assessment methodologies, it is imperative to obtain a larger sample of human data before applying autoregulation measurements as a valid tool in clinical practice. Using more standardized data collection procedures in future CA studies is essential for providing more homogenized information about the relationship between CA and brain disorders.

3.4.3 Limitations

Potential limitations of this study should be considered. We used the linear regression slope between MAP and CBF (MCAv) to compare the effectiveness of autoregulation for falling and rising blood pressure, which assumed a linear response of cerebral circulation to blood pressure perturbations. This simple approach is a compromise to the limited studies describing the relationship between MAP and CBF. The lack of experimental data is mainly due to the technical limitations in manipulating blood pressure and recording CBF.

Difficulties in blood pressure manipulation

It is challenging to manipulate MAP over a sufficiently wide range in human subjects. The experimental methods of manipulating blood pressure included in this study can be basically divided into physical and pharmacological methods.

These experimental methods can produce fluctuations in mean arterial pressure of about 5 to 30 mmHg, which are largely buffered via cerebral autoregulation. Normal baroreflex function limits the effective range within which MAP can be altered normally. Therefore, we could only analyse the cerebral pressure-blood flow relationship based on experimental data of MAP between 53 and 138 mmHg, which cannot fully cover the autoregulatory plateau of 60 to 150 mmHg proposed by Lassen [28] and Paulson et al. [154].

Pharmacological methods can perturb blood pressure by intravenous injection of vasodilator and/or vasoconstrictor drugs, such as nitroprusside and phenylephrine. The obvious advantage of the pharmacological approaches is that the response of CBF to rising and falling MAP can be studied simultaneously by injecting different drugs. In addition, pharmacological methods allow blood pressure to be altered over a relatively long period of time, as opposed to physical actions that tend to stimulate the cerebral circulation abruptly, resulting in more stable and accurate measurements of MAP and CBF. However, many studies have pharmacologically manipulated CBF with anaesthetics, angiotensin and α-adrenergic receptor agonists and/or nitric oxide donors [49, 151, 198, 238], and their effects on cerebrovascular tone are controversial; for example, the drugs used to manipulate MAP may have as yet unknown effects on the autoregulation response by directly altering cerebrovascular resistance downstream from the middle cerebral arteries.

Physical methods of blood pressure manipulation include tilt (head-up tilt), low body negative pressure (LBNP), etc. Of these, tilt tests can induce the greatest fluctuations in MAP, up to 43% change in MAP. Physical methods can only induce unidirectional hypotension or hypertension, and therefore cannot reliably explore autoregulatory asymmetry. In addition, the stability and reproducibility of blood pressure changes induced by physical methods are poor. However, physical methods are still widely used in dCA studies as they can noninvasively and quickly change blood pressure, and have minimal direct effects on vascular tone or indirect effect on arterial CO_2 or cerebral metabolism, independently from cerebral autoregulation.

Although accurate measurement of MAP and CBF is crucial for clinical purposes, so far there is no "gold standard" for autoregulation assessment. There is also no evidence to suggest significant differences in conclusions obtained from different assessment methods.

Accuracy of CBF measurements

CBF measurement techniques commonly used for static autoregulation studies in humans include TCD, Kety Schmidt technique, ^{133}Xenon clearance or other indicator methods, arterio-venous O_2 difference, near-infrared spectroscopy, and X-ray imaging [68, 239]. Notably, the experiments reviewed in this study primarily used TCD to measure CBF. Using MCAv as an index of CBF requires the assumption that the diameter of the artery remains constant. Multiple studies in humans have shown that the diameters of the middle cerebral artery and other large cerebral vessels remain relatively constant despite changes in ABP and blood gases [240–242]. Furthermore, changes in MCAv were highly correlated with CBF changes measured by two MRI techniques using the tracer gadolinium and arterial spin labeling, again validating TCD as a representative assessment of CBF [243]. Given the strict exclusion criteria employed in this study to limit the influence of factors such as blood gases changes on cerebrovascular, it can be assumed that the diameter of cerebral arteries remains relatively constant. Therefore, in the present study, we suggest that the cerebral blood flow velocity measured by TCD may accurately reflect the response to CBF.

Another limitation of TCD is that it measures regional changes in blood flow velocity rather than global CBF [244]. Given the complex physiological mechanisms of autoregulation, it is not yet known whether monitoring CA based on flow measurements in a large artery is reflective of the autoregulation behaviour in the entire brain (including regions perfused by other large arteries) as well as at the microcirculation level. In addition to the physiological variables directly affecting CBF, such as $PaCO_2$ and brain activation, there are many other factors that can

influence CBF through metabolic coupling (such as haematocrit, temperature), making it challenging to find appropriate methods to assess cerebral autoregulation.

This also leads to few studies attempting to reproduce the entire autoregulation curve. In most cases, researchers induce changes in MAP to determine the lower or upper limits of autoregulation or assess whether specific patients retain intact autoregulatory capacity. Patients with impaired or absent autoregulation (such as severe head injury or subarachnoid haemorrhage) are at a significantly higher risk of cerebral ischaemia or secondary brain damage caused by hyperperfusion. Cerebral autoregulation assessment is crucial in the clinical management of such patients. Therefore, more efforts are needed to improve the reproducibility and stability of autoregulation assessment to facilitate its clinical application.

3.4.4 Future research on static cerebral autoregulation assessment

The availability of measurement techniques that allow high temporal resolution for continuous recording of CBF changes has made dynamic CA the focus of most current research and clinical assessment. It is worth emphasizing that our findings are highly consistent with other studies on dCA. This strong consistency suggests a close relationship between these two phenomena. While dynamic testing overcomes some limitations of static methods, it is important to note that the interchangeability of the two approaches is still unclear. Previous studies have produced conflicting results regarding the association between dynamic and static autoregulation: de Jong et al. [162] found no correlation, whereas Tiecks et al. [64] found a strong linear relationship between them. Several factors may explain the opposite findings, including methodological differences, heterogeneity of study subjects, and variations in data processing and analysis methods. Additionally, the time frame over which changes in BP occur also influences the effectiveness and stabilization of CBF by autoregulation [232].

For clinical applications, it is conceivable that patients with impaired autoregulation may exhibit slowed adaptation to rapid blood pressure changes (i.e., impaired dynamic autoregulation), while their adaptation to slow blood pressure changes remains intact (i.e., normal static autoregulation) [3, 245]. Further research is needed to determine the consistency and complementarity between dynamic and static autoregulation. The combination of these two approaches may provide a more comprehensive assessment of cerebral autoregulation in different physiological and clinical contexts.

Considering the diversity of experimental designs and clinical practices, proposing a "gold standard" for cerebral autoregulation testing is challenging. However, the following guidelines can be recommended: a minimum change of 10% from baseline in MAP, a duration of each assessment of more than 5 minutes, minimizing autonomic nervous system stimulation, controlling brain activation, measuring $PaCO_2$ simultaneously with ABP and CBF, and focusing on individual data for each subject. These guidelines not only contribute to improving the reproducibility and inter-method agreement of autoregulation assessment but also enhance the accuracy of different tests on individuals. Despite some limitations, the present study provides a further update on the static cerebral pressure-flow relationship. With further research and technological advancements, we can expect a better understanding and application of dynamic and static cerebral autoregulation assessment methods.

3.5 Conclusion

Although the concept of cerebral autoregulation has been widely accepted after its proposal, increasing evidence suggests that the classic view of autoregulation may be incomplete or inaccurate. We performed a reanalysis of the dataset originally published by Numan et al. [68], adding papers published between 2013 and 2022, to provide new insights for updating the classical cerebral autoregulation curve. A total of 143 experiments (including Numan's original dataset) were included in the analysis. The cerebral pressure-flow relationship was comprehensively explored by

multiple analyses of absolute and relative CBF values. The main findings of this paper are:

1. The cerebrovascular system in healthy subjects does have autoregulatory ability, but CBF cannot maintain constant over the wide MAP range between 60 and 150 mmHg proposed by Lassen [28]. First-order linear regression and third-order polynomial functions were used to fit the relationship between absolute CBF (MCAv) and MAP. An autoregulatory plateau region of only approximately 20 mmHg (MAP between 80 and 100mmHg) was found using a data-driven approach, indicating a considerably narrower autoregulation range than previously accepted. Furthermore, within the autoregulatory plateau region, the cerebral pressure-flow relationship is not a straight line but with a slight positive slope.

2. The results of the relative CBF analysis showed asymmetry in the autoregulatory curve: the slope of $\%\Delta CBF/\%\Delta MAP$ were found to be 1.47 ± 0.71 for decreasing blood pressure and 0.37 ± 0.38 for increasing blood pressure, which were altered to $1.11 \pm 0.78\%/\%$ and $0.24 \pm 0.60\%/\%$ respectively after CO_2 correction. The significant difference in CBF directional sensitivity suggests that the cerebral vasculature defends more effectively against MAP increase than MAP decrease.

Based on the above findings, we proposed a new cerebral pressure-flow relationship, as shown in Figure 3.11. It should be noted that this new curve is based on the limited experimental data available so far, with many assumptions. Despite some advances in physiological measurement of cerebral blood flow and perfusion pressure, the ability to quantify cerebral autoregulation in health and disease remains limited. The physiological mechanisms that regulate CBF, how CBF changes when MAP is above 140 mmHg, and how autoregulation is altered in pathological conditions remain unclear, reminding us that more explicit assessments of CBF are needed under a range of non-pharmacological and pharmacological perturbations of blood

pressure while maintaining $PaCO_2$. Only by understanding these mechanisms can we clarify the role of impaired autoregulation in numerous cerebrovascular diseases, such as hypertension, Alzheimer's disease, and dementia [49, 151, 198, 238], thus providing more insights for clinical application.

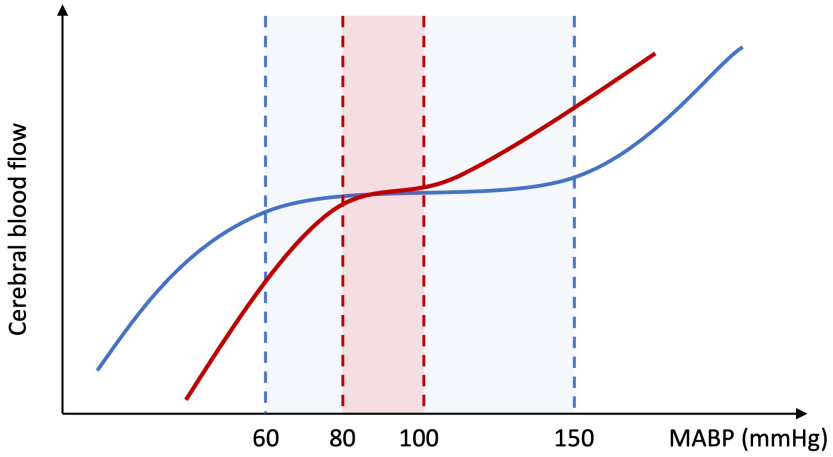


Figure 3.11: Classical view and updated view of the cerebral autoregulation curve. The blue line and shaded area represent the autoregulation curve and plateau proposed by Lassen [28] and Paulson et al. [154]. The red line and shaded area represent the new autoregulation curve and plateau proposed in this study, based on the dataset from Numan et al. [68] and studies from 2013 to 2022. It should be noted that the new curve is asymmetric (with a lower slope for MAP $>$ 100 mmHg than for MAP $<$ 80 mmHg) and has a slight slope between the "autoregulation plateau" of MAP and CBF.

With the increasing aging population and the rising incidence of hypertension, stroke, and dementia, it is crucial to enhance our understanding of cerebral blood flow regulation in both health and disease. We quantitatively investigated dynamic and static autoregulation by reviewing literature on different physiological and pathological conditions and found that autoregulation was altered in stroke and AD patients compared to healthy subjects, suggesting impaired autoregulation. The more passive cerebral pressure-flow relationship in these patients indicates a decreased ability to resist changes in blood pressure, highlighting the need for real-time monitoring and blood pressure management to reduce the risk of haemorrhage.

Although experimental data are limited, and we used a simple linear regression method to calculate the relative changes in cerebral blood flow when blood pressure

changes, the consistency shown by studies using different blood pressure manipulations and evaluation methods suggested that the relative changes in cerebral pressure and blood flow velocity have clinical significance in predicting disease such as stroke and Alzheimer's disease. This analysis provided a simplified approach to quantitative analysis of autoregulation that can be easily updated as more experimental data become available.

However, it should be noted that distinguishing the effects of normal ageing and disease regulation on CBF regulation is difficult due to the presence of many confounding factors. Vascular risk factors such as hypertension, diabetes, dyslipidaemia or congestive heart failure are more common in the elderly. In addition, the incidence of neurodegenerative diseases such as Alzheimer's disease, vascular dementia and mixed dementia also increases sharply with ageing [235]. As these diseases remain asymptomatic in their early stages and thus are difficult to identify clinically, some studies may have unknowingly included older subjects with reduced CBF caused by neurodegenerative diseases. It is necessary to conduct further experiments that can disentangle age-related vascular risk factors from normal ageing to gain a better understanding of the mechanisms underlying various cerebrovascular disorders.

Overall, an in-depth investigation of changes in cerebral autoregulation under various physiological and pathological conditions has the potential to enhance the prevention and treatment of CBF dysregulation and related brain disorders. This can be achieved by providing real-time information to clinicians about the patient's cerebral autoregulation status and informing targeted interventions to achieve optimal CBF. However, due to the substantial heterogeneity in patient conditions and autoregulation assessment methodologies, it is imperative to obtain a larger sample of human data before applying autoregulation measurements as a valid tool in clinical practice. Using more standardized data collection procedures in future CA studies is essential for providing more homogenized information about the relationship between CA and brain disorders.

4

A physiological-based mathematical model of cerebral vasculature

A physiological-based mathematical model is proposed that predicts the response of cerebral vasculature to changes in arterial blood pressure and neural stimulation. Cerebral blood flow is assumed to be controlled through changes in arterial compliance, and hence arterial resistance and volume, through nonlinearly interdependent feedback mechanisms to achieve autoregulation. This physiological based mathematical model of arterial, together with capillary and venous compartments, constructs a lumped compartment model to simulate whole-brain blood flow. The model also includes a BOLD response compartment for outputting the response to neural activation. Steady-state and dynamic simulations of the model under different conditions show that there is significant interaction between the autoregulation and activation processes, and that the level of autoregulation has a strong influence on the CBF and neural activation responses.

4.1 Introduction

Although the NVC and autoregulation mechanisms share a great deal in common, they have traditionally been studied separately. To the best of our knowledge, no model in the literature attempts to capture the underlying physiology while also being able to simulate both the activation and autoregulatory responses. Therefore, the primary aim of this chapter is to construct a physiologically based mathematical model capable of performing a comprehensive investigation of both the NVC and cerebral autoregulation. The global nature of the autoregulatory response makes it relatively easy to obtain a benchmark input-output figure (the canonical Lassen curve) to validate the model [28] On the contrary, producing a canonical input-output characteristic for the activation response is hindered by the 'local' nature of the NVC. During activation, CBF is observed to overcompensate in response to the increased metabolism, resulting in venous blood becoming more oxygenated giving a decrease in deoxyhaemoglobin. As deoxyhaemoglobin is paramagnetic, the increased signal in response to mental activation can thus be captured by the BOLD functional magnetic resonance imaging (fMRI) [58]. Quantifying cerebral metabolism plays a key role in replicating the BOLD signal and hence verifying the NVC response.

After directly reproducing a wide range of experimental observations to validate the model, the use of this integrated approach allows us to provide key insights into the underlying NVC and autoregulation mechanisms to help to better understand CBF control. Given the importance of SMC calcium in regulating blood flow, it is vital to understand the physiology that governs the changes in this substance. Since the sarcoplasmic reticulum is the primary calcium-storage organelle of SMC, its role in controlling SMC calcium dynamics will first be ascertained. The myogenic response has been shown to be driven by mechanically activated channels as well as membrane voltage activated channels, but the initiating factor is still unclear. It is thus necessary to fully investigate the process of the SMC transforming stretch into active force. In addition, the detailed physiological basis of our model enables us

to explore the underlying pathway of shear-stress-induced additional vasodilation. Finally, the interaction between the various mechanisms will be investigated through the NO signalling pathway.

4.2 A Model of Vascular Regulation

In order to ensure an adequate physiological basis, an arterial vessel model is first constructed before integrating into a whole brain vasculature model, as shown in Figure 4.1. This model is a composite of several studies: the electrochemical processes of ion exchange through various channels are modified from Mathias et al. (2018) [95], the NO dynamics are taken from Dormanns et al. (2016) [89] and the kinetic and mechanical models are extended from Hai et al. (1988) [78], Yang et al. (2003) [79] and Stalhand et al. (2008) [85]. Therefore, this model can be used to investigate the vasodilating effects of NO, the release and uptake of calcium in the SMC, the kinetics of phosphorylation of myosin cross bridges, and the mechanical interactions that ultimately determine the vessel radius. Since the NVC pathways modelled in the literature are highly detailed and complete, the focus of this study will be on how the different subsystems couple with the other compartments of the single vessel model.

4.2.1 NVC Model

The NVU subsystem provides the physiological basis behind the synaptic release of potassium and glutamate. The potassium signalling mechanism is primarily driven by the astrocyte and couples to the SMC through the perivascular space (PVS). The NO that diffuses to the SMC results from glutamate release during neural activation.

The neuron model also captures the tissue oxygen dynamics associated with the increase in metabolism through a mass balance between vascular supply, background demand and neuronal pump demand. The three elements are represented in the

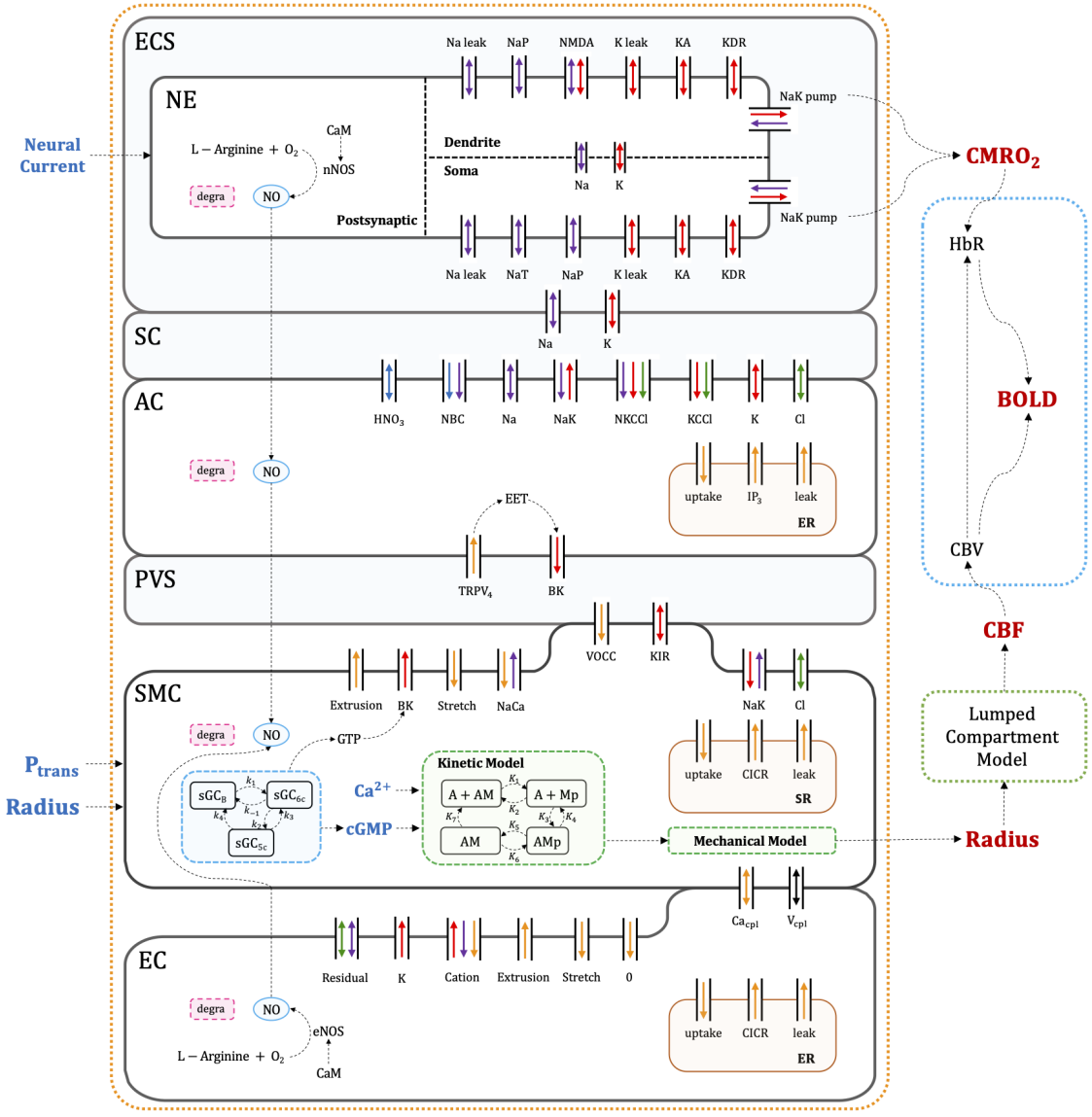


Figure 4.1: Schematic of the integrated model and the BOLD model. Different coloured arrows represent different ion pathways. NE: neuron, AC: astrocyte, PVS: perivascular space, ER: endoplasmic reticulum, ECS: extracellular space, degra: degradation. Figure adapted and modified from Mathias et al. [95]

following state equation:

$$\frac{d[\mathrm{O_2}]}{dt} = CBF \cdot \frac{[\mathrm{O_2}]_b - [\mathrm{O_2}]}{[\mathrm{O_2}]_b - [\mathrm{O_2}]_0} - CBF_0 \cdot P([\mathrm{O_2}]) \cdot (1-\theta) - CBF_0 \cdot P([\mathrm{O_2}]) \cdot \theta \cdot E_P \quad (4.1)$$

where $[\mathrm{O_2}]_b$ and $[\mathrm{O_2}]_0$ are constants, $P([\mathrm{O_2}])$ is a function that represents the decreased activity of the pumps with decreasing oxygen concentrations, θ denotes the proportion of metabolic activity attributable to the neuronal membrane sodium/potassium (NaK) pump and E_P represents the normalized activity of NaK pump. Note that the background demand (the second term in Eq. (4.1)) and the neuronal pump demand (the third term in Eq. (4.1)) both depend on the tissue oxygen concentration, since the activity of the pumps is ATP dependent and the production of ATP by mitochondria is, in turn, oxygen dependent.

Prediction of BOLD response

The BOLD model used here is based on the work of Buxton et al. (2004) and is used to validate the activation response against experimental data. Figure 2 summarizes the inputs and outputs of the BOLD model and there are two contributing elements: changes in deoxyhaemoglobin (HbR) and CBV. HbR in turn depends on the cerebral metabolic rate of oxygen consumption and CBV. The mass balance for HbR is simply the difference between that generated by the consumption of oxygen by the neuron and that flowing into the varying volume v(t) (or balloon), given by:

$$\frac{dHbR}{dt} = \frac{1}{\tau_{\mathrm{MTT}}} \left(\frac{CMRO_2}{CMRO_{20}} - \frac{HbR}{CBV} f_{\mathrm{out}} \right) \quad (4.2)$$

$\mathrm{CMRO_2}$ reflects the demand for extra oxygen during increased neural activity, $\mathrm{CMRO_{20}}$ is the baseline value of $\mathrm{CMRO_2}$, and f_{out} is the outflow from the balloon. Due to the limited ability of the brain to store glucose and oxygen, $\mathrm{CMRO_2}$ and CBF are tightly coupled. This is captured by the following mass conservation equation which, in the steady state, relates $\mathrm{CMRO_2}$, the oxygen extraction factor (OEF), arterial oxygen concentration C_a and CBF:

$$CMRO_2 = CBF \cdot OEF \cdot C_a \quad (4.3)$$

The rate of change of blood volume is the difference between the non-dimensional blood flow into a varying volume and that flowing out given by f_{out} with the characteristic time scale of τ_{MTT}, hence:

$$\frac{dCBV}{dt} = \frac{1}{\tau_{\text{MTT}}}\left(\frac{CBF}{CBF_0} - f_{\text{out}}\right) \tag{4.4}$$

The time-dependent outflow f_{out} from the venous compartment, which is transiently different from CBF, is composed of two parts, namely the relationship between blood flow and the blood volume and the rate at which the blood volume changes due to viscous effects of the vessel wall. Hence the outflow is defined as:

$$f_{\text{out}}(v) = v^{\frac{1}{\alpha}} + \tau\frac{\mathrm{d}v}{\mathrm{d}t} \tag{4.5}$$

v is the volume of the balloon, α is the steady state flow–volume relation, and τ depicts the associated time constant. The balloon model of Buxton et al. (2004) [246] provides the change in the BOLD signal as a function of the venous volume and deoxyhaemoglobin:

$$BOLD_{\text{signal}} = V_0[a_1(1 - HbR_N) - a_2(1 - CBV_N)] \tag{4.6}$$

Baseline venous volume is denoted by V_0, while a_1 and a_2 are dimensionless constants based on several experimental and physiological parameters [246].

4.2.2 CA Model

Endothelium subsystem

Gap junctions are vital to generating arterial contraction and vasomotion through the recruitment and synchronization of calcium oscillations. Koenigsberger et al. [247] noted that calcium diffusion and electrical coupling pathways are responsible for generating calcium oscillations and synchronizing oscillations respectively, whereas the inositol 1,4,5-trisphosphate (IP3) diffusion pathway has little effect on the SMC calcium dynamics. Therefore, in order to keep our model as simple as possible whilst still providing enough physiological detail, we only add two gap junctions via electrical (V_{cpl}) and calcium (Ca_{cpl}) coupling in the lumen/endothelium subsystem

for the transfer of species and intercellular communication between the SMC and the endothelial cell (EC).

The EC plays a crucial role in the cerebrovascular NO dynamics, particularly when compared to its small effect on calcium dynamics and the myogenic response [247]. The flow-induced shear stress initiates the production of NO in the EC, which is related to the radius of the arteriole r, the axial pressure across the arteriole ΔP, and the length of the arteriole L (assuming Poiseuille flow):

$$\tau_{\text{wall}} = \frac{r\Delta P}{2L} \tag{4.7}$$

The activation of the enzyme eNOS depends on the dominant contribution of elastic strain energy, the minor contribution of endothelial calcium and the associated deactivation process, which is outlined by Comerford et al. [91]:

$$\frac{d[\text{eNOS}]_{\text{EC}}}{dt} = \gamma_{\text{eNOS}} \frac{K_{\text{dis}}[\text{Ca}^{2+}]_{\text{EC}}}{K_{m,\text{eNOS}} + [\text{Ca}^{2+}]_{\text{EC}}} + (1 - \gamma_{\text{eNOS}}) g_{\max} F_{\text{wSS}} - \mu_{\text{deact}}[\text{eNOS}]_{\text{EC}} \tag{4.8}$$

The Michaelis constant for a process x is given by K_x, γ_{eNOS} denotes the fraction of the activation of $[\text{eNOS}]_{\text{EC}}$ that is due to the calcium pathway, F_{wSS} is the elastic strain energy stored within the membrane, $g_{\max}$ is the maximal shear stress induced eNOS activation rate and μ_{deact} is the deactivation rate. The resulting accumulation equation for the NO in the EC contains three elements: the production term $p_{\text{NO,EC}}$, the net diffusive term $d_{\text{NO,EC}}$ and the consumption term $c_{\text{NO,EC}}$. For brevity, the reader is referred to Dormanns et al. [89] for the detailed NO dynamics in the EC.

$$\frac{d[\text{NO}]_{\text{EC}}}{dt} = p_{\text{NO,EC}} + d_{\text{NO,EC}} + c_{\text{NO,EC}} \tag{4.9}$$

Smooth muscle cell subsystem

The full biochemical model of the SMC with all the associated ionic currents and channel activations is the pivotal element of the single vessel model due to its dominant role in controlling vascular tone through 'cross-bridge cycling'. It is

primarily driven by the rise in perivascular potassium and the net diffusion of NO from the neuron (both NVC mechanisms), the transmural pressure from the lumen and the net diffusion of NO from the EC (both autoregulation mechanisms).

The key to the SMC calcium dynamics lies in the exchange and movement of calcium through ion channels and pumps. The cytoplasmic concentration of SMC calcium $[Ca^{2+}]_{SMC}$ is thought to be driven by mechanically activated channels as well as membrane voltage activated channels:

$$\frac{d[Ca^{2+}]_{SMC}}{dt} = -\frac{d[Ca^{2+}]_{SR}}{dt} + J_{VOCC} + J_{stretch} + J_{Na/Ca} - J_{ATPase} + J_{SMC\text{-}EC}^{Ca\ cpl} \quad (4.10)$$

The SR calcium concentration $[Ca^{2+}]_{SR}$ is determined by the balance between the calcium uptake into the SR (J_{uptake}), calcium-induced calcium release (J_{CICR}), and the calcium release from the SR (J_{leak}), given by Dormanns et al. [87]:

$$\frac{d[Ca^{2+}]_{SR}}{dt} = J_{uptake} - J_{CICR} - J_{leak} \quad (4.11)$$

These channels, which exchange species with intracellular spaces, generally have simple sigmoidal or linear relationships with calcium in cytoplasm. Uptake of calcium into the SR is given by Koenigsberger et al. [247]:

$$J_{uptake} = B_{SMC}\frac{[Ca^{2+}]_{SMC}^2}{c_b^2 + [Ca^{2+}]_{SMC}^2} \quad (4.12)$$

where B_{SMC} and c_b are free constants, representing the SR uptake rate constant and the half-point of the SR ATPase activation sigmoidal, respectively. By contrast, J_{VOCC} and $J_{stretch}$ are channels which control the movement of ions across the SMC membrane, connecting the SMC cytoplasm to extracellular spaces. These are typically very fast and depend on the membrane voltage of the SMC and the Nernst potential of the flux species. The flux of calcium exchanging with sodium and calcium extrusion by Ca^{2+}-ATPase pumps are represented by $J_{Na/Ca}$ and J_{ATPase}, respectively, which depend on both membrane potential and calcium concentration.

The stretch channel is the only channel with a dependence on the transmural pressure (P_{trans}), given by:

$$J_{\text{stretch}} = \frac{G_{\text{stretch}}}{1 + \exp\left[-\alpha_{\text{stretch}}\left(\frac{P_{\text{trans}} r}{t_w} - \sigma_0\right)\right]}(v_{\text{SMC}} - E_{\text{SAC}}) \tag{4.13}$$

where G_{stretch} and E_{SAC} are the whole cell conductance and reversal potential for stretch-activated channels (SACs), respectively. α_{stretch} and σ_0 are the slope of stress dependence and half-point of the SAC activation sigmoidal, respectively. t_w is the thickness of the arteriole wall.

The electrochemical processes of ions entering and leaving the cell allow us to keep track of all of the ionic currents between the compartments and therefore the concentrations of each species within each compartment as well as the potential of the cell membrane (v_{SMC}). Since the main electrically charged substances which can cross the membrane are sodium, potassium and chloride ions:

$$\frac{dv_{\text{SMC}}}{dt} = \gamma_{\text{SMC}}\left(-J_{\text{NaK}} - J_{\text{Cl}} - J_{\text{VOCC}} - J_{\text{Na/Ca}} - J_{\text{K}} - J_{\text{stretch}} - J_{\text{KIR}}\right) + V_{\text{cpl}}^{\text{SMC-EC}} \tag{4.14}$$

Although these channels are not involved directly in exchanging calcium, they can alter the membrane voltage by changing the concentration of charged ions in the SMC, thereby exerting an indirect influence on the SMC contractile mechanism. γ_{SMC} is a scaling factor inversely related to cell capacitance. Among the different ions, potassium has the dominant influence. The effects of membrane potential and calcium on the potassium channels is reflected by the equilibrium distribution of open channel states for the voltage and calcium activated potassium channels K_{act}, given by Koenigsberger et al. [247]:

$$K_{\text{act}} = \frac{\left([\text{Ca}^{2+}]_{\text{SMC}} + c_w\right)^2}{\left([\text{Ca}^{2+}]_{\text{SMC}} + c_w\right)^2 + \beta_{\text{SMC}} \exp\left[-\frac{(v_{\text{SMC}} - v_{ca3})}{R_K}\right]} \tag{4.15}$$

where β_{SMC}, v_{ca3} and R_K are the translation factor for membrane potential dependence, half-point and maximum slope of calcium activated potassium channel

sigmoidal, respectively. The translation factor c_w was originally modelled as a constant, whereas Stockand and Sansom [248] found that the presence of cGMP increased the open probability of calcium activated potassium channels. Therefore, this was modified to include a dependence on cGMP with two constants $(c_{w,0}, c_{w,1})$, given by:

$$c_w = \frac{1}{2}\left[1 + \tanh\left(\frac{[\text{cGMP}]_{\text{SMC}} - c_{w,0}}{c_{w,1}}\right)\right] \tag{4.16}$$

The SMC NO dynamics are much simpler than the intricate SMC calcium dynamics. Since there is negligible NO produced in the SMC, the NO concentration is simply the sum of the net NO fluxes to the SMC and a degradation term. The production of cGMP is catalysed by the intermediary enzyme soluble guanylyl cyclase (sGC) which depends on the SMC NO concentration. The NO-sGC and sGC-cGMP pathways captured by Dormanns et al. [89] are key to this process and thus taken unaltered here.

4-state Kinetic Model

The kinetic model is able to translate intracellular concentrations of calcium and cGMP to describe the attachment and phosphorylation of actin and myosin filaments, which provides the molecular basis for the SMC contraction. The phosphorylation rate constants are assumed to depend on the concentration of calcium, whereas the de-phosphorylation rates are negatively modulated by calcium and positively modulated by cGMP. It is via these rate constants in the kinetic model that the intramural pressure and flow along with NO exert their influence on the mechanical model, and so on the vasculature's behaviour.

The 4-state kinetic model from [78] describes the attachment and phosphorylation of myosin cross-bridges. The proportions of the total number of cross-bridges are: M, myosin cross-bridges; Mp, phosphorylated cross-bridges; AMp, phosphorylated and attached cross-bridges; and AM, attached, non-phosphorylated cross-bridges. Rate constants, K, govern the transitions between states (i.e., phosphorylation/dephosphorylation and attachment/detachment). The four species

are connected by 7 rate constants: K1 and K6 are the rate constants representing the phosphorylation of M to Mp and AM to AMp by the active myosin light-chain kinase, Ca^{2+} - calmodulin complex. K2 and K5 are the rate constants for the dephosphorylation of Mp to M and AMp to AM by myosin light-chain phosphatase. K3 and K4 are the rate constants representing the attachment of the fast cycling phosphorylated cross bridges. K7 is the rate constant for latch-bridge detachment. The kinetic model can be described by four differential equations:

$$\frac{d}{dt}\begin{bmatrix} M \\ Mp \\ AMp \\ AM \end{bmatrix} = \begin{bmatrix} -K_1 & K_2 & 0 & K_7 \\ K_1 & -K_2 - K_3 & K_4 & 0 \\ 0 & K_3 & -K_4 - K_5 & K_6 \\ 0 & 0 & K_5 & -K_6 - K_7 \end{bmatrix} \cdot \begin{bmatrix} M \\ Mp \\ AMp \\ AM \end{bmatrix} \tag{4.17}$$

subject to:

$$M + Mp + AMp + AM = 1 \tag{4.18}$$

The phosphorylation and dephosphorylation rate constants are assumed to depend on $[Ca^{2+}]$ and [cGMP] in order that the effects of myosin light-chain kinase (MLCK) and myosin light-chain phosphatase (MLCP) respectively can be simulated. It is via these rate constants that the myogenic response and the NO model exert their influence on the mechanical model, and so on the behaviour of the vessel.

The phosphorylation rates are modulated by the concentration of Ca^{2+}:

$$K_1 = K_6 = \frac{[\mathrm{Ca}^{2+}]^{n_{\mathrm{ca1}}} k_{\mathrm{ca1}}}{[\mathrm{Ca}^{2+}]^{n_{\mathrm{ca1}}} + k_{\mathrm{ca1}}^{n_{\mathrm{ca1}}}} \tag{4.19}$$

n_{ca1} represents the sensitivity of the phosphorylation reaction to calcium ions, k_{ca1} is the constant that adjusts the phosphorylation rate. The de-phosphorylation rates are negatively modulated by $[Ca^{2+}]$ and positively modulated by [cGMP]:

$$K_2 = K_5 = 0.55 + 2 \cdot \frac{[\mathrm{cGMP}]^{n_{\mathrm{cGMP}}}}{[\mathrm{cGMP}]^{n_{\mathrm{cGMP}}} + k_{\mathrm{cGMP}}^{n_{\mathrm{cGMP}}}} \cdot \frac{k_{\mathrm{ca2}}^{n_{\mathrm{ca2}}}}{[\mathrm{Ca}^{2+}]^{n_{\mathrm{ca2}}} + k_{\mathrm{ca2}}^{n_{\mathrm{ca2}}}} \tag{4.20}$$

Mechanical Model

The wall mechanical subsystem mainly describes the relationship between the concentrations of the species in the SMC and the contraction and the effect of NO on the dephosphorylation of myosin cross bridges. The mechanical model is based on [79, 85]. The mechanical model consists of an active element and a passive element, representing the overlapping actin and myosin filaments and the passive stiffness of the cell respectively. The force in the active element is determined by the viscous friction coefficients f_1 and f_2 (for phosphorylated and un-phosphorylated attached myosin cross bridges respectively):

$$F_a = l_0(f_1 AMp(\hat{v} + \hat{\lambda}) + f_2 AM\hat{\lambda})e^{\frac{-(\lambda-\lambda_{\text{opt}})^2}{2\eta}} \tag{4.21}$$

where normalized cross-bridge cycling speed $\hat{v} = v/10$ and normalized cell length $\lambda = l_{\text{cell}}/l_0$. The passive element takes the form of an exponential spring-like element, giving a passive force:

$$F_p = q_1 \left(e^{q_2(\lambda^3-1)} - 1\right) \tag{4.22}$$

The sum of the active and passive forces gives the total force in the cell:

$$F_T = F_a + F_p \tag{4.23}$$

The expansive force of the blood pressure can be equated with the contractive force of the muscle, for a single cell of width w_c:

$$F_T = F_{\text{cell}} = w_c \cdot P \cdot r \tag{4.24}$$

where P denotes intramural pressure; the difference in pressure between the blood within the vessel and the tissue surrounding the vessel. The resulting mechanical effects of myosin 'cross-bridge cycling' can thus be captured, in which the rate of change of the SMC length is calculated and converted into the rate of change of vessel radius.

$$r = \frac{1}{2}\left(\frac{\lambda l_0 n_c}{\pi} - t_w\right) \tag{4.25}$$

where n_c is the number of SMCs end-to-end around the circumference of the vessel and λ is the cell length which is determined by the force in the active element.

To solve the mechanical model in the steady state we set $\dot{\lambda} = 0$, giving the relation:

$$F_T = F_p + F_a\Big|_{\dot{\lambda}=0} = q_1\left(e^{q_2(\lambda^{a_3}-1)} - 1\right) + l_0 f_1 \alpha_3 \hat{v} e^{\frac{-(\lambda-\lambda_{\text{opt}})^2}{2\eta}} \tag{4.26}$$

Here force in the cell is a function only of its current length and the proportion of cycling cross-bridges ($\alpha_3 = AMp$). The value of λ at which $F_T = F_{\text{cell}}$ is then found by solving:

$$0 = F_p + F_a\Big|_{\dot{\lambda}=0} - F_{\text{cell}} \tag{4.27}$$

$$0 = q_1\left(e^{q_2(\lambda^{a_3}-1)} - 1\right) + l_0 f_1 \alpha_3 \hat{v} e^{\frac{-(\lambda-\lambda_{\text{opt}})^2}{2\eta}} - w_c P \frac{1}{2}\left(\frac{\lambda l_0 n_c}{\pi} - t_w\right) \tag{4.28}$$

Unfortunately, there is no analytical solution to this equation, instead it must be solved numerically; in this case a modified Newton-Raphson method was used.

4.2.3 Fitting and analysis

We use approximately 60 ordinary differential equations to describe the model variables based on the conservation of mass and Kirchhoff's law. This system is solved using the MATLAB stiff solver 'ode15s' with a relative tolerance of 1e-3, absolute tolerance of 1e-6 and maximum stop of 1.

Autoregulatory response

Kuo et al. (1991b) [35] measured the steady state responses of an isolated coronary arteriole from a pig across a range of intramural pressures and a range of pressure differences between the vessel ends. In addition to separate the effects of flow and intramural pressure, they also observed the dynamic responses of arterioles to step changes in pressure and flow, thus providing enough information to verify the autoregulatory response of the single vessel model.

All physiologically significant parameter values were directly sourced from prior literature, with detailed descriptions and references available therein. To ensure the model closely matched experimental measurements, parameters of purely numerical significance were fitted multiple times to minimise the root mean square error between the model and the data. Following optimisation, the steady state radius output from the model is in good agreement with the experimental data from Kuo et al. (1991) [35] under two experimental regimes, as shown in Figure 4.2. The gradient across the arterioles determines the magnitude of the flow through the vessel. In the 'no flow' case, no pressure gradient was applied resulting in no flow and hence no shear stress was applied to the arteriole, in contrast to the 'flow' case where an axial pressure of $\Delta P = 4\,\mathrm{cmH_2O}$ was applied. The myogenic element of autoregulation is largely isolated in the 'no flow' regime, which provides the validity of the calcium dynamics of the single vessel model in the steady state. In the 'flow' case, the magnitude of vasodilation provided by the shear stress response indicates that the endothelium-driven NO pathway exhibits accurate steady state behaviour.

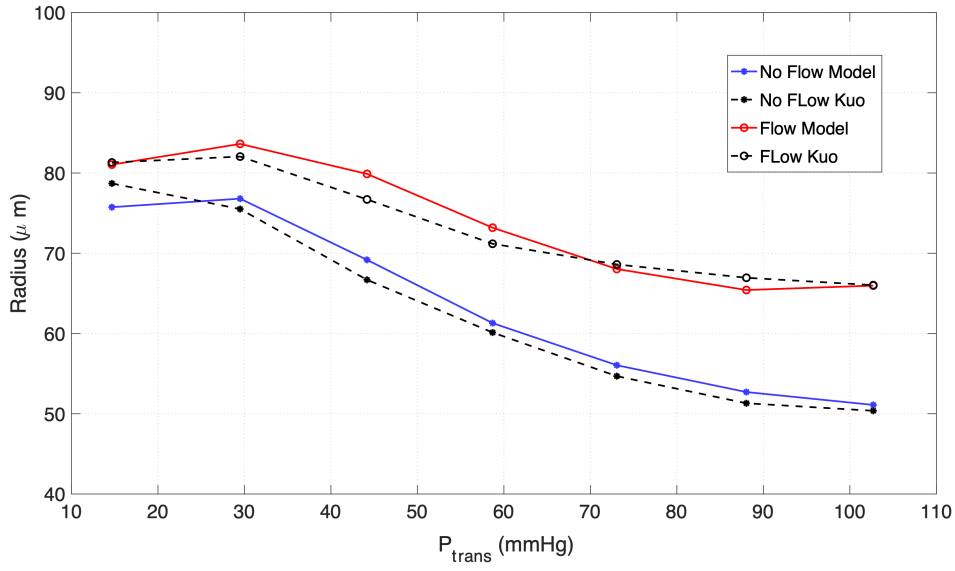


Figure 4.2: Comparison of the model arteriole radius responses (flow-red lines; no flow-blue lines) and arteriole radius experimental data from Kuo et al. (1991) [35] (black lines) across a range of transmural pressures.

The dynamic responses of arterioles to different steps changes in pressure and flow allow us to examine the role of flow and intramural pressure separately. Figure

4.3 shows the effect of flow (shear stress response) on pressure-induced myogenic response. For the first 240s, there was no pressure difference between the ends of the vessel and hence the myogenic response to intramural pressure under no-flow condition was captured. When IP was increased from 60mmHg to 80mmHg, the vessel initially dilated but gradually contracted down to a new active equilibrium radius which was smaller than the initial radius (from 69 to 61μm). In response to the brief period of flow, when ΔP was increased from 0 to 4 cmH_2O, the vessel distended from 61 to 76μm, and gradually decreased to the pre-flow value upon the cessation of flow.

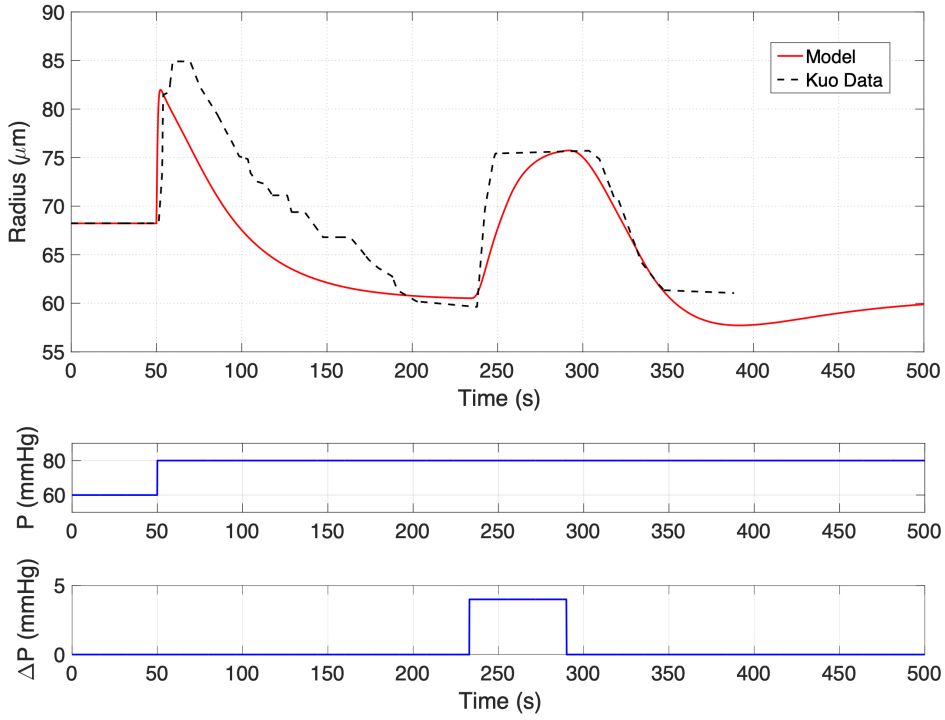


Figure 4.3: The resulting arteriole radius against time in response to variations in transmural pressure and axial pressure gradient. The top panel presents the arteriole radius over time, with the black dashed line indicating experimental data from Fig.2A in Kuo et al. (1991) [35], and the red line representing model output. The middle panel illustrates the axial pressure gradient applied during the experiment, while the bottom panel illustrates the changes in transmural pressure applied during the experiment.

Figure 4.4 shows that the flow-induced vasodilation was counterbalanced by the myogenic response when pressure was increased (117s). However, the rate of vasoconstriction in the flow condition between 117s to 270s was slower than in the

no-flow case in Figure 4.3 (50s to 200s), indicating that the presence of flow could also reduce the vasoconstriction caused by myogenic response. The discrepancies between model results and the experimental data in the process of radius variation may result from the relatively low calcium concentration in the SR compared with reality. Stokes and Wagenknecht (2000) [24] stated that a thousandfold concentration gradient of calcium across the SR is required to raise the intracellular calcium concentration sufficiently to cause contraction. Although the conductivities and the sigmoid functions relating to the SR channels were scaled to increase its calcium concentration in this study, it was still found to be too low to induce the thousandfold gradient (only a hundred times greater than the typical cytoplasmic concentration). As a result, the SMC calcium dynamics were relatively dominated by the ion channels that connect to the space outside the SMC, leading to the excessively fast dynamic response when fitted to experimental data from Kuo et al. (1991) [35].

It also should be noted that the animal experimental data from Kuo and the model results indicate that the time course of the autoregulatory response spans several tens of seconds, whereas typical autoregulatory responses in human experiments usually take only a few seconds. This discrepancy in time course warrants further investigation to explore its underlying causes and potential implications for blood flow autoregulation.

Activation response

Sadaghiani et al. (2009) performed a study measuring both the BOLD contrast signal and CBF using arterial spin labelling, and also captured the difference of the BOLD post stimulus undershoot when human subjects were exposed to static checkerboard and flickering checkerboard patterns [249]. Therefore, the simulation and validation of the activation response largely centres around this data set. The results of the model are shown in Figure 4.5 along with experimental data from Sadaghiani et al. (2009). It should be noted that shape and relative magnitude

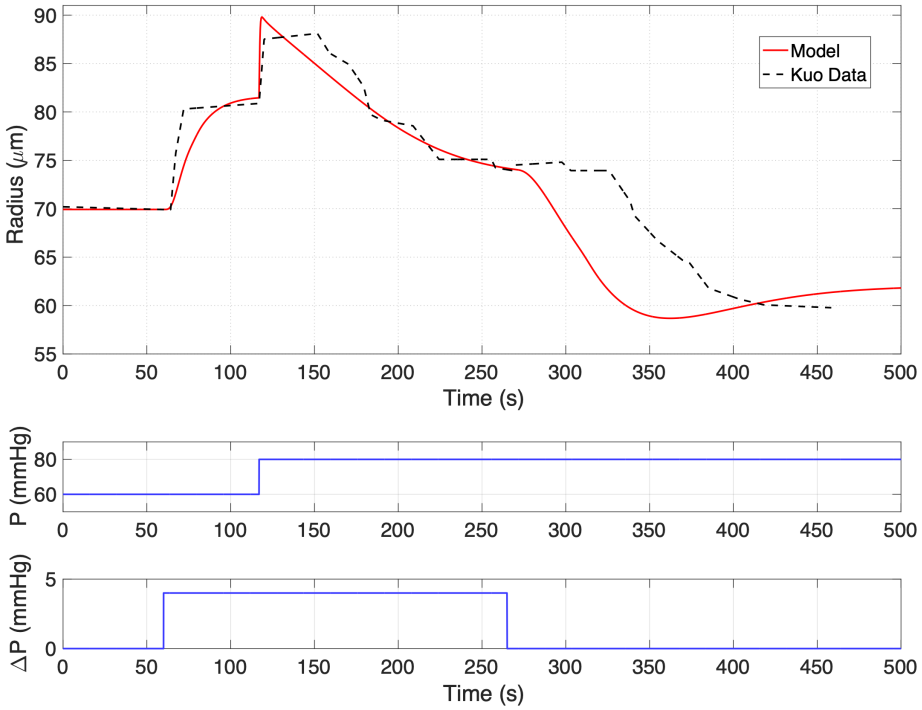


Figure 4.4: The resulting arteriole radius against time in response to variations in transmural pressure and axial pressure gradient. The top panel presents the arteriole radius over time, with the black dashed line indicating experimental data from Fig.2C in Kuo et al. (1991) [35], and the red line representing model output. The middle panel illustrates the axial pressure gradient applied during the experiment, while the bottom panel illustrates the changes in transmural pressure applied during the experiment.

provide more meaningful comparisons between the experimental data and model responses than absolute values. Therefore, the experimental data has been linearly scaled in order to lie in a similar range to the maximum stimulation of the model. The model output largely displays the canonical elements of a typical BOLD response: an initial dip, main response, and post stimulus undershoot. At the cessation of the neural stimulus, the small undershoot of the model fits closely with the static data but poorly with the flicker data. This can be explained by the finding of Zheng et al. (2010) [250], that a vasoconstriction mechanism working in parallel to the vasodilatory mechanisms is required to cause the BOLD signal to undershoot. Since both of the NVC mechanisms in this model are vasodilatory, the small undershoot may be a result of the absence of a suitable vasoconstriction mechanism.

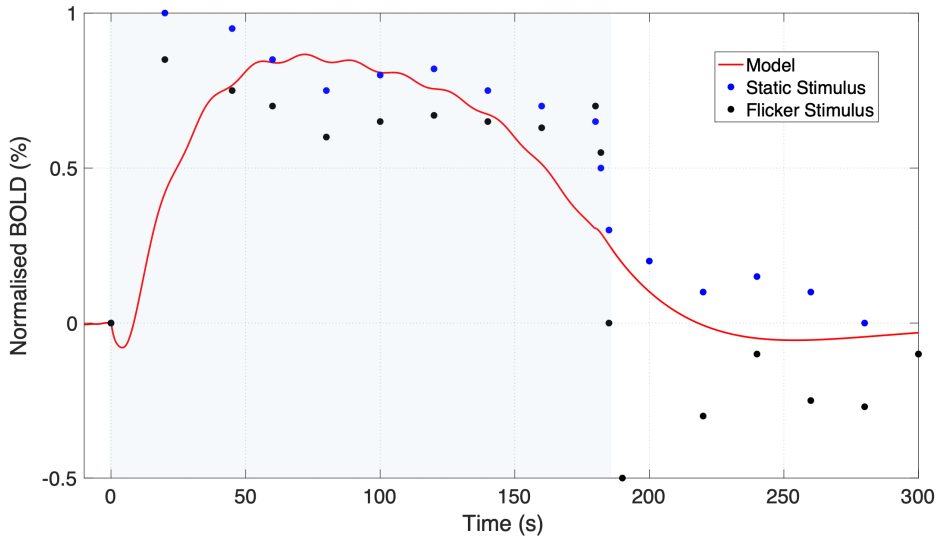


Figure 4.5: Resulting BOLD contrast signal. Light blue shading indicates the period of stimulation. Red line represents the model output. Blue circles indicate the static stimulus while black circles indicate flicker stimulus, manually extracted from Sadaghiani et al. (2009) [249].

4.3 Whole brain vasculature model

4.3.1 Integration of arteriole model into existing whole-brain model

In the previous section we presented a model of an individual arteriole and showed that its behaviour is representative of that of a real arteriole. In this chapter we integrate that model of a single arteriole into a model of the vasculature of the whole brain. We then examine the effect that our arteriolar model has within a larger vascular system. The integration into a whole brain model also allows comparison of model results with in-vivo data from humans. In-vivo flow data for single arterioles is not available for humans, whereas data for the flow in the middle cerebral artery and arterial blood pressure in humans are readily available.

A lumped compartment model was constructed that can simulate whole-brain blood circulation, including arterial, capillary, and venous compartments, as shown in Figure 4.6. Each compartment has its function: arteries regulate CBF, capillaries regulate gas transport, and veins regulate CBV. The haemodynamic model uses

the system of equivalents between hydrodynamic and electrical circuits used by numerous authors [8, 245].

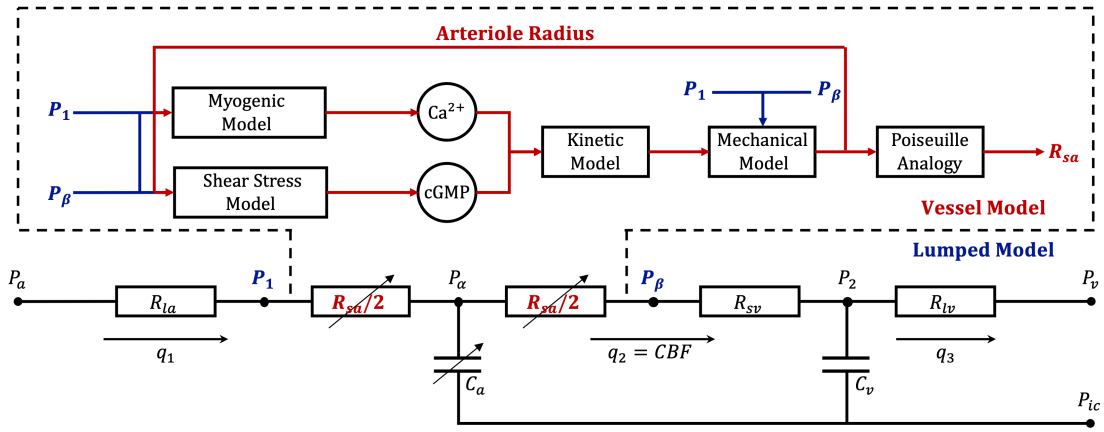


Figure 4.6: Schematic of the electrical equivalence model coupled with single vessel model. P_a, P_{ic} and P_v, arterial input, intracranial and venous output blood pressure, respectively. R_{la}, resistance of non-regulating arterial compartment. R_{sa} and C_a, resistance and compliance of regulating arterial compartment; R_{sv}, resistance of capillary compartment and small veins; C_v, venous compliance; R_{lv}, resistance of large veins.

The arterial compartment is divided into regulating and non-regulating compartments. The first segment (R_{la}) represents the larger arteries, while the smaller arteries and arterioles are represented by the second segment (R_{sa}). To allow for changes in arterial volume due to arterial compliance (C_a), the smaller arteries are sub-divided into two parts, with the first segment assumed to have fixed resistance and blood volume, and the second segment having varying resistance and volume. The capillary compartment is assumed to have a fixed resistance and volume, while the volume of the venous compartment changes but has a fixed flow resistance for simplicity. The venous compartment is thus modelled as two resistors separated by a venous compliance (C_v). To simplify the model, the smaller veins and venules are combined with the capillaries and represented by the first resistor (R_{sv}), while the larger veins are represented by the second resistor (R_{lv}). ICP is assumed constant since the time constants governing ICP are significantly different from those of autoregulation or neural activation.

Because it is the arterioles, or the small arteries, which have the greatest effect in

the autoregulation feedback loop, it is the properties of this level of the vascular tree which change in response to haemodynamic and metabolic stimuli. We thus replace the variable components of the arterial compartment with components whose properties are determined by a physiologically based arterial vessel model (which will be discussed in detail in the following section), as shown in Figure 4.6. Arterial volume is assumed to include a fixed part corresponding to non-regulating vessels (V_{la}) and a variable part corresponding to regulating vessels (V_{sa}):

$$V_a = V_{la} + V_{sa} \tag{4.29}$$

The resistance of the vessels can be related to the radius via the analogous form of Poiseuille's equation:

$$R_{sa} = \frac{8\mu_b L}{\pi r^4} \cdot \frac{1}{n_{sa}} \tag{4.30}$$

where n_{sa} is the effective number of parallel arterioles in the vascular tree. The volume of blood in the arterioles is equivalent to the charge on the capacitor in the arterial compartment and its derivative is equivalent to the current down that branch of the circuit, given by:

$$\frac{dV_{sa}}{dt} = 2\pi r L n_{sa} \frac{dr}{dt} \tag{4.31}$$

The pressures in the haemodynamic model and arterial volume can also be calculated from conservation of volume at the relevant nodes:

$$\frac{dV_{sa}}{dt} = \frac{P_a - P_1}{R_{la} + R_{sa}/2} - \frac{P_1 - P_2}{R_{sa}/2 + R_{sv}} \tag{4.32}$$

These relationships are sufficient to combine the arterial vessel model with the whole brain lumped model. In this way, we can investigate the behaviour of the arterial model in the context of the entire cerebral vascular system and ensure that any output behaviour observed from the relatively large-scale lumped model has a physiological basis. By comparing the results to experimental data measured in-vivo from humans, the overall model's behaviour in terms of the whole-brain response can thus be examined.

4.3.2 Fitting and analysis

The integration of the single vessel model into an equivalent circuit model of the whole brain vasculature next allows the autoregulatory response of the whole organ vasculature to be observed. The results presented in McCarron et al. (1997) [251] and Harper et al. (1984) [157] are suitable to validate our model as McCarron et al. (1997) [251] presented the low-pressure side of the Lassen curve in eight anaesthetized cats and Harper et al. (1984) [157] further studied the responsiveness of arteries during cerebral cortical autoregulation in rats which determined the maximum and minimum pressures for the lower and upper limits of autoregulation.

The predicted membrane voltage and the model's Lassen curve show good consistency with experimental data at both low and elevated ABP, as shown in Figure 4.6. The steady state plot of CBF against ABP exemplifies the autoregulatory response which contains the LLA, the plateau region and ULA. At pressures below 60 mmHg and above 120 mmHg, CBF was directly affected by ABP and changed significantly. However, the blood flow remained essentially constant to changes of ABP ranging from 60 to 120 mmHg. This plateau region, where changes in ABP have little impact on CBF, shows the importance of cerebral autoregulation, since it can ensure that the brain is sufficiently and continuously supplied with nutrients to maintain healthy function under various conditions.

4.4 Discussion

Since the integrated model can closely reproduce experimentally observed behaviour, i.e., the Lassen curve and the BOLD response, we can next investigate key mechanisms in NVC and autoregulation, as well as the interaction between the autoregulation and activation processes.

4.4.1 The role of the SR in the SMC

The physiologically detailed model proposed here allows us to investigate the potential role of the SR in governing the dynamic behaviour of the autoregulatory

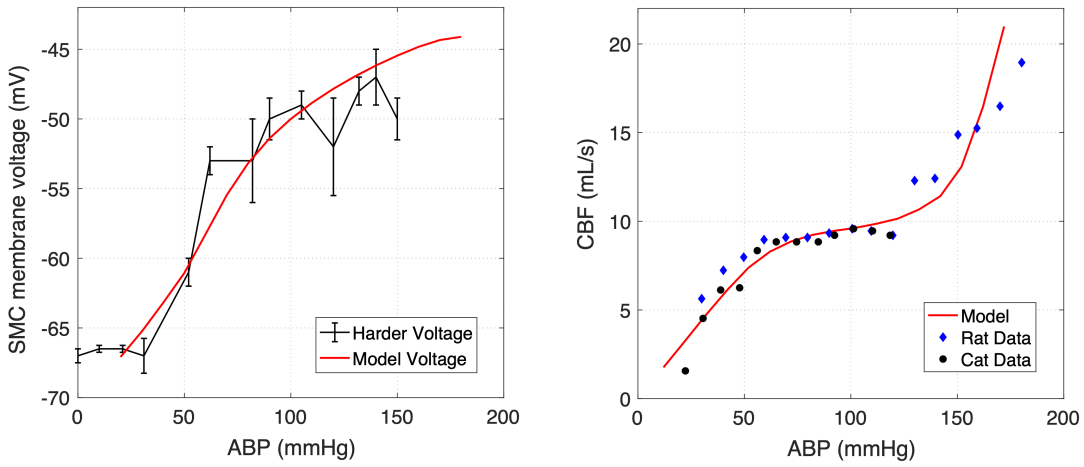


Figure 4.7: (a) SMC membrane voltage plotted against ABP. The black line represents the data from [157] and the red line represents the model output; (b) Steady state CBF plotted against ABP. The red line displays the model response, while the black circles indicate cat data from [251] and the blue diamonds indicate rat data from [157].

response. The SR has shown to be the key governor in calcium cycling, since it can provide automatic feedback control required to balance the processes of calcium storage, release, and reuptake. Figure 4.8(a) displays two stages of changes in SMC calcium concentration to an external stimulus. When pressure is elevated ($t = 50$s), membrane depolarization instantaneously triggers activation and opening of SR calcium-release channels, rapidly altering the intracellular calcium. In this case, uptake into the SR increases, thereby slowing down the rise in cytoplasmic calcium. Due to the mechanical constraints of energy coupling, the reuptake pumping is $\approx 10^5$ slower than release [24]. It should be noted that although uptake does increase, efflux from the SR will also increase owing to the higher concentration of SR calcium.

This reveals that the SR plays a key role in SMC calcium cycling and can effectively buffer the perturbation to the internal calcium concentration due to its significant calcium storage. However, as found by McCarron et al. (1997) [251], the SR has little effect on the steady state behaviour of the SMC's response to a stimulus, as shown in Figure 4.8(b). This means that the SR only increases the time constant of the dynamic response and adds inertia to the system to resist sharp changes but has

little steady state influence in the autoregulatory response. It should be noted that the volume of the SR and thus its contribution to intracellular calcium varies as a function of artery size: larger arteries have a more extensive SR and smaller arteries have little SR capacity. This is one of the major sources of structural and functional cerebral heterogeneity. Considering that large and medium-sized arteries contribute a major fraction of cerebrovascular resistance in the brain, models based on regional arterial data can still highlight the importance of SR in overall cerebrovascular regulation to a large extent.

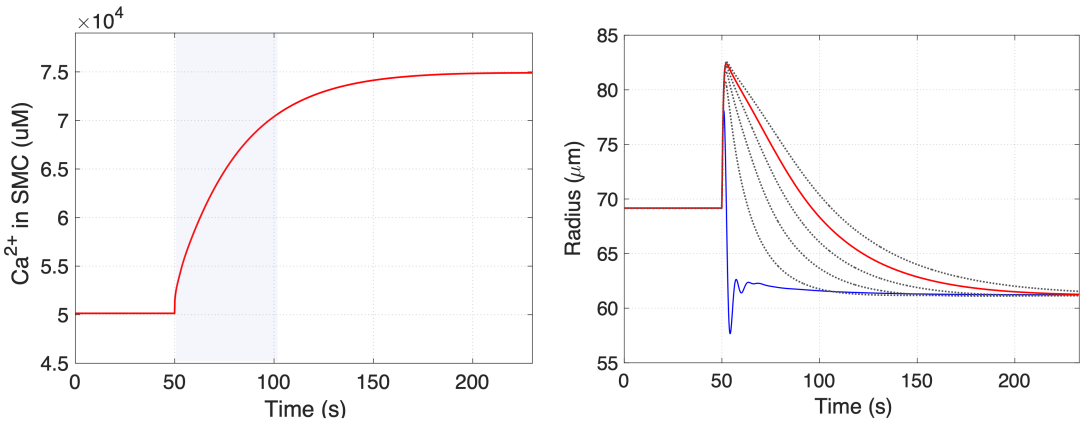


Figure 4.8: (a) SMC calcium concentration plotted against time; (b) Resulting arteriole radius against time. Blue line shows the output without uptake ($B_{SMC} = 0$). Grey lines show outputs when B_{SMC} is equal to 20, 40, 60 and 100, from left to right respectively. Red line shows the original output from the model ($B_{SMC} = 80$). The input is a step increase in transmural pressure from 60 mmHg to 80 mmHg.

4.4.2 The role of stretch channels in the myogenic response

Owing to the fact that transmural pressure only directly affects the stretch channels in this study, its role in the transformation of stretch into active force development by the SMC contractile activity can be determined. Takenaka et al. (1998) [31] found that elevated transmural pressure can increase intracellular calcium through the activation of SACs. Kirber et al. (1992) [252] proposed that membrane stretch can exert influence on the gating behaviour of the VOCCs. These findings have led to the hypothesis that the SACs initiate the myogenic response and consequently elevate intracellular calcium. The results of this study can contribute to recognising

the role of SACs in increasing the SMC calcium during changes in transmural pressure.

At membrane potentials in the range -70 mV to -40 mV, the activation of the VOCCs increases exponentially with membrane depolarization, thereby providing a sustained calcium influx [253]. However, as shown in Figure 4.7, when ABP is greater than 140 mmHg, both the membrane voltage of the model and the experimental data from Harper et al. (1984) [157] are shown to saturate (at about -45 mV). At the same time, CBF rises sharply with increasing transmural pressure, revealing that the membrane voltage is unable to exert adequately autoregulatory control on the system. Interestingly, the SACs are observed to saturate at transmural pressures around 140 mmHg. Therefore, it is plausible that the SACs are a key driving force in the myogenic response and play a role in the activation of the VOCCs. Otherwise, the ULA would be higher and the plateau region would be wider because the increased VOCCs activity at high potentials could maintain an adequate autoregulatory response. In other words, the depolarization of the SMC following an increase in cytoplasmic calcium, caused by the activation of SACs, results in the recruitment of the VOCCs and consequent vasoconstriction. This finding is consistent with the myogenic mechanism model proposed by Davis et al. (1992) [32], in which transmural pressure modulated stretch channels drive the myogenic response.

4.4.3 Impact of the Shear Stress Response on the SMC Membrane Voltage

In addition to directly inducing vasodilation through the production of cGMP in the SMC, the shear stress response can also indirectly increase the arteriole radius by altering the SMC membrane voltage. Stockand and Sansom (1996) [248] pointed out that the presence of cGMP in the SMC causes additional vasodilation by reducing the SMC calcium concentration, which has been confirmed by the results of the model. Figure 4.9(a) show that the steady state open probability of calcium activated potassium channels is greater in the flow case than in the no flow

case. This, in turn, causes the steady state efflux of potassium from the SMC to be larger, leading to a lower membrane potential under the flow case, as shown in Figure 4.9(b). The additional vasodilatory element is a result of the fact that at lower membrane voltages, the VOCCs are less active, thereby causing slight hyperpolarization and reducing the intracellular calcium concentration. Although this vasodilation effect is relatively small, this behaviour is important to note as it reveals another influential element of the shear stress response. This result and hyperpolarization caused by the cGMP emphasis the central role played by potassium ions in setting the membrane voltage of the SMC.

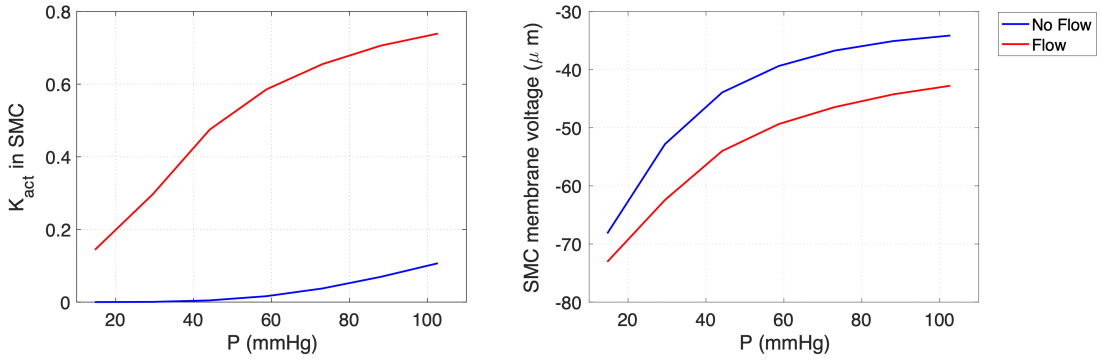


Figure 4.9: (a) Steady state open probability of calcium activated potassium channels against transmural pressure (b) SMC membrane voltage against transmural pressure. (Conditions are taken from Figure 4.7)

4.4.4 The role of NO in autoregulation and NVC

While it is widely known that NO is a vital cerebral vasodilator, there is wide debate about how much of an active role it plays in NVC and which pathway provides the governing source of NO for regulating vascular dynamics. As shown in Figure 4.10, the inclusion of the neuronal NO pathway results in only a moderate increase in the SMC NO concentration. Furthermore, during periods of stimulation (where it would be expected that neuronal NO would drive an increase in SMC NO), the contribution of neuronal NO is relatively minor in comparison to endothelial NO, which indicates that the endothelium acts as the primary supply of vasodilatory NO. However, the endothelial mechanism responsible for the NO dynamics is not

the shear-stress-induced release of NO but instead the rise in endothelial calcium initiating the activation of eNOS.

Although the neuronal NO is not the prominent provider for the SMC, it plays a key role in modulating other neurovascular pathways. The increase of cGMP via NO signalling pathway enhances potassium efflux due to the larger opening probability of the BK channel. This leads to a decrease in the SMC membrane potential and consequently calcium concentration, resulting in a further vasodilation. Our finding that nNOS-derived NO is involved in mediating cerebrovascular regulation is supported by several experimental studies. Lindauer et al. (1999) [254] found that neuronal NO production largely acts as a modulator as opposed to a mediator in the coupling of neuronal activation and regional CBF in the rat cortex. Mulligan and MacVicar (2004) [255] found that the inhibition of nitric oxide synthase (NOS) blocked vascular constrictions caused by 20-HETE. In addition, the NO directly released from the cerebral perivascular parasympathetic nitrergic nerve terminals may influence contractile dynamics.

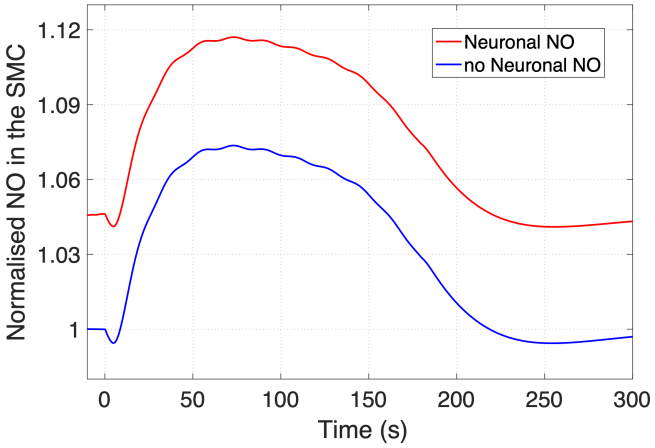


Figure 4.10: Normalized NO Concentration in the SMC. Baseline is taken as the case where the neuronal NO pathway is not activated. Blue line indicates no neuronal NO production while red line indicates that neuronal NO production is activated.

4.5 Sensitivity Analysis

This model involves hundreds of parameters, and the values of these parameters are often derived from animal experiments. However, the poor translation rate

between animal models and human subjects has been acknowledged for many years. The uncertainty in parameter values contributes to the uncertainty in the model outputs. Sensitivity analysis can determine the influence of parameters by assigning the relative contribution to output uncertainty to individual parameters. By only correcting the parameters with larger influence and fixing the parameters with smaller or no influence, the workload of model correction can be reduced.

Parameter sensitivity analysis methods are mainly divided into local sensitivity analysis and global sensitivity analysis. The local sensitivity analysis only analyses the influence of a single parameter change on the model output, while the global sensitivity can analyse the influence of the entire parameter space on the model result. Because global sensitivity analysis has the characteristics of analysing the influence of each parameter and the interaction between parameters on the model results, it is applied to this study to determine which of the many parameters have the greatest effect and which have very little effect.

Although there is a substantial amount of research current being done in applied mathematics and statistics in the corresponding field of GSA, it is still difficult to meaningfully define 'influential' and 'non-influential' and develop methods applicable to high-dimensional problems. Morris method, an important GSA technique, employs a differential approach to assess the sensitivity of each parameter, thereby reducing computational costs. It is particularly suitable for analysing models with a large number of parameters, making it a suitable choice for our model.

4.5.1 Methods

This integrated model consists of 331 parameters, most of which are derived from non-human experiments. Some essential physiological pathways, such as nitric oxide, potassium, and calcium pathways, have been established to play a significant role in the normal functioning of NVC and autoregulation. However, certain parameters in the model, such as leak terms, are known to have minimal effects on blood flow regulation. Therefore, these parameters will be fixed at nominal values to reduce

computational costs. By permitting variability in only the parameters that support important physiological pathways, the dimension of the parameter space is reduced from 331 to 196, greatly facilitating subsequent calculations and analyses.

There are many ways to define the parameter space. While some parameters may have inherent bounds, for others, it is possible to arbitrarily choose the limits of the parameter space for sensitivity analysis samples. Alternatively, we can define the parameter space to extend a fixed percentage on either side of the best-fitting values. This may be a better strategy as it ensures that the parameter space is centred on a point where all the mechanisms of the model are active. Conversely, increasing the width of the interval resulted in many samples for which the solution exhibited atypical or non-physical behaviour, or in some cases ode15s was unable to solve the system.

Therefore, we give each $\theta_i, i = 1, \ldots, 196$, a nominal value $\bar{\theta}_i$ and assume each parameter to be independent and uniformly distributed over the interval $[0.9\bar{\theta}_i, 1.1\bar{\theta}_i]$ (within $\pm 10\%$ of the nominal value). Our choice of $\pm 10\%$ uncertainty is considered a reasonable compromise between accounting for uncertainty and ensuring computational feasibility. The results of sensitivity analysis are typically presented as a graph showing the relationship between the variance (σ) and the mean (μ), representing the sensitivity of the output to variations in each parameter.

In order to get high efficiency, we use the Linear Regression model in MATLAB to fit our model after determining the parameter distribution. We evaluate the model outputs at M (M=300) different samples, denote them $\theta^k, k = 1, 2, \ldots, M$:

$$g(\theta^k) = g(\theta_1^k, \ldots, \theta_P^k) \approx \beta_0 + \sum_{j=1}^{196} \beta_j \theta_j^k, \quad k = 1, \ldots, M \tag{4.33}$$

This approach yields a crude GSA of the model with respect to the θ_j's, $j = 1, \ldots, 196$. We assign a preliminary importance measure to each θ_j by computing for each of them the relative size of their coefficient in the above linear approximation, i.e.

$$L_j = \frac{|\beta_j|}{\sum_{\ell=1}^{196} |\beta_\ell|}, \quad j = 1, \ldots, 196 \tag{4.34}$$

To obtain a model with a more manageable size, we reduce the parameter space to only the θ_j's for which $L_j > 0.01$. We denote these r parameters $\{\theta_{j_i}\}_{i=1}^{r}$. The rest of the parameters are regarded as non-influential and treated as latent variables, even though they are uncertain, their specific values have little effect on the model results within the given range. In other words, we consider the approximation:

$$g(\theta_1, \ldots, \theta_{196}) \approx h(\theta_{j_1}, \ldots, \theta_{j_r}) \tag{4.34}$$

where h is obtained from g by treating the non-influential parameters as latent.

This reduction yields 11 parameters instead of the original 196. Parameters located closer to the origin have less effect on the model output than parameters found further away. We use $\hat{\theta}$ to denote the reduced parameter vector. The reduced parameter vector being defined to extend $\pm 10\%$ or $\pm 20\%$ either side of the optimal values is shown in Table 4.1. Then we used the elementary effects method proposed by Morris [256], contained in the SAFE toolbox to conduct sensitivity analysis and explore the most influential factors that determine CBF.

Table 4.1: Bounds placed on variables during optimization and used to define the limits of the parameter space for additive sensitivity analysis.

Parameter	Description	Optimal Value
$g_{NaP,GHK}$	channel conductance	2e-6
R_0	steady state values of radius	1.9341e-5
k_{O2}	O_2 reaction rate constant	9.6e-6
$\alpha_{stretch}$	Slope of stress dependence of the SAC activation sigmoidal	1.05e-4
t_w	thickness of vessel wall	15e-6
k_{Ca1}	phosphorylation Ca2+ sensitivity constant	3e-6
k_{cGMP}	dephosphorylation [cGMP] sensitivity constant	3e-5
f_i	friction from cycling cross-bridges	9.34e-6
l_0	relaxed length of cell	7.7479e-5
λ_{opt}	normalized cell length at max overlap	1.49
w_c	effective width of muscle cell	2.6667e-6

4.5.2 Results

The results of the sensitivity analysis were shown in Figure 4.11. The mean value (x-axis) quantifies the influence of each parameter, while the standard deviation

(y-axis) quantifies the non-linear and interaction effects of each parameter on the output variations. It can be observed that the parameters of the mechanical model in the SMCs have the greatest impact on the model's output, while the parameters in the NVU exhibit considerably lower significance. This disparity arises due to the greater level of detail in the NVU's physiological pathways compared to the mechanical model, with each pathway involving a larger number of parameters that affect calcium and cGMP levels in SMCs. Consequently, the lower apparent importance of these parameters should not be interpreted as a direct reflection of the physiological relevance of the mechanisms involved; rather, it is a result of the sensitivity analysis outcomes.

The two ranges of sensitivity analysis yield quite similar results with only the different order of R_0 and $g_{NaP,GHK}$. This is not surprising considering that myogenic response is the primary regulatory mechanism within the autoregulatory range. Except for the saturation level of [cGMP], all the parameters in the NO (nitric oxide) system are relatively unimportant. Our findings suggest that perturbations in Ca2+ levels will greatly affect the regulation of blood flow. Conversely, excessive NO has little influence on vessel diameter since cGMP is already saturated.

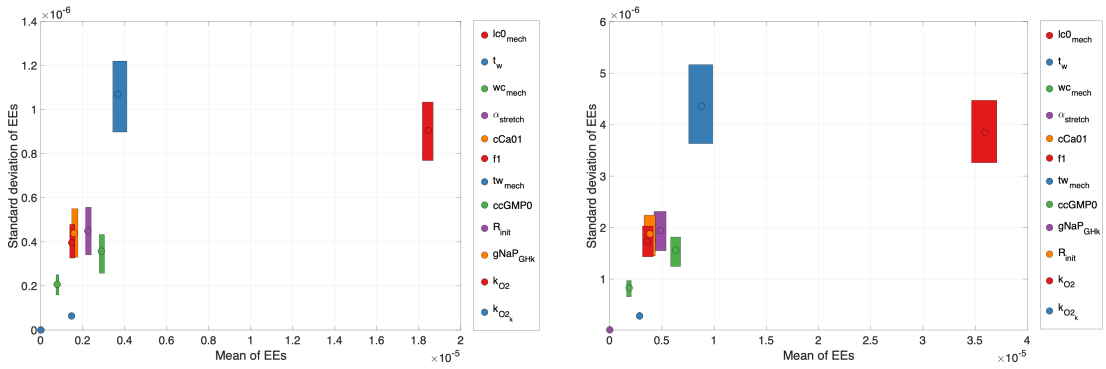


Figure 4.11: Mean and standard deviation of elementary effects for integrated model based on fractional changes (10%, 20%) in each model parameter.

4.6 Conclusions

The physiological based mathematical model for the whole brain vasculature proposed in this study investigates the responses of both cerebral autoregulation

and NVC for the first time. This is achieved by firstly constructing a single vessel model and then scaling it as a part of the lumped compartment model. The good consistency between model simulations and experimental data under both steady state and dynamic conditions provides initial validation of the model. We can thus use this combined approach to further examine the key physiological mechanisms in CBF control, which would not have been feasible if either autoregulation or NVC were studied purely in isolation.

Since the SR in the SMC governs calcium release and reuptake during muscle contraction through feedback control, it is able to moderate sharp changes in the dynamic response to different intramural pressures and pressure gradients. The plateau along with the relatively low ULA observed in the Lassen curve reveals that SACs appear to be the crucial initiating factor to the recruitment of VOCCs and the subsequent myogenic response. Apart from the direct impact on cGMP production, the shear stress response also has a relatively small effect on the membrane potential and hence the SMC calcium concentration, leading to additional vasodilation. Although the endothelium has been shown to be the most influential NO producer, the neuronal NO plays an important role in modulating NVC mechanisms and hence smooth muscle tone.

In order to improve clinical guidelines for cerebrovascular diseases, more work is required in developing further these quantitative approaches. Since the activation responses are purely a result of vasodilatory mechanisms, more detailed mathematical models need to be developed to include vasoconstriction mechanisms in the NVC, i.e. considering the AA metabolite, 20-HETE [21]. In addition, CBF is sensitive to changes in blood gas levels, whereas our model is not able to consider this response. There is substantial evidence that changes in arterial CO_2 blood gas levels significantly impact the autoregulatory response [27]. It is thus logical to include the cerebrovascular reactivity mechanism in a future study due to its importance in interpreting measurements such as the BOLD signal [257]. In addition, it is assumed that arterioles are the sole controller of CBF in this study. However, pericytes

have been shown to affect the blood flow and to prolong the decrease of CBF after ischaemia and reperfusion [258]. These additional pathways open up new fields for future exploration and go further in ensuring the physiological reality of this CBF model.

5

Integrated model of cerebral oedema and osmotherapy

This chapter aims to evaluate the clinical application potential of cerebral autoregulation model developed in Chapter 4. By employing the CA model, relationships between arterial blood pressure, vessel radius, and cerebral blood flow were established. These relationships are then applied to dynamically adjust arterial permeability within a multi-compartment porous Finite Element model, aiming to enhance the accuracy of computational modelling for cerebral oedema treatment. Compared to the original model, the improved model demonstrates enhanced consistency in managing intracranial pressure during the rebound phase following osmotherapy and aligns more closely with clinical data. Sensitivity analysis reveals that parameters such as tissue hydraulic conductivity and capillary wall permeability are crucial for the effectiveness of osmotherapy. These results underscore the potential of the enhanced model to tailor treatment protocols based on individual patient needs, thereby potentially improving treatment outcomes and minimizing side effects.

5.1 Introduction

The healthy functioning of the human brain relies on a consistent and adequate perfusion to support cerebral metabolism. Stroke is one of the most important causes of brain damage, ranking as a leading cause of death and disability worldwide. Ischaemic stroke, the much more common type of stroke, is primarily caused by vascular obstructions such as thrombosis. When this occurs, a certain area of the brain experiences a reduction in blood supply, leading to insufficient oxygen and nutrients reaching the brain tissue, resulting in brain cell damage or death. The clinical significance of stroke has spurred extensive research into developing treatments for improved outcomes. Reperfusion therapy is a principal treatment for ischaemic stroke, utilizing pharmacological agents (e.g., thrombolytics) or mechanical procedures (e.g., endovascular surgery) to remove vascular obstructions and quickly restore blood flow to the affected area, thereby minimizing brain cell damage. However, when blood flow to the Ischaemic areas is suddenly restored, it can lead to fluid accumulation in the brain tissues, known as cerebral oedema. This condition can increase intracranial pressure and brain tissue stress, exacerbating damage to the blood-brain barrier and cellular injury, resulting in more severe neurological impairments [259].

Osmotherapy is a treatment modality widely employed to reduce ICP and manage cerebral oedema. By administering osmotic agents intravenously to elevate blood osmolarity, it facilitates the movement of water from brain tissues into the bloodstream, thereby alleviating cerebral oedema and lowering ICP. Although osmotherapy holds significant therapeutic value in treating acute brain conditions such as traumatic brain injuries, cerebral haemorrhage, and stroke, it must be used with caution, as improper application can lead to electrolyte imbalances, dehydration, and other adverse effects [260]. Therefore, this treatment is typically administered under strict medical supervision to ensure both safety and efficacy.

Mannitol, hypertonic saline, sorbitol, and glycerol are common osmotic agents used in osmotherapy. Compared to traditional mannitol, hypertonic saline offers a more sustained effect in reducing ICP, which is particularly crucial for patients requiring long-term ICP management. Unlike glycerol and sorbitol, which may cause risks of electrolyte imbalance and dehydration, hypertonic saline effectively increases blood osmolarity, facilitating the movement of water from brain tissues into the vascular space, thus alleviating cerebral oedema [261]. Additionally, hypertonic saline can improve the rheological properties of blood, aiding in the restoration of CPP and MAP. Given the increasing clinical use of hypertonic saline and its unique benefits, this study focuses on this osmotic agent.

The multi-compartment porous Finite Element model, by simulating the complex fluid dynamics and tissue interactions within the brain, has been demonstrated to effectively predict the therapeutic outcomes of osmotherapy [262]. Compared to traditional clinical trials, modelling analysis offers more flexibility and accuracy in assessing the effects of different therapeutic parameters such as dosage, infusion time, and retention time of osmotic agents, thereby reducing the costs and resources associated with traditional clinical experiments. However, the existing model does not include the mechanism of cerebral autoregulation. During Ischaemic stroke and subsequent treatments, particularly when osmotic agents are used, arterial blood pressure fluctuations can be severe. The fixed values for vessel permeability in the existing model may lead to inaccurate predictions of ICP changes. Additionally, the existing model fails to account for impaired cerebral autoregulation in pathological conditions such as post-stroke, limiting its clinical applicability.

Therefore, this study aims to incorporate the cerebral autoregulation mechanism into the existing multi-compartment porous finite element model to enhance the accuracy and practicality of the model. The ultimate goal of this work is to provide more precise treatment protocols for the clinic and minimize potential side effects, thereby improving outcomes for patients suffering from Ischaemic stroke and other conditions that lead to increased ICP. The study consists of the following parts:

(1) coupling the cerebral autoregulation model with the multi-compartment porous finite element model to refine its predictive capabilities; (2) comparing the results of the optimized model against both the original model and actual clinical data to validate its effectiveness; (3) conducting a sensitivity analysis of physiological parameters that influence the success of osmotherapy. The results of this analysis help to achieve a balance between reducing ICP and controlling potential side effects, thus providing new insights for clinical treatment.

5.2 Methods

The brain is assumed to consist of four compartments, i.e., tissue, arterioles, capillaries, and venular networks, it can be regarded as a multi-network fluid dynamics system. The multi-compartment porous finite element model comprises three 3D models, each dedicated to simulating blood perfusion, oedema, and osmotherapy. This chapter begins with a brief introduction to these three 3D models, followed by a detailed explanation of how the cerebral autoregulation model introduced in Chapter 4 is coupled into the multi-compartment porous finite element model through vascular permeability.

5.2.1 Perfusion Model

Governing equations

In the perfusion component, the brain is modelled as a three-compartment porous medium, consisting of arteriolar, venular, and capillary blood compartments [263]. The governing equations for the three porous compartments are based on fluid dynamics and porous media flow theory, where the left-hand side of the equations represents the blood flow within each compartment, while the right-hand side describes the fluid transfer between different compartments:

$$\nabla \cdot (K_a \nabla p_a) = \omega_{ac} \cdot (p_a - p_c) \tag{5.1}$$

$$\nabla \cdot (K_c \nabla p_c) = -\omega_{ac} \cdot (p_a - p_c) + \omega_{cv} \cdot (p_c - p_v) \tag{5.2}$$

$$\nabla \cdot (K_v \nabla p_v) = -\omega_{cv} \cdot (p_c - p_v) \tag{5.3}$$

where p_a, p_c and p_v are the Darcy pressures in the arteriole, capillary, and venule compartments respectively. K_i is the permeability tensor of compartment i, whereas ω_{ij} represents the fluid transfer coefficient between compartments i and j. Note that the transfer coefficients are different in white matter and grey matter and can thus be further defined by ω_{ac}^{w}, ω_{ac}^{g} and ω_{cv}^{w}, ω_{cv}^{g}, respectively.

In mathematical models, differences in permeability in different directions of porous media can be described by a tensor field to reflect anisotropy. According to previous studies [262, 263], the arterioles and venules are assumed to comprise penetrating vessels perpendicular to the pial surface, and arteriole and venule compartments are therefore modelled as anisotropic and inhomogeneous porous media. In these compartments, the resistance and directionality of blood flow vary due to the characteristics of vascular structure and arrangement. Conversely, the capillary vessels form an interconnected network, and this compartment is thus considered a porous medium with isotropic and homogeneous permeability [264]. Using a scalar field instead of a tensor field can simplify the equations while still accurately describing the fluid movement within this vascular structure.

Boundary conditions

Different boundary conditions were used to simulate blood entry and exit through different compartments. Blood flows through penetrating arteriolar branches into the brain and returns via penetrating venular branches on the surface of the brain membrane. Each of the posterior, middle, and anterior cerebral arteries on both the left and right hemispheres supplies a distinct sub-territory at the pial surface. As no modifications were made to the original perfusion model, for details regarding the perfusion territories corresponding to large arteries and a summary of the boundary conditions of the perfusion model, refer to [262].

Blood flows exclusively within the capillary network and does not directly exchange with these surfaces. Therefore, blood flow through pial surface and ventricle surface in the capillary compartment is set to be zero. Based on experimental data, the

pressure in the venular compartment on the cortical surface is assumed to be 15 mmHg, while the pressure in the arteriolar compartment on the pial surface is approximately 90 mmHg [265]. These values represent the normal pressure levels of blood vessels in different regions of the brain. To account for arterial occlusion scenarios, blood flow through the perfusion territory of an occluded vessel is set to zero whereas pressure on the pial surface is assumed to remain constant in other regions. Boundary conditions of the perfusion model are summarized in Table 5.1.

Table 5.1: Boundary conditions for the perfusion model.

	Cortical Surface	**Ventricle Surface**
Arteriole Blood	$p_a = 90$ mmHg (non-occluded regions); $K_a \nabla p_a = 0$ (occluded regions);	$K_a \nabla p_a = 0$
Capillary Blood	$K_c \nabla p_c = 0$	$K_c \nabla p_c = 0$
Venule Blood	$p_v = 15$ mmHg	$K_v \nabla p_v = 0$

5.2.2 Oedema and Osmotherapy Model

The exchange of flow between the capillary network and the interstitial space is negligible in a healthy brain. However, in a damaged brain, this flow exchange becomes significant, and therefore, an extra compartment for interstitial fluid is needed to accurately model oedema and osmotherapy. Another distinction from the Perfusion Model is that modelling oedema and osmotherapy requires consideration of time-dependent effects, whereas the perfusion model only estimates steady-state blood flow in the microcirculation. Due to the large difference between the BBB permeability in the damaged region and the healthy region, the flow from capillary blood to the interstitial space and the flow of interstitial fluid in healthy tissue is thus neglected.

Governing equations

Governed by the laws of mass conservation and Darcy's law, the governing equations are as follows:

$$c_w \frac{\partial p_w}{\partial t} = \nabla \cdot (K_w \nabla p_w) + S_{cw}, \tag{5.4}$$

$$c_b \frac{\partial p_a}{\partial t} = \nabla \cdot (K_a \nabla p_a) - \omega_{ac} \cdot (p_a - p_c), \tag{5.5}$$

$$c_b \frac{\partial p_c}{\partial t} = \nabla \cdot (K_c \nabla p_c) + \omega_{ac} \cdot (p_a - p_c) - \omega_{cv} \cdot (p_c - p_v) - S_{cw}, \tag{5.6}$$

$$c_b \frac{\partial p_v}{\partial t} = \nabla \cdot (K_v \nabla p_v) + \omega_{cv} \cdot (p_c - p_v), \tag{5.7}$$

where:

- c_w and c_b are the storage factors of the interstitial fluid and blood in the brain tissue.
- p_w, p_a, p_c, and p_v represent the pressure in the interstitial space, arteries, capillaries, and veins, respectively.
- K_w, K_a, K_c, and K_v denote the hydraulic conductance.
- S_{cw} is the fluid transport from the vasculature into the interstitial space. The value of the S_{cw} term in the normal BBB has been estimated by Ref. [266] and this value can increase by more than 100 times its normal value in pathology [267].

The S_{cw} represents fluid transfer between the capillary and the interstitial fluid compartments in oedema model [262]:

$$S_{cw} = 2n_b \frac{L_p}{R_c} \left[(p_c - p_w) - \sigma \Pi_c \right] \tag{5.8}$$

where:

- L_p is the hydraulic permeability of the capillary wall.
- Π_c is the osmotic pressure for the plasma components in the blood before osmotherapy.
- σ is the reflection coefficient of the original plasma composition.
- n_b is the volume fraction of blood vessels in a unit volume of brain tissue.
- R_c is the mean vessel radius.

Boundary conditions

In osmotherapy model, an additional term $\sigma_{\mathrm{NaCl}} \Pi_{\mathrm{NaCl}}$ is introduced to describe the osmotic pressure rise induced by the hypertonic saline:

$$S_{cw} = 2n_b \frac{L_p}{R_c} \left[(p_c - p_w) - \sigma \Pi_c - \sigma_{\mathrm{NaCl}} \Pi_{\mathrm{NaCl}} \right] \tag{5.9}$$

where:

- σ_{NaCl} is the reflection coefficient of hypertonic saline.
- Π_{NaCl} is the osmotic pressure of the saline.

In the oedema model, it is assumed that there is no occlusion and therefore blood perfusion is restored. Since normal ICP is around 5–15 mmHg, the baseline value of the interstitial fluid pressure is taken here to be 10 mmHg and the boundary conditions are as summarized in Table 5.2.

Table 5.2: Boundary conditions for the oedema and osmotherapy model.

	Cortical Surface	**Ventricle Surface**
Arteriole Blood	$p_a = 90$ mmHg	$K_a \nabla p_a = 0$
Capillary Blood	$K_c \nabla p_c = 0$	$K_c \nabla p_c = 0$
Venule Blood	$p_v = 15$ mmHg	$K_v \nabla p_v = 0$
Interstitial Fluid	$p_w = 10$ mmHg	$p_w = 10$ mmHg

5.2.3 Model Coupling

Coupling between perfusion model and oedema and osmotherapy model

The location of leaking vessels obtained from the perfusion model is then used within the oedema model. The perfusion in brain tissue of the healthy and stroke scenarios can thus be compared. The perfusion (F) and perfusion change (ΔF) are given as:

$$F = \omega_{ac} \cdot (p_a - p_c) \tag{5.10}$$

$$\Delta F = \frac{F_{\mathrm{healthy}} - F_{\mathrm{occluded}}}{F_{\mathrm{healthy}}} \times 100\% \tag{5.11}$$

A threshold of 70% or greater reduction in blood perfusion is used to define the location of leaking vessels. Thereafter, the pressure field in the oedema is simulated until the ICP (defined to be the same as p_w) reaches equilibrium. Finally, the osmotherapy is assumed to be performed after the ICP reaches equilibrium and thus the pressures at the final step in oedema model are used as the initial pressures in the osmotherapy model, as shown in Figure 5.1. Most parameters of the model

are taken from experimental studies; however, it should be noted that some of these values are difficult to obtain and thus are associated with relatively high uncertainty.

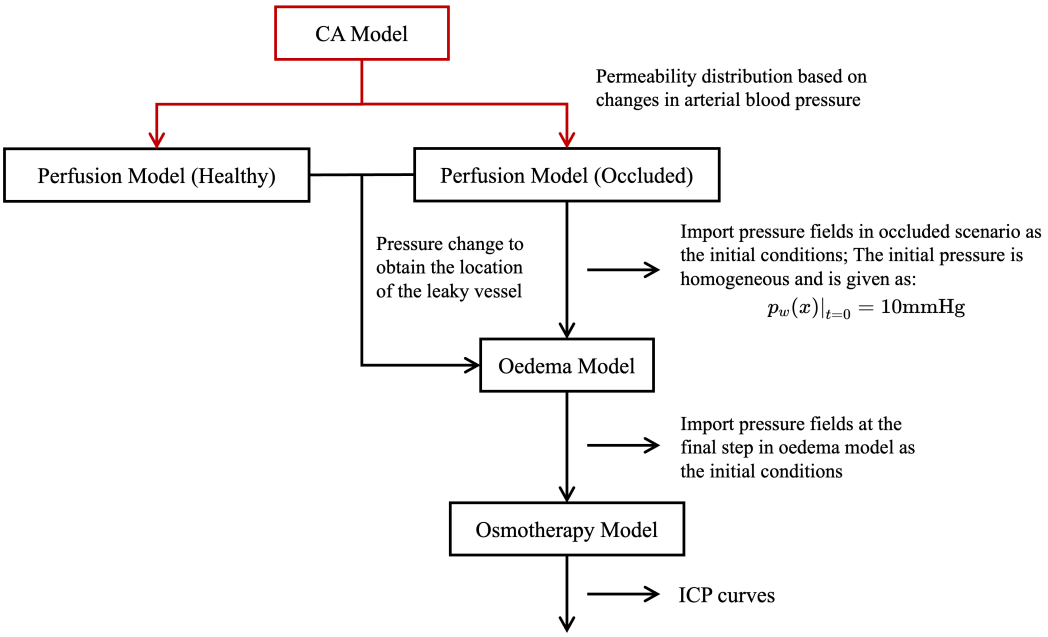


Figure 5.1: Flowchart demonstrating how the CA model and the Finite Element models are coupled.

Coupling between CA Model and Finite Element Model

The permeability tensors (K_a, K_c and K_v) of the porous model need to represent the complex structure of the vasculature. Penetrating vessels, including Descending Arterioles and Ascending Veins, in the cortex tend to be aligned normal to the pial surface. Consequently, the permeability tensors of the arteriole and venule compartments are similar but anisotropic and inhomogeneous. On the contrary, it has been reported that the permeability tensor of the capillary compartment is approximately isotropic [268, 269]. Based on statistically accurate capillary network simulations [270], the capillary permeability in the grey matter can be described by a single scalar: $K_c = 4.28 \times 10^{-4}[\text{mm}^3\text{skg}^{-1}]$. For simplicity we use the assumptions first proposed by [271]:

$$K_v = 2K_a \tag{5.12}$$

The permeability k_a of a "vessel bundle" with laminar flow within k_{vb} can be estimated as:

$$k_a \approx k_{vb} = \frac{n_v D^4 \pi}{128 \mu_b A_{ref}} \tag{5.13}$$

where:

- n_v is the number of vessels corresponding to a reference cortical surface area A_{ref}.
- D is the characteristic diameter of the vessels.
- μ_b is the in vitro dynamic viscosity of blood depending on the diameter and the haematocrit.

In previous chapter, we have established a physiologically based mathematical model to simulate CBF autoregulation mechanisms in response to changes in arterial blood pressure. The model functions by altering the vascular resistance, primarily through changes in the vascular diameter, to buffer against blood pressure volatility thereby safeguarding cerebral perfusion. Using the Hagen-Poiseuille Equation, the vascular diameter is given by:

$$D = 2 \cdot R = \sqrt[4]{\frac{8 \mu Q L}{\pi \Delta p}} \tag{5.14}$$

Through these steps, we can simulate the dynamic adjustments of vascular permeability in response to changes in ABP. This is consistent with experimental findings: an increase in blood flow as a consequence of vasodilation will increase vascular permeability [272].

Numerical method

The numerical solution of the governing equations for this study is carried out using Python with a high performance open source Finite Element library, FEniCS [273, 274]. Within the finite element model, highly coupled equations are solved in a mixed function space that represents a multi-compartment dynamic system. The pressures in each compartment (p_i) are discretized using piecewise linear Lagrange

elements. Permeability (K_i) and other coefficients (ω_{ij}, L_p, etc.) are represented in piecewise constant tensor and scalar function spaces, respectively. The flow fields and blood perfusion are computed within dP0 elements and solved using the Bi-Conjugate Gradient Stabilized method (BiCGSTAB) with an Algebraic Multigrid (AMG) preconditioner. The model employs a backward Euler scheme for discretizing time steps. The mesh used in this study comprises 1.4 million tetrahedral elements, and a grid convergence study has been conducted as detailed in a previous study [275].

5.3 Results

5.3.1 Model Validation

The effective osmotic pressure of hypertonic saline is fitted with data points measured during clinical treatment of patients who suffered from hemispheric stroke and underwent osmotherapy [214]. In this study, the concentration of hypertonic saline during infusion (T_{in}) is set at 15 minutes, reaching a peak value of 11.2 mmol/L, and gradually decreases to 5.9 mmol/L 45 minutes after the infusion ends. To model the experimental concentration curve accurately, the increase in concentration during the injection phase is assumed to follow a sigmoid function, expressed as:

$$\sigma_{\mathrm{NaCl}}\Pi_{\mathrm{NaCl}} = \frac{\Pi_{\mathrm{Max}}}{1 + e^{\frac{15(0.5T_{in}-t)}{T_{in}}}}, \quad 0 \leq t \leq T_{in} \tag{5.15}$$

After the injection phase, the concentration of hypertonic saline is assumed to decline exponentially as it is excreted from the body. This decay is characterized by a rate ($\dot{D} = 0.01424\,\mathrm{min}^{-1}$), and the concentration drop is modelled as:

$$\sigma_{\mathrm{NaCl}}\Pi_{\mathrm{NaCl}} = \Pi_{\mathrm{Max}} e^{-\dot{D}(t-T_{in})}, \quad T_{in} < t \leq 240\,\mathrm{min} \tag{5.16}$$

The maximum effective osmotic pressure (Π_{Max}) induced by the increase in NaCl osmolarity is determined to be 1800 Pa. This osmotic pressure ($\sigma_{\mathrm{NaCl}}\Pi_{\mathrm{NaCl}}$) captures the dynamic response of the osmotic agent over time within the human body as illustrated in Figure 5.2(a).

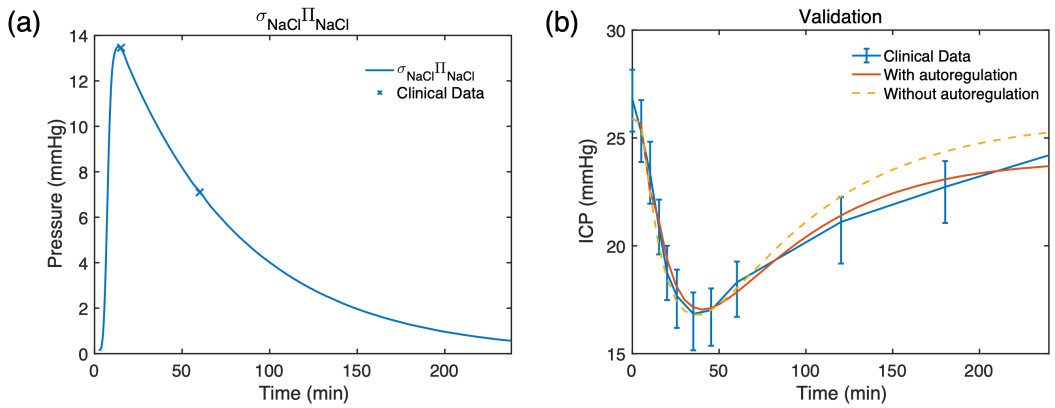


Figure 5.2: (a) The effective osmotic pressure of hypertonic saline with clinical data points. The clinical data obtained from 22 osmotherapy episodes are presented as mean ±SE (right). (b) The validation curve of the ICP under different conditions, including clinical data, simulation results with autoregulation, and simulation results without autoregulation.

The perfusion model is used to identify the location of leaking vessels. Since the exact location of the ICP probe in the clinical study is unknown, the maximum simulated ICP at different time instants is used for comparison with the clinically measured ICP curves. By substituting the effective osmotic pressure $\sigma_{\mathrm{NaCl}}\Pi_{\mathrm{NaCl}}$ into the governing equations, we obtain the simulation results of the dynamic ICP during an episode of osmotherapy, as shown in Figure 5.2(b).

Both the initial model (yellow dashed line) and the optimized model (orange line), which incorporated cerebral autoregulation, captured that the ICP is significantly elevated due to cerebral oedema. Following the injection of the hypertonic saline, the ICP rapidly decreases to a nadir before gradually rising back to near-peak levels after approximately 35 minutes as the agent is excreted. However, the optimized model aligns more closely with the observed clinical data (blue line with error bars) compared to the original model, particularly in the later stages following hypertonic saline injection. This comparison indicates that incorporating the autoregulation mechanism may enhance the model's capability to capture and forecast the ICP response to osmotherapy more accurately. Consequently, this optimized model has the potential to serve as a more powerful tool for effective clinical application and the formulation of therapeutic strategies.

Studies indicate that strokes can impair autoregulation. Therefore, we explored the impact of autoregulatory capacity on the effectiveness of osmotherapy. This was achieved by multiplying the arterial permeability obtained from the CA model by a preservation factor ranging between 0 and 1, where 0 represents completely impaired autoregulation and 1 indicates normal autoregulatory function. Simulation results (as shown in Figure 5.3) indicate that patients with normal autoregulatory capabilities exhibit a rapid decline in ICP following saline injection, followed by a gradual increase, ultimately stabilizing at a lower level, suggesting better therapeutic outcomes. Conversely, in cases of partial or severe impairment of autoregulation, ICP rises more swiftly and stabilizes at higher levels, indicating that reduced autoregulation leads to diminished effectiveness of osmotherapy. In the absence of autoregulation, ICP experiences the greatest fluctuations, underscoring the critical importance of a fully functional autoregulatory mechanism in maintaining ICP stability. These findings emphasize the importance of maintaining and restoring autoregulatory functions during treatment.

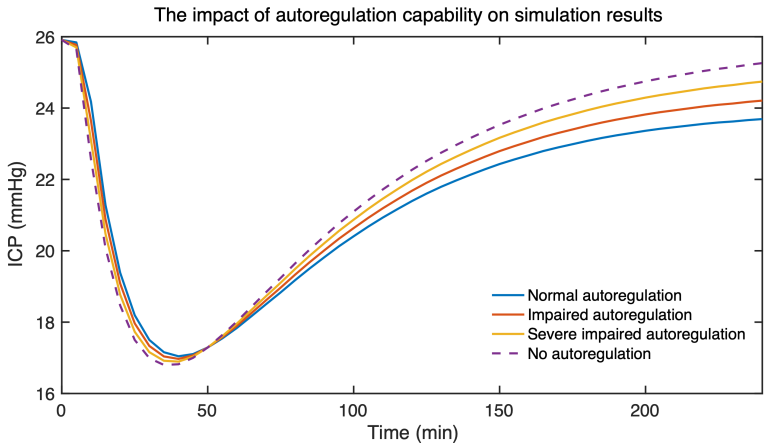


Figure 5.3: The impact of autoregulatory capacity on the effectiveness of osmotherapy.

5.3.2 Sensitivity analysis of physiological parameters

Parameter variability introduces uncertainty in therapeutic outcomes, thus making it crucial to study the effects of changes in various physiological parameters. The governing equation of the interstitial fluid pressure indicates key parameters influencing simulation results, including hydraulic conductivity, capillary wall

permeability, capillary blood pressure, blood osmotic pressure, and baseline ICP. Additionally, the size of malignant strokes (such as L-MCA and hemispheric strokes) also has clinical significance. The values of σ and L_p are estimated from the initial ICP value between 20 and 25 mmHg, as osmotherapy is only necessary within this range. The parameter values of c_w and K_w are varied from 50% to 200% of their baseline values to ensure physiological rationality. To discuss the effectiveness of the osmotherapy, E_{Mean} is introduced as the ratio of the mean ICP drop over 240 min (same as the time frame of the clinical data) and the mean increased effective osmotic pressure induced by the hypertonic saline infusion:

$$E_{\text{Mean}} = \frac{\int_0^{240}(ICP_{t=0} - ICP) \cdot dt}{\int_0^{240} \sigma_{\text{NaCl}} \Pi_{\text{NaCl}} \cdot dt} \tag{5.17}$$

Figure 5.4 shows the ICP evolution under various physiological parameters. The reference value of E_{Mean} is 94.22%. The ranges and E_{Mean} of parameter values in the sensitivity analysis tests are summarized in Table 5.3. It can be seen that capillary wall permeability significantly influences treatment outcomes, leading to a difference of up to -37.51% in E_{Mean}, significantly affecting the rate and extent of ICP reduction. Additionally, the hydraulic conductivity also shows relatively significant effect on the treatment effectiveness. However, the reflection coefficient of the original plasma composition and the storage factor of the interstitial fluid exhibit only minor effects on the effectiveness of osmotherapy. Sensitivity analysis results are largely consistent with the original model, indicating that the introduction of autoregulation mechanisms does not alter the impact of different parameters on the effectiveness of osmotherapy.

Table 5.3: Ranges and values of E_{Mean} of parameter values in the sensitivity analysis tests.

Parameters	**Range**	$E_{\textbf{Mean}}$
σ	$0.35 - 0.65$	92.10% to 92.87%
L_p	$6.0 \times 10^{-12} - 6.0 \times 10^{-11}$ m/s $\cdot$ Pa	56.71% to 101.17%
c_w	$1.54 \times 10^{-4} - 6.16 \times 10^{-4}$ Pa^{-1}	93.55% to 96.68%
K_w	$1.8 \times 10^{-3} - 7.2 \times 10^{-3}$ mm^{3}kg^{-1}	83.63% to 95.62%

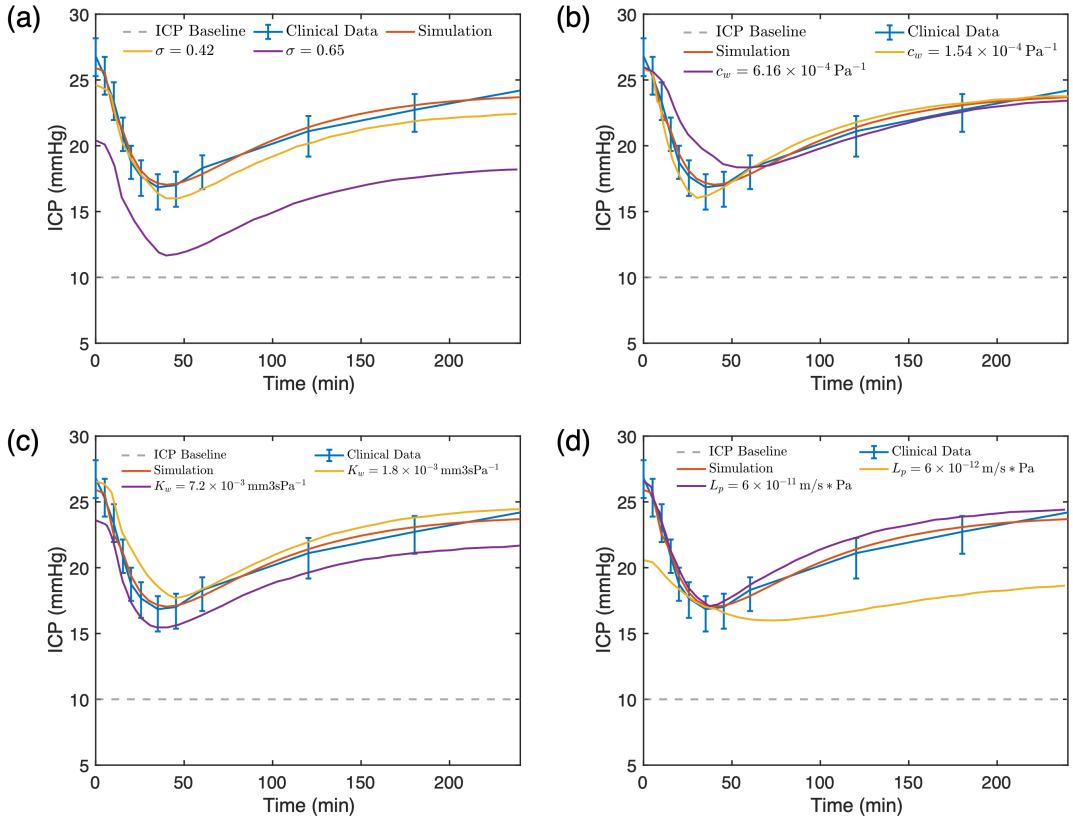


Figure 5.4: The evolution of ICP in osmotherapy under varying physiological parameters. (a) Varying the reflection coefficient of the original plasma composition. (b) Varying the storage factor of the interstitial fluid. (c) Varying the hydraulic conductivity of interstitial fluid in the interstitial space. (d) Varying the hydraulic permeability of the capillary wall. The reference curve corresponds to the validation case shown in Figure 5.2.

5.4 Discussions

Simulation results indicate that the optimized model aligns closely with clinical data collected from eight patients who underwent 22 osmotherapy sessions. As illustrated in Figure 5.2(b), the optimized model demonstrates improved consistency with clinical data during the ICP rebound phase than the original porous medium model, and it maintains a lower level of ICP, highlighting the critical role of preserved autoregulation in enhancing therapeutic outcomes. Although the infusion lasts only 15 minutes, the brain takes about 35 minutes to respond, with ICP reaching its lowest value post-injection. The optimized model slightly delays reaching this nadir compared to the original model, likely due to the time required for autoregulation mechanisms to stabilize, typically 3-5 minutes. During the ICP rebound phase, the

optimized model adjusts the arterial radius in response to changes in arterial pressure, affecting capillary permeability. This higher permeability facilitates the osmotic draw of water from the brain, improving osmotherapy's effectiveness. Overall, incorporating autoregulation mechanisms enhances the model's predictive accuracy, demonstrating that the detailed physiological-based CA model from the previous chapter integrates well with other mathematical models, suggesting substantial potential for clinical application.

Research indicates that variations in physiological parameters play a crucial role in the effectiveness of osmotherapy, thereby impacting treatment outcomes. While osmotherapy and its side effects have been extensively reviewed in meta-analyses, the specific impact of certain physiological parameters on ICP remains unclear. In this study, we have quantitatively investigated the effects of these varying physiological parameters. Our findings identify tissue hydraulic conductivity and reflection coefficient as key parameters in osmotherapy. Understanding these relationships can aid in developing more targeted therapeutic methods that consider individual patient characteristics, potentially improving clinical outcomes.

5.4.1 Limitations

It should be noted that this study has several limitations. Firstly, the multi-compartment model relies on numerous parameters that are difficult to measure precisely from existing experimental data. Additionally, parameters such as reflection coefficient of the original plasma composition and the hydraulic permeability of the capillary wall are related to the severity of oedema, necessitating personalized adjustments for accurate clinical predictions. Furthermore, the scarcity of brain-specific experimental data and the diversity in experimental methodologies mean that even real physiological parameters may vary significantly, typically within a range of 50% - 200%.

Secondly, the model depends on the homogenization of brain behaviour, which disregards the variability in tissue characteristics across different brain regions,

focusing only on the differences between white and grey matter. The lack of detailed anatomical data limits the development of a more refined brain model.

Thirdly, while the inclusion of cerebral autoregulation adds more physiological basis to the model, this integration is achieved solely through modifications in arterial permeability. The model does not account for the interactions of autoregulation with other parameters of the porous medium model or the highly complex biochemical reactions that occur during the injection of hypertonic saline. This omission limits a deeper understanding of the effects of osmotherapy.

5.5 Conclusions

In this study, cerebral autoregulation is innovatively incorporated into a multi-compartment porous Finite Element model, enabling the model to dynamically adjust vascular permeability in response to fluctuations in arterial blood pressure. The enhanced model not only aligns more closely with actual clinical outcomes but also serves as a platform for analysing the impact of various physiological parameters, such as hydraulic conductivity and capillary wall permeability, on the effectiveness of osmotherapy. This improved model provides more detailed guidelines to maximize therapeutic efficacy and minimize potential risks, ultimately enhancing patient care and treatment outcomes.

6

Conclusions

In this chapter, we will summarize our findings and explore future work that can build on this foundation to further investigate cerebral autoregulation. This is crucial for revealing the complete physiological processes of the brain and can also advance the clinical translation of cerebral autoregulation applications.

6.1 Summary of Results

This thesis first provides new insights into the cerebrovascular pressure-flow response in healthy subjects under steady-state conditions and examines the static and dynamic alterations in autoregulation associated with pathological states such as ageing and hypertension. The study reveals that cerebrovascular autoregulation may be more effective during elevated ABP compared to decreased ABP. Furthermore, both non-pharmacological and pharmacological BP manipulation methods demonstrate varying degrees of robustness, underscoring the need for more standardized data collection procedures in future CA studies is essential for providing more homogenized information about the relationship between CA and brain disorders. Given the limited human experimental data, defining the "normal" and "impaired" states of static CA remains challenging.

In Chapter 4, a physiological based mathematical model for the whole brain vasculature is introduced, which for the first time investigates the cerebrovascular system's responses to arterial blood pressure and neural stimulation. A single-vessel mathematical model is first constructed, encompassing subsystems such as neurons, astrocytes, smooth muscle cells, and endothelial cells. This comprehensive physiological basis facilitates the inclusion of myogenic and shear stress responses, along with potassium signalling and neuronal NO mechanisms. The model output largely displays the canonical elements of a typical BOLD response: an initial dip, main response, and post stimulus undershoot.

By using the analogy between cerebral vasculature and electrical circuits, integrating our single-vessel model into a whole-brain vasculature model successfully replicates experimental pressure-flow data observed in rats and cats, exhibiting classical autoregulation curves (Lassen's curve) characteristics, including the LLA, the plateau region, and the ULA. Since the SR in the SMC governs calcium release and reuptake during muscle contraction through feedback control, it is able to moderate sharp changes in the dynamic response to different intramural pressures and pressure gradients. The plateau along with the relatively low ULA observed in the Lassen curve reveals that SACs appear to be the crucial initiating factor to the recruitment of VOCCs and the subsequent myogenic response. Apart from the direct impact on cGMP production, the shear stress response also has a relatively small effect on the membrane potential and hence the SMC calcium concentration, leading to additional vasodilation. Although the endothelium has been shown to be the most influential NO producer, the neuronal NO plays an important role in modulating NVC mechanisms and hence smooth muscle tone.

Finally, we integrate the CA model into a multi-compartment porous Finite Element model for osmotherapy, and simulation results align well with clinical data. The results of the parameter sensitivity analysis identify the tissue hydraulic conductivity and reflection coefficient as key parameters in osmotherapy. It is hoped that further development of this model will help predict optimized therapeutic strategies for

patients with various types of unsuccessful treatments, providing more detailed guidelines for the clinical management of oedema.

6.2 Future Work

6.2.1 Unified quantitative techniques for cerebral autoregulation analysis

As evident from the meta-analysis in Chapter 3, a wide variety of analytical techniques are available for quantifying CA. This diversity allows for detailed interpretations of autoregulation, yet also results in significant variability across studies using different techniques, complicating the drawing of conclusions about specific pathophysiologies. Invasive arterial pressure monitoring may only be applicable to a small subset of patients and is not feasible as a routine procedure. Future efforts are necessary to improve CA assessment methods to identify a technique that balances accuracy and reliability.

6.2.2 Detailed capillary network models

Although the model in this article considers highly detailed physiological pathways, it simplifies the capillary network into a single layer. The capillary network, known to be a highly complex and interconnected system with a vascular density of about 8,000 per cubic metre, has rarely been modelled at the capillary level. Current cerebral blood flow mathematical models are rudimentary in terms of spatial information and differentiation between layers, with a major challenge being the computational difficulty of simulating each individual vessel. Therefore, new mathematical approaches are required to model blood flow dynamics across every length scale of vessels. The studies by El-Bouri and Payne may play a crucial role in future modelling efforts [264].

6.2.3 Incorporation of physiological and pathological variations

The model needs further refinement to include dynamic responses under various physiological and pathological states. For example, existing models often focus on describing blood flow autoregulation in healthy adults, with insufficient detail for paediatric, elderly, or specific disease states. Age is a significant factor affecting vascular elasticity, blood flow velocity, and vascular reactivity. Mathematical models could integrate age-related physiological parameters, such as changes in vascular wall thickness and stiffness, and neuroregulatory alterations, to simulate cerebral blood flow autoregulation mechanisms from infancy to old age. Additionally, different pathological states such as hypertension, diabetes, and Alzheimer's disease alter the structure and function of cerebral vessels, impacting the efficiency of blood flow autoregulation. The model should include the specific effects of these pathological factors on vascular reactivity and blood flow regulation, as well as their interactions with age.

6.2.4 Consideration of brain regions

Current models rely on the assumption of brain homogeneity. Future models need to classify different brain regions more finely, as each region has unique structural and functional characteristics, and the specific blood flow properties, metabolic activities, and neural activities of each area should be considered individually. High-resolution medical imaging technologies, such as fMRI or PET, could be utilized to acquire detailed information on blood flow, oxygen consumption, and metabolic data for specific brain regions. This information could link specific brain functions to neurovascular and neurometabolic responses in a region-specific manner, facilitating the development and validation of regional-specific blood flow regulation models.

References

[1] *Stroke statistics*. Stroke Association. Oct. 7, 2020. URL: https://www.stroke.org.uk/what-is-stroke/stroke-statistics (visited on 04/24/2023).

[2] Gill Livingston et al. "Dementia prevention, intervention, and care: 2020 report of the Lancet Commission". In: *The Lancet* 396.10248 (Aug. 8, 2020). Publisher: Elsevier, pp. 413–446. DOI: 10.1016/S0140-6736(20)30367-6.

[3] Jurgen A. H. R. Claassen et al. "Regulation of cerebral blood flow in humans: physiology and clinical implications of autoregulation". In: *Physiological Reviews* 101.4 (Oct. 1, 2021), pp. 1487–1559. DOI: 10.1152/physrev.00022.2020.

[4] Melanie D. Sweeney et al. "Vascular dysfunction-The disregarded partner of Alzheimer's disease". In: *Alzheimer's & Dementia: The Journal of the Alzheimer's Association* 15.1 (Jan. 2019), pp. 158–167. DOI: 10.1016/j.jalz.2018.07.222.

[5] Mathieu Cloutier et al. "An integrative dynamic model of brain energy metabolism using in vivo neurochemical measurements". In: *Journal of Computational Neuroscience* 27.3 (Dec. 2009), pp. 391–414. DOI: 10.1007/s10827-009-0152-8.

[6] Piotr Orlowski et al. "Modelling of pH dynamics in brain cells after stroke". In: *Interface Focus* 1.3 (June 6, 2011), pp. 408–416. DOI: 10.1098/rsfs.2010.0025.

[7] S. J. Payne and W. K. El-Bouri. "Modelling dynamic changes in blood flow and volume in the cerebral vasculature". In: *NeuroImage* 176 (Aug. 1, 2018), pp. 124–137. DOI: 10.1016/j.neuroimage.2018.04.037.

[8] M. Ursino et al. "Cerebral hemodynamics during arterial and CO(2) pressure changes: in vivo prediction by a mathematical model". In: *American Journal of Physiology. Heart and Circulatory Physiology* 279.5 (Nov. 2000), H2439–2455. DOI: 10.1152/ajpheart.2000.279.5.H2439.

[9] S. J. Payne. "A model of the interaction between autoregulation and neural activation in the brain". In: *Mathematical Biosciences* 204.2 (Dec. 1, 2006), pp. 260–281. DOI: 10.1016/j.mbs.2006.08.006.

[10] Seymour S. Kety and Carl F. Schmidt. "THE EFFECTS OF ALTERED ARTERIAL TENSIONS OF CARBON DIOXIDE AND OXYGEN ON CEREBRAL BLOOD FLOW AND CEREBRAL OXYGEN CONSUMPTION OF NORMAL YOUNG MEN 1". In: *Journal of Clinical Investigation* 27.4 (July 1948), pp. 484–492.

[11] K. R. Jessen and R. Mirsky. "Glial cells in the enteric nervous system contain glial fibrillary acidic protein". In: *Nature* 286.5774 (Aug. 14, 1980), pp. 736–737. DOI: 10.1038/286736a0.

[12] Stephen W. Kuffler and John G. Nicholls. "The physiology of neuroglial cells". In: *Ergebnisse der Physiologie Biologischen Chemie und Experimentellen Pharmakologie* 57.1 (Dec. 1, 1966), pp. 1–90. DOI: 10.1007/BF02259903.

[13] Christine R. Rose, Bruce R. Ransom, and Stephen G. Waxman. "Pharmacological Characterization of Na $^+$ Influx via Voltage-Gated Na $^+$ Channels in Spinal Cord Astrocytes". In: *Journal of Neurophysiology* 78.6 (Dec. 1, 1997), pp. 3249–3258. DOI: 10.1152/jn.1997.78.6.3249.

[14] J. M. Ritchie. "Voltage-gated cation and anion channels in mammalian Schwann cells and astrocytes". In: *Journal De Physiologie* 82.4 (1987), pp. 248–257.

[15] Agnès Aubert and Robert Costalat. "A Model of the Coupling between Brain Electrical Activity, Metabolism, and Hemodynamics: Application to the Interpretation of Functional Neuroimaging". In: *NeuroImage* 17.3 (Nov. 2002), pp. 1162–1181. DOI: 10.1006/nimg.2002.1224.

[16] Païkan Marcaggi and David Attwell. "Role of glial amino acid transporters in synaptic transmission and brain energetics". In: *Glia* 47.3 (Aug. 15, 2004), pp. 217–225. DOI: 10.1002/glia.20027.

[17] Ragnhildur Káradóttir et al. "NMDA receptors are expressed in oligodendrocytes and activated in ischaemia". In: *Nature* 438.7071 (Dec. 22, 2005), pp. 1162–1166. DOI: 10.1038/nature04302.

[18] Alexei Verkhratsky et al. "Purinoceptors on neuroglia". In: *Molecular Neurobiology* 39.3 (June 2009), pp. 190–208. DOI: 10.1007/s12035-009-8063-2.

[19] P. Kofuji and E. A. Newman. "Potassium buffering in the central nervous system". In: *Neuroscience* 129.4 (2004), pp. 1045–1056. DOI: 10.1016/j.neuroscience.2004.06.008.

[20] Olaf B. Paulson and Eric A. Newman. "Does the Release of Potassium from Astrocyte Endfeet Regulate Cerebral Blood Flow?" In: *Science (New York, N.Y.)* 237.4817 (Aug. 21, 1987), pp. 896–898.

[21] Monica R. Metea and Eric A. Newman. "Glial Cells Dilate and Constrict Blood Vessels: A Mechanism of Neurovascular Coupling". In: *The Journal of Neuroscience* 26.11 (Mar. 15, 2006), pp. 2862–2870. DOI: 10.1523/JNEUROSCI.4048-05.2006.

[22] Hélène Girouard et al. "Astrocytic endfoot Ca2+ and BK channels determine both arteriolar dilation and constriction". In: *Proceedings of the National Academy of Sciences of the United States of America* 107.8 (Feb. 23, 2010), pp. 3811–3816. DOI: 10.1073/pnas.0914722107.

[23] Jessica A. Filosa and Víctor M. Blanco. "Neurovascular coupling in the mammalian brain". In: *Experimental Physiology* 92.4 (2007). _eprint: https://physoc.onlinelibrary.wiley.com/doi/pdf/10.1113/expphysiol.2006.036368, pp. 641–646. DOI: https://doi.org/10.1113/expphysiol.2006.036368.

[24] David L. Stokes and Terence Wagenknecht. "Calcium transport across the sarcoplasmic reticulum". In: *European Journal of Biochemistry* 267.17 (2000). _eprint: https://febs.onlinelibrary.wiley.com/doi/pdf/10.1046/j.1432-1327.2000.01569.x, pp. 5274–5279. DOI: https://doi.org/10.1046/j.1432-1327.2000.01569.x.

[25] Philip N Ainslie et al. "Elevation in cerebral blood flow velocity with aerobic fitness throughout healthy human ageing". In: *The Journal of Physiology* 586 (Pt 16 Aug. 15, 2008), pp. 4005–4010. DOI: 10.1113/jphysiol.2008.158279.

[26] Philip N. Ainslie and James Duffin. "Integration of cerebrovascular CO $_2$ reactivity and chemoreflex control of breathing: mechanisms of regulation, measurement, and interpretation". In: *American Journal of Physiology-Regulatory, Integrative and Comparative Physiology* 296.5 (May 2009), R1473–R1495. DOI: 10.1152/ajpregu.91008.2008.

[27] Stephen Payne. *Cerebral blood flow and metabolism: a quantitative approach*. New Jersey: World Scientific, 2018. 440 pp.

[28] Niels A. Lassen. "Cerebral Blood Flow and Oxygen Consumption in Man". In: *Physiological Reviews* 39.2 (Apr. 1, 1959), pp. 183–238. DOI: 10.1152/physrev.1959.39.2.183.

[29] Patrice Brassard et al. "Losing the dogmatic view of cerebral autoregulation". In: *Physiological Reports* 9.15 (2021). _eprint: https://onlinelibrary.wiley.com/doi/pdf/10.14814/phy2.14982, e14982. DOI: 10.14814/phy2.14982.

[30] Paulo W. Pires et al. "The effects of hypertension on the cerebral circulation". In: *American Journal of Physiology - Heart and Circulatory Physiology* 304.12 (June 15, 2013), H1598–H1614. DOI: 10.1152/ajpheart.00490.2012.

[31] Tsuneo Takenaka et al. "Mechanosensitive cation channels mediate afferent arteriolar myogenic constriction in the isolated rat kidney". In: *The Journal of Physiology* 511 (Pt 1 Aug. 15, 1998), pp. 245–253. DOI: 10.1111/j.1469-7793.1998.245bi.x.

[32] M. J. Davis, G. A. Meininger, and D. C. Zawieja. "Stretch-induced increases in intracellular calcium of isolated vascular smooth muscle cells". In: *American Journal of Physiology-Heart and Circulatory Physiology* 263.4 (Oct. 1, 1992), H1292–H1299. DOI: 10.1152/ajpheart.1992.263.4.H1292.

[33] D. D. Rees et al. "Characterization of three inhibitors of endothelial nitric oxide synthase in vitro and in vivo." In: *British Journal of Pharmacology* 101.3 (Nov. 1990), pp. 746–752.

[34] J. C. Falcone, M. J. Davis, and G. A. Meininger. "Endothelial independence of myogenic response in isolated skeletal muscle arterioles". In: *American Journal of Physiology-Heart and Circulatory Physiology* 260.1 (Jan. 1, 1991). Publisher: American Physiological Society, H130–H135. DOI: 10.1152/ajpheart.1991.260.1.H130.

[35] L. Kuo, W. M. Chilian, and M. J. Davis. "Interaction of pressure- and flow-induced responses in porcine coronary resistance vessels". In: *American Journal of Physiology-Heart and Circulatory Physiology* 261.6 (Dec. 1, 1991), H1706–H1715. DOI: 10.1152/ajpheart.1991.261.6.H1706.

[36] Aaron A Phillips et al. "Neurovascular coupling in humans: Physiology, methodological advances and clinical implications". In: *Journal of Cerebral Blood Flow & Metabolism* 36.4 (Apr. 2016), pp. 647–664. DOI: 10.1177/0271678X15617954.

[37] Jessica A. Filosa et al. "Local potassium signaling couples neuronal activity to vasodilation in the brain". In: *Nature Neuroscience* 9.11 (Nov. 2006). Number: 11 Publisher: Nature Publishing Group, pp. 1397–1403. DOI: 10.1038/nn1779.

[38] Micaela Zonta et al. "Neuron-to-astrocyte signaling is central to the dynamic control of brain microcirculation". In: *Nature neuroscience* 6 (Feb. 1, 2003), pp. 43–50. DOI: 10.1038/nn980.

[39] Xinqi Peng et al. "Dependency of cortical functional hyperemia to forepaw stimulation on epoxygenase and nitric oxide synthase activities in rats". In: *Journal of Cerebral Blood Flow and Metabolism: Official Journal of the International Society of Cerebral Blood Flow and Metabolism* 24.5 (May 2004), pp. 509–517. DOI: 10.1097/00004647-200405000-00004.

[40] Grant R. J. Gordon et al. "Brain metabolism dictates the polarity of astrocyte control over arterioles". In: *Nature* 456.7223 (Dec. 2008). Number: 7223 Publisher: Nature Publishing Group, pp. 745–749. DOI: 10.1038/nature07525.

[41] Hiroki Kitaura et al. "Roles of nitric oxide as a vasodilator in neurovascular coupling of mouse somatosensory cortex". In: *Neuroscience Research* 59.2 (Oct. 2007), pp. 160–171. DOI: 10.1016/j.neures.2007.06.1469.

[42] J. W. Denninger and M. A. Marletta. "Guanylate cyclase and the .NO/cGMP signaling pathway". In: *Biochimica Et Biophysica Acta* 1411.2 (May 5, 1999), pp. 334–350. DOI: 10.1016/s0005-2728(99)00024-9.

[43] David Attwell et al. "Glial and neuronal control of brain blood flow". In: *Nature* 468.7321 (Nov. 2010). Number: 7321 Publisher: Nature Publishing Group, pp. 232–243. DOI: 10.1038/nature09613.

[44] Philip N. Ainslie and Patrice Brassard. "Why is the neural control of cerebral autoregulation so controversial?" In: *F1000Prime Reports* 6 (Mar. 3, 2014), p. 14. DOI: 10.12703/P6-14.

[45] Walter D. Obrist et al. "Determination of Regional Cerebral Blood Flow by Inhalation of 133-Xenon". In: *Circulation Research* 20.1 (Jan. 1967). Publisher: American Heart Association, pp. 124–135. DOI: 10.1161/01.RES.20.1.124.

[46] James M. Warwick. "Imaging of Brain Function Using SPECT". In: *Metabolic Brain Disease* 19.1 (June 1, 2004), pp. 113–123. DOI: 10.1023/B:MEBR.0000027422.48744.a3.

[47] Max Wintermark et al. "Comparative Overview of Brain Perfusion Imaging Techniques". In: *Stroke* 36.9 (Sept. 2005). DOI: 10.1161/01.STR.0000177884.72657.8b.

[48] Rune Aaslid, Thomas-Marc Markwalder, and Helge Nornes. "Noninvasive transcranial Doppler ultrasound recording of flow velocity in basal cerebral arteries". In: *Journal of Neurosurgery* 57.6 (Dec. 1982), pp. 769–774. DOI: 10.3171/jns.1982.57.6.0769.

[49] Jie Liu et al. "Cerebral Autoregulation of Blood Velocity and Volumetric Flow During Steady-State Changes in Arterial Pressure". In: *Hypertension* 62.5 (Nov. 2013). Publisher: American Heart Association, pp. 973–979. DOI: 10.1161/HYPERTENSIONAHA.113.01867.

[50] J. M. Serrador et al. "MRI measures of middle cerebral artery diameter in conscious humans during simulated orthostasis". In: *Stroke* 31.7 (July 2000), pp. 1672–1678. DOI: 10.1161/01.str.31.7.1672.

[51] C. K. Willie et al. "Regional brain blood flow in man during acute changes in arterial blood gases". In: *The Journal of Physiology* 590.14 (2012). _eprint: https://onlinelibrary.wiley.com/doi/pdf/10.1113/jphysiol.2012.228551, pp. 3261–3275. DOI: 10.1113/jphysiol.2012.228551.

[52] M. J. Poulin, P. J. Liang, and P. A. Robbins. "Dynamics of the cerebral blood flow response to step changes in end-tidal PCO2 and PO2 in humans". In: *Journal of Applied Physiology (Bethesda, Md.: 1985)* 81.3 (Sept. 1996), pp. 1084–1095. DOI: 10.1152/jappl.1996.81.3.1084.

[53] C. A. Giller et al. “Cerebral arterial diameters during changes in blood pressure and carbon dioxide during craniotomy”. In: *Neurosurgery* 32.5 (May 1993), 737–741, discussion 741–742.

[54] Shigehiko Ogoh et al. “The effect of phenylephrine on arterial and venous cerebral blood flow in healthy subjects”. In: *Clinical Physiology and Functional Imaging* 31.6 (2011). _eprint: https://onlinelibrary.wiley.com/doi/pdf/10.1111/j.1475-097X.2011.01040.x, pp. 445–451. DOI: 10.1111/j.1475-097X.2011.01040.x.

[55] Julian M. Stewart et al. “Middle cerebral O2 delivery during the modified Oxford maneuver increases with sodium nitroprusside and decreases during phenylephrine”. In: *American Journal of Physiology - Heart and Circulatory Physiology* 304.11 (June 1, 2013), H1576–H1583. DOI: 10.1152/ajpheart.00114.2013.

[56] Navpreet Reehal et al. “Differentiating Dynamic Cerebral Autoregulation Across Vascular Territories”. In: *Frontiers in Neurology* 12 (2021).

[57] Marc E. Wolf. “Functional TCD: regulation of cerebral hemodynamics–cerebral autoregulation, vasomotor reactivity, and neurovascular coupling”. In: *Frontiers of Neurology and Neuroscience* 36 (2015), pp. 40–56. DOI: 10.1159/000366236.

[58] S Ogawa et al. “Brain magnetic resonance imaging with contrast dependent on blood oxygenation.” In: *Proceedings of the National Academy of Sciences of the United States of America* 87.24 (Dec. 1990), pp. 9868–9872.

[59] S. Ogawa et al. “Intrinsic signal changes accompanying sensory stimulation: functional brain mapping with magnetic resonance imaging.” In: *Proceedings of the National Academy of Sciences of the United States of America* 89.13 (July 7, 1992). Publisher: National Academy of Sciences, p. 5951. DOI: 10.1073/pnas.89.13.5951.

[60] Marlies Wagner et al. “T2’- and PASL-based perfusion mapping at 3 Tesla: influence of oxygen-ventilation on cerebral autoregulation”. In: *Journal of magnetic resonance imaging: JMRI* 36.6 (Dec. 2012), pp. 1347–1352. DOI: 10.1002/jmri.23777.

[61] Mark A. Horsfield et al. “Regional Differences in Dynamic Cerebral Autoregulation in the Healthy Brain Assessed by Magnetic Resonance Imaging”. In: *PLOS ONE* 8.4 (Apr. 30, 2013). Publisher: Public Library of Science, e62588. DOI: 10.1371/journal.pone.0062588.

[62] Emily L. Sammons et al. “Influence of noninvasive peripheral arterial blood pressure measurements on assessment of dynamic cerebral autoregulation”. In: *Journal of Applied Physiology* 103.1 (July 2007). Publisher: American Physiological Society, pp. 369–375. DOI: 10.1152/japplphysiol.00271.2007.

[63] Nils H. Petersen et al. “Comparison of non-invasive and invasive arterial blood pressure measurement for assessment of dynamic cerebral autoregulation”. In: *Neurocritical care* 20.1 (Feb. 2014), pp. 60–68. DOI: 10.1007/s12028-013-9898-y.

[64] Frank P. Tiecks et al. “Comparison of Static and Dynamic Cerebral Autoregulation Measurements”. In: *Stroke* 26.6 (June 1995). Publisher: American Heart Association, pp. 1014–1019. DOI: 10.1161/01.STR.26.6.1014.

[65] R. B. Panerai et al. “Cerebral blood flow velocity response to induced and spontaneous sudden changes in arterial blood pressure”. In: *American Journal of*

Physiology. Heart and Circulatory Physiology 280.5 (May 2001), H2162–2174. DOI: 10.1152/ajpheart.2001.280.5.H2162.

[66] Arenda H. E. A. van Beek et al. "Dynamic Cerebral Autoregulation in the Old Using a Repeated Sit-Stand Maneuver". In: *Ultrasound in Medicine & Biology* 36.2 (Feb. 1, 2010), pp. 192–201. DOI: 10.1016/j.ultrasmedbio.2009.10.011.

[67] Farzaneh A. Sorond et al. "The sit-to-stand technique for the measurement of dynamic cerebral autoregulation". In: *Ultrasound in Medicine & Biology* 35.1 (Jan. 2009), pp. 21–29. DOI: 10.1016/j.ultrasmedbio.2008.08.001.

[68] Tianne Numan et al. "Static autoregulation in humans: a review and reanalysis". In: *Medical Engineering & Physics* 36.11 (Nov. 1, 2014), pp. 1487–1495. DOI: 10.1016/j.medengphy.2014.08.001.

[69] Rune Aaslid. "Cerebral autoregulation and vasomotor reactivity". In: *Frontiers of Neurology and Neuroscience* 21 (2006), pp. 216–228. DOI: 10.1159/000092434.

[70] Y. C. Tzeng et al. "Assessment of cerebral autoregulation: the quandary of quantification". In: *American Journal of Physiology-Heart and Circulatory Physiology* 303.6 (Sept. 15, 2012). Publisher: American Physiological Society, H658–H671. DOI: 10.1152/ajpheart.00328.2012.

[71] Jurgen AHR Claassen et al. "Transfer function analysis of dynamic cerebral autoregulation: A white paper from the International Cerebral Autoregulation Research Network". In: *Journal of Cerebral Blood Flow & Metabolism* 36.4 (Apr. 2016), pp. 665–680. DOI: 10.1177/0271678X15626425.

[72] L. Beishon et al. "INFOMATAS multi-center systematic review and meta-analysis individual patient data of dynamic cerebral autoregulation in ischemic stroke". In: *International Journal of Stroke: Official Journal of the International Stroke Society* 15.7 (Oct. 2020), pp. 807–812. DOI: 10.1177/1747493020907003.

[73] Mauro Ursino. "A mathematical study of human intracranial hydrodynamics. Part 1–The cerebrospinal fluid pulse pressure". In: *Annals of biomedical engineering* 16 (Feb. 1, 1988), pp. 379–401. DOI: 10.1007/BF02364625.

[74] M. Ursino, M. Iezzi, and N. Stocchetti. "Intracranial pressure dynamics in patients with acute brain damage: a critical analysis with the aid of a mathematical model". In: *IEEE transactions on bio-medical engineering* 42.6 (June 1995), pp. 529–540. DOI: 10.1109/10.387192.

[75] Mauro Ursino and Carlo Alberto Lodi. "A simple mathematical model of the interaction between intracranial pressure and cerebral hemodynamics". In: *Journal of Applied Physiology* 82.4 (Apr. 1997). Publisher: American Physiological Society, pp. 1256–1269. DOI: 10.1152/jappl.1997.82.4.1256.

[76] S. J. Payne, J. Selb, and D. A. Boas. "Effects of autoregulation and CO2 reactivity on cerebral oxygen transport". In: *Annals of Biomedical Engineering* 37.11 (Nov. 2009), pp. 2288–2298. DOI: 10.1007/s10439-009-9763-5.

[77] Bart Spronck et al. "A lumped parameter model of cerebral blood flow control combining cerebral autoregulation and neurovascular coupling". In: *American Journal of Physiology-Heart and Circulatory Physiology* 303.9 (July 9, 2012). Publisher: American Physiological Society, H1143–H1153. DOI: 10.1152/ajpheart.00303.2012.

[78] C. M. Hai and R. A. Murphy. "Cross-bridge phosphorylation and regulation of latch state in smooth muscle". In: *The American Journal of Physiology* 254.1 (Jan. 1988), pp. C99–106. DOI: 10.1152/ajpcell.1988.254.1.C99.

[79] Jin Yang et al. "The myogenic response in isolated rat cerebrovascular arteries: smooth muscle cell model". In: *Medical Engineering & Physics*. Cerebrovascular Modelling 25.8 (Oct. 1, 2003), pp. 691–709. DOI: 10.1016/S1350-4533(03)00100-0.

[80] Murad Banaji et al. "A physiological model of cerebral blood flow control". In: *Mathematical Biosciences* 194.2 (Apr. 2005), pp. 125–173. DOI: 10.1016/j.mbs.2004.10.005.

[81] Murad Banaji et al. "A Model of Brain Circulation and Metabolism: NIRS Signal Changes during Physiological Challenges". In: *PLoS Computational Biology* 4.11 (Nov. 7, 2008), e1000212. DOI: 10.1371/journal.pcbi.1000212.

[82] Michèle Koenigsberger et al. "Effects of Arterial Wall Stress on Vasomotion". In: *Biophysical Journal* 91.5 (Sept. 1, 2006), pp. 1663–1674. DOI: 10.1529/biophysj.106.083311.

[83] D. Parthimos, D. H. Edwards, and T. M. Griffith. "Minimal model of arterial chaos generated by coupled intracellular and membrane Ca2+oscillators". In: *American Journal of Physiology-Heart and Circulatory Physiology* 277.3 (Sept. 1, 1999). Publisher: American Physiological Society, H1119–H1144. DOI: 10.1152/ajpheart.1999.277.3.H1119.

[84] Mark Catherall. *Modelling the Role of Nitric Oxide in Cerebral Autoregulation*. Dec. 30, 2015. arXiv: 1512.09160[q-bio].

[85] J. Stålhand, A. Klarbring, and G. A. Holzapfel. "Smooth muscle contraction: Mechanochemical formulation for homogeneous finite strains". In: *Progress in Biophysics and Molecular Biology*. Cardiovascular Physiome 96.1 (Jan. 1, 2008), pp. 465–481. DOI: 10.1016/j.pbiomolbio.2007.07.025.

[86] Hannah Farr and Tim David. "Models of neurovascular coupling via potassium and EET signalling". In: *Journal of Theoretical Biology* 286 (Oct. 2011), pp. 13–23. DOI: 10.1016/j.jtbi.2011.07.006.

[87] K. Dormanns et al. "Neurovascular coupling and the influence of luminal agonists via the endothelium". In: *Journal of Theoretical Biology* 364 (Jan. 2015), pp. 49–70. DOI: 10.1016/j.jtbi.2014.08.029.

[88] Ivar Østby et al. "Astrocytic Mechanisms Explaining Neural-Activity-Induced Shrinkage of Extraneuronal Space". In: *PLOS Computational Biology* 5.1 (Jan. 23, 2009). Publisher: Public Library of Science, e1000272. DOI: 10.1371/journal.pcbi.1000272.

[89] K. Dormanns, R.G. Brown, and T. David. "The role of nitric oxide in neurovascular coupling". In: *Journal of Theoretical Biology* 394 (Apr. 2016), pp. 1–17. DOI: 10.1016/j.jtbi.2016.01.009.

[90] Kejing Chen and Aleksander S. Popel. "Theoretical analysis of biochemical pathways of nitric oxide release from vascular endothelial cells". In: *Free Radical Biology and Medicine* 41.4 (Aug. 15, 2006), pp. 668–680. DOI: 10.1016/j.freeradbiomed.2006.05.009.

[91] A. Comerford, M. J. Plank, and T. David. "Endothelial Nitric Oxide Synthase and Calcium Production in Arterial Geometries: An Integrated Fluid Mechanics/Cell Model". In: *Journal of Biomechanical Engineering* 130.1 (Feb. 1, 2008). Publisher: American Society of Mechanical Engineers Digital Collection. DOI: 10.1115/1.2838026.

[92] Kathryn M. Dunn and Mark T. Nelson. "Potassium Channels and Neurovascular Coupling". In: *Circulation Journal* 74.4 (2010), pp. 608–616. DOI: 10.1253/circj.CJ-10-0174.

[93] Allanah Kenny, Michael J. Plank, and Tim David. "The role of astrocytic calcium and TRPV4 channels in neurovascular coupling". In: *Journal of Computational Neuroscience* 44.1 (Feb. 1, 2018), pp. 97–114. DOI: 10.1007/s10827-017-0671-7.

[94] Allanah Kenny et al. "Massively parallel simulations of neurovascular coupling with extracellular diffusion". In: *Journal of Computational Science* 24 (Jan. 1, 2018), pp. 116–124. DOI: 10.1016/j.jocs.2017.07.001.

[95] Elshin J. Mathias et al. "Integrated models of neurovascular coupling and BOLD signals: Responses for varying neural activations". In: *NeuroImage* 174 (July 1, 2018), pp. 69–86. DOI: 10.1016/j.neuroimage.2018.03.010.

[96] R. B. Buxton, E. C. Wong, and L. R. Frank. "Dynamics of blood flow and oxygenation changes during brain activation: the balloon model". In: *Magnetic Resonance in Medicine* 39.6 (June 1998), pp. 855–864. DOI: 10.1002/mrm.1910390602.

[97] Richard B. Buxton. "Dynamic models of BOLD contrast". In: *NeuroImage* 62.2 (Aug. 15, 2012), pp. 953–961. DOI: 10.1016/j.neuroimage.2012.01.012.

[98] Joshua C. Chang et al. "A Mathematical Model of the Metabolic and Perfusion Effects on Cortical Spreading Depression". In: *PLOS ONE* 8.8 (Aug. 14, 2013). Publisher: Public Library of Science, e70469. DOI: 10.1371/journal.pone.0070469.

[99] Brian J. Carey et al. "Dynamic Cerebral Autoregulation Is Unaffected by Aging". In: *Stroke* 31.12 (Dec. 2000). Publisher: American Heart Association, pp. 2895–2900. DOI: 10.1161/01.STR.31.12.2895.

[100] Brian J. Carey, Ronney B. Panerai, and John F. Potter. "Effect of Aging on Dynamic Cerebral Autoregulation During Head-Up Tilt". In: *Stroke* 34.8 (Aug. 2003). Publisher: American Heart Association, pp. 1871–1875. DOI: 10.1161/01.STR.0000081981.99908.F3.

[101] Lewis A. Lipsitz et al. "Dynamic Regulation of Middle Cerebral Artery Blood Flow Velocity in Aging and Hypertension". In: *Stroke* 31.8 (Aug. 2000), pp. 1897–1903. DOI: 10.1161/01.STR.31.8.1897.

[102] Arenda HEA van Beek et al. "Cerebral Autoregulation: An Overview of Current Concepts and Methodology with Special Focus on the Elderly". In: *Journal of Cerebral Blood Flow & Metabolism* 28.6 (June 2008), pp. 1071–1085. DOI: 10.1038/jcbfm.2008.13.

[103] Alan T Yam et al. "Cerebral autoregulation and ageing". In: *Journal of Clinical Neuroscience* 12.6 (Aug. 1, 2005), pp. 643–646. DOI: 10.1016/j.jocn.2004.08.017.

[104] Fiona G. Brodie et al. "Long-term changes in dynamic cerebral autoregulation: a 10 years follow up study". In: *Clinical Physiology and Functional Imaging* 29.5 (2009). _eprint: https://onlinelibrary.wiley.com/doi/pdf/10.1111/j.1475-097X.2009.00880.x, pp. 366–371. DOI: 10.1111/j.1475-097X.2009.00880.x.

[105] Chang-Yang Xing et al. "Arterial Pressure, Heart Rate, and Cerebral Hemodynamics across the Adult Life Span". In: *Hypertension (Dallas, Tex. : 1979)* 69.4 (Apr. 2017), pp. 712–720. DOI: 10.1161/HYPERTENSIONAHA.116.08986.

[106] Brian M. Deegan et al. "Gender related differences in cerebral autoregulation in older healthy subjects". In: *Conference proceedings : ... Annual International Conference of the IEEE Engineering in Medicine and Biology Society. IEEE Engineering in Medicine and Biology Society. Conference* 2009 (2009), pp. 2859–2862. DOI: 10.1109/IEMBS.2009.5333604.

[107] Jorge M. Serrador et al. "Cerebral pressure-flow relations in hypertensive elderly humans: transfer gain in different frequency domains". In: *Journal of Applied Physiology* 98.1 (Jan. 2005), pp. 151–159. DOI: 10.1152/japplphysiol.00471.2004.

[108] Anne Pavy-Le Traon et al. "Dynamics of cerebral blood flow autoregulation in hypertensive patients". In: *Journal of the Neurological Sciences* 195.2 (Mar. 30, 2002), pp. 139–144. DOI: 10.1016/S0022-510X(02)00010-2.

[109] Lewis A. Lipsitz et al. "Antihypertensive Therapy Increases Cerebral Blood Flow and Carotid Distensibility in Hypertensive Elderly Subjects". In: *Hypertension* 45.2 (Feb. 2005). Publisher: American Heart Association, pp. 216–221. DOI: 10.1161/01.HYP.0000153094.09615.11.

[110] Elio Troisi et al. "Cerebral hemodynamics in young hypertensive subjects and effects of atenolol treatment". In: *Journal of the Neurological Sciences* 159.1 (July 1998), pp. 115–119. DOI: 10.1016/S0022-510X(98)00147-6.

[111] Rong Zhang et al. "Cerebral Hemodynamics After Short- and Long-Term Reduction in Blood Pressure in Mild and Moderate Hypertension". In: *Hypertension* 49.5 (May 2007). Publisher: American Heart Association, pp. 1149–1155. DOI: 10.1161/HYPERTENSIONAHA.106.084939.

[112] T. Michael De Silva and Frank M. Faraci. "Effects of angiotensin II on the cerebral circulation: role of oxidative stress". In: *Frontiers in Physiology* 3 (Jan. 3, 2013), p. 484. DOI: 10.3389/fphys.2012.00484.

[113] Marcel J.H. Aries et al. "Cerebral Autoregulation in Stroke". In: *Stroke* 41.11 (Nov. 2010). Publisher: American Heart Association, pp. 2697–2704. DOI: 10.1161/STROKEAHA.110.594168.

[114] Osian Llwyd et al. "Cerebral Haemodynamics following Acute Ischaemic Stroke: Effects of Stroke Severity and Stroke Subtype". In: *Cerebrovascular Diseases Extra* 8.2 (July 11, 2018), pp. 80–89. DOI: 10.1159/000487514.

[115] Pedro Castro, Elsa Azevedo, and Farzaneh Sorond. "Cerebral Autoregulation in Stroke". In: *Current Atherosclerosis Reports* 20.8 (May 21, 2018), p. 37. DOI: 10.1007/s11883-018-0739-5.

[116] Sushmita Purkayastha et al. "Impaired Cerebrovascular Hemodynamics are Associated with Cerebral White Matter Damage". In: *Journal of Cerebral Blood Flow & Metabolism* 34.2 (Feb. 1, 2014). Publisher: SAGE Publications Ltd STM, pp. 228–234. DOI: 10.1038/jcbfm.2013.180.

[117] E. D. Gommer et al. "Dynamic cerebral autoregulation and cerebrovascular reactivity: a comparative study in lacunar infarct patients". In: *Physiological Measurement* 29.11 (Oct. 2008), p. 1293. DOI: 10.1088/0967-3334/29/11/005.

[118] John Stirling Meyer et al. "Impaired Neurogenic Cerebrovascular Control and Dysautoregulation After Stroke". In: *Stroke* 4.2 (Mar. 1973). Publisher: American Heart Association, pp. 169–186. DOI: 10.1161/01.STR.4.2.169.

[119] Angela S.M. Salinet, Ronney B. Panerai, and Thompson G. Robinson. "The Longitudinal Evolution of Cerebral Blood Flow Regulation after Acute Ischaemic

Stroke". In: *Cerebrovascular Diseases Extra* 4.2 (Aug. 26, 2014), pp. 186–197. DOI: 10.1159/000366017.

[120] P Zhao et al. "Vasoreactivity and peri-infarct hyperintensities in stroke". In: *Neurology* 72.7 (Feb. 17, 2009), pp. 643–649. DOI: 10.1212/01.wnl.0000342473.65373.80.

[121] Alexandre Krainik et al. "Regional Impairment of Cerebrovascular Reactivity and BOLD Signal in Adults After Stroke". In: *Stroke* 36.6 (June 2005). Publisher: American Heart Association, pp. 1146–1152. DOI: 10.1161/01.STR.0000166178.40973.a7.

[122] R. Pineiro et al. "Altered Hemodynamic Responses in Patients After Subcortical Stroke Measured by Functional MRI". In: *Stroke* 33.1 (Jan. 2002). Publisher: American Heart Association, pp. 103–109. DOI: 10.1161/hs0102.100482.

[123] P. M. Rossini et al. "Does cerebrovascular disease affect the coupling between neuronal activity and local haemodynamics?" In: *Brain* 127.1 (Jan. 1, 2004), pp. 99–110. DOI: 10.1093/brain/awh012.

[124] ALEXANDER KUNZ and COSTANTINO IADECOLA. "Cerebral vascular dysregulation in the ischemic brain". In: *Handbook of clinical neurology* 92 (2009), pp. 283–305. DOI: 10.1016/S0072-9752(08)01914-3.

[125] Martin Soehle et al. "Continuous Assessment of Cerebral Autoregulation in Subarachnoid Hemorrhage". In: *Anesthesia & Analgesia* 98.4 (Apr. 2004), p. 1133. DOI: 10.1213/01.ANE.0000111101.41190.99.

[126] Christian Zweifel et al. "Continuous Assessment of Cerebral Autoregulation With Near-Infrared Spectroscopy in Adults After Subarachnoid Hemorrhage". In: *Stroke* 41.9 (Sept. 2010). Publisher: American Heart Association, pp. 1963–1968. DOI: 10.1161/STROKEAHA.109.577320.

[127] Karol P Budohoski et al. "Cerebral Autoregulation after Subarachnoid Hemorrhage: Comparison of Three Methods". In: *Journal of Cerebral Blood Flow & Metabolism* 33.3 (Mar. 1, 2013). Publisher: SAGE Publications Ltd STM, pp. 449–456. DOI: 10.1038/jcbfm.2012.189.

[128] Johann Fontana et al. "Impairment of Dynamic Pressure Autoregulation Precedes Clinical Deterioration after Aneurysmal Subarachnoid Hemorrhage". In: *Journal of Neuroimaging* 26.3 (2016). _eprint: https://onlinelibrary.wiley.com/doi/pdf/10.1111/jon.12295, pp. 339–345. DOI: 10.1111/jon.12295.

[129] Maximilian Oeinck et al. "Dynamic Cerebral Autoregulation in Acute Intracerebral Hemorrhage". In: *Stroke* 44.10 (Oct. 2013). Publisher: American Heart Association, pp. 2722–2728. DOI: 10.1161/STROKEAHA.113.001913.

[130] Karol P. Budohoski et al. "Impairment of Cerebral Autoregulation Predicts Delayed Cerebral Ischemia After Subarachnoid Hemorrhage". In: *Stroke* 43.12 (Dec. 2012). Publisher: American Heart Association, pp. 3230–3237. DOI: 10.1161/STROKEAHA.112.669788.

[131] Lionel Calviere et al. "Prediction of Delayed Cerebral Ischemia After Subarachnoid Hemorrhage Using Cerebral Blood Flow Velocities and Cerebral Autoregulation Assessment". In: *Neurocritical Care* 23.2 (Oct. 1, 2015), pp. 253–258. DOI: 10.1007/s12028-015-0125-x.

[132] Joseph M Darby. "Acute cerebral blood flow response to dopamine-induced hypertension after subarachnoid hemorrhage". In: (1994).

[133] M. P. Heilbrun, J. Olesen, and N. A. Lassen. "Regional cerebral blood flow studies in subarachnoid hemorrhage". In: *Journal of Neurosurgery* 37.1 (July 1972), pp. 36–44. DOI: 10.3171/jns.1972.37.1.0036.

[134] Li Zhang et al. "Steady-state cerebral autoregulation in older adults with amnestic mild cognitive impairment: linear mixed model analysis". In: *Journal of Applied Physiology (Bethesda, Md.: 1985)* 129.2 (Aug. 1, 2020), pp. 377–385. DOI: 10.1152/japplphysiol.00193.2020.

[135] Guoyu Zhou et al. "Impaired Cerebral Autoregulation in Alzheimer's Disease: A Transcranial Doppler Study". In: *Journal of Alzheimer's disease: JAD* 72.2 (2019), pp. 623–631. DOI: 10.3233/JAD-190296.

[136] Rianne A.A. de Heus et al. "Dynamic Regulation of Cerebral Blood Flow in Patients With Alzheimer Disease". In: *Hypertension* 72.1 (July 2018). Publisher: American Heart Association, pp. 139–150. DOI: 10.1161/HYPERTENSIONAHA.118.10900.

[137] Jurgen A.H.R. Claassen et al. "Altered Cerebral Hemodynamics in Early Alzheimer Disease: A Pilot Study Using Transcranial Doppler". In: *Journal of Alzheimer's disease : JAD* 17.3 (2009), pp. 621–629. DOI: 10.3233/JAD-2009-1079.

[138] Erik D. Gommer et al. "Dynamic Cerebral Autoregulation in Subjects with Alzheimer's Disease, Mild Cognitive Impairment, and Controls: Evidence for Increased Peripheral Vascular Resistance with Possible Predictive Value". In: *Journal of Alzheimer's Disease* 30.4 (Jan. 1, 2012). Publisher: IOS Press, pp. 805–813. DOI: 10.3233/JAD-2012-111628.

[139] D. SIMARD et al. "REGIONAL CEREBRAL BLOOD FLOW AND ITS REGULATION IN DEMENTIA". In: *Brain* 94.2 (Jan. 1, 1971), pp. 273–288. DOI: 10.1093/brain/94.2.273.

[140] Arenda H.E.A. van Beek et al. "Cortical Oxygen Supply During Postural Hypotension is Further Decreased in Alzheimer's Disease, but Unrelated to Cholinesterase-Inhibitor Use". In: *Journal of Alzheimer's Disease* 21.2 (Aug. 11, 2010), pp. 519–526. DOI: 10.3233/JAD-2010-100288.

[141] Allyson R Zazulia et al. "Autoregulation of cerebral blood flow to changes in arterial pressure in mild Alzheimer's disease". In: *Journal of Cerebral Blood Flow & Metabolism* 30.11 (Nov. 2010), pp. 1883–1889. DOI: 10.1038/jcbfm.2010.135.

[142] Aisha S. S. Meel-van den Abeelen et al. "Impaired cerebral autoregulation and vasomotor reactivity in sporadic Alzheimer's disease". In: *Current Alzheimer Research* 11.1 (Jan. 2014), pp. 11–17. DOI: 10.2174/1567205010666131119234845.

[143] Arenda H. E. A. van Beek et al. "Oscillations in cerebral blood flow and cortical oxygenation in Alzheimer's disease". In: *Neurobiology of Aging* 33.2 (Feb. 1, 2012), 428.e21–428.e31. DOI: 10.1016/j.neurobiolaging.2010.11.016.

[144] Jade L. Taylor et al. "Functionally linked potassium channel activity in cerebral endothelial and smooth muscle cells is compromised in Alzheimer's disease". In: *Proceedings of the National Academy of Sciences of the United States of America* 119.26 (June 28, 2022), e2204581119. DOI: 10.1073/pnas.2204581119.

[145] Philip B. Gorelick et al. "Vascular Contributions to Cognitive Impairment and Dementia". In: *Stroke; a journal of cerebral circulation* 42.9 (Sept. 2011), pp. 2672–2713. DOI: 10.1161/STR.0b013e3182299496.

[146] Kassandra Kisler et al. "Cerebral blood flow regulation and neurovascular dysfunction in Alzheimer's disease". In: *Nature reviews. Neuroscience* 18.7 (July 2017), pp. 419–434. DOI: 10.1038/nrn.2017.48.

[147] Y. Iturria-Medina et al. "Early role of vascular dysregulation on late-onset Alzheimer's disease based on multifactorial data-driven analysis". In: *Nature Communications* 7 (June 21, 2016), p. 11934. DOI: 10.1038/ncomms11934.

[148] Belinda Yew and Daniel A. Nation. "Cerebrovascular resistance: effects on cognitive decline, cortical atrophy, and progression to dementia". In: *Brain* 140.7 (July 2017), pp. 1987–2001. DOI: 10.1093/brain/awx112.

[149] Yufan Wang and Stephen J Payne. "Static autoregulation in humans". In: *Journal of Cerebral Blood Flow & Metabolism* (Nov. 7, 2023). Publisher: SAGE Publications Ltd STM, p. 0271678X231210430. DOI: 10.1177/0271678X231210430.

[150] Samuel J.E. Lucas et al. "Influence of Changes in Blood Pressure on Cerebral Perfusion and Oxygenation". In: *Hypertension* 55.3 (Mar. 2010). Publisher: American Heart Association, pp. 698–705. DOI: 10.1161/HYPERTENSIONAHA.109.146290.

[151] Rong Zhang, Khosrow Behbehani, and Benjamin D Levine. "Dynamic pressure–flow relationship of the cerebral circulation during acute increase in arterial pressure". In: *The Journal of Physiology* 587 (Pt 11 June 1, 2009), pp. 2567–2577. DOI: 10.1113/jphysiol.2008.168302.

[152] MOGENS FOG. "CEREBRAL CIRCULATION: THE REACTION OF THE PIAL ARTERIES TO A FALL IN BLOOD PRESSURE". In: *Archives of Neurology & Psychiatry* 37.2 (Feb. 1, 1937), pp. 351–364. DOI: 10.1001/archneurpsyc.1937.02260140137007.

[153] B. Ekström-Jodal et al. "Cerebral Blood Flow Autoregulation at High Arterial Pressures and Different Levels of Carbon Dioxide Tension in Dogs". In: *European Neurology* 6.1 (1971). Publisher: Karger Publishers, pp. 6–10. DOI: 10.1159/000114457.

[154] Olaf Paulson, S Strandgaard, and L Edvinsson. "Cerebral autoregulation". In: *Cerebrovascular and brain metabolism reviews* 2 (Feb. 1, 1990), pp. 161–92.

[155] S. Strandgaard et al. "Autoregulation of Brain Circulation in Severe Arterial Hypertension". In: *British Medical Journal* 1.5852 (Mar. 3, 1973), pp. 507–510.

[156] Donald D. Heistad et al. "Regulation of cerebral blood flow in atherosclerotic monkeys". In: *American Journal of Physiology-Heart and Circulatory Physiology* 239.4 (Oct. 1980). Publisher: American Physiological Society, H539–H539. DOI: 10.1152/ajpheart.1980.239.4.H539.

[157] S. L. Harper, H. G. Bohlen, and M. J. Rubin. "Arterial and microvascular contributions to cerebral cortical autoregulation in rats". In: *American Journal of Physiology-Heart and Circulatory Physiology* 246.1 (Jan. 1, 1984). Publisher: American Physiological Society, H17–H24. DOI: 10.1152/ajpheart.1984.246.1.H17.

[158] W. Fitch et al. "Autoregulation of cerebral blood flow during controlled hypotension in baboons". In: *Journal of Neurology, Neurosurgery, and Psychiatry* 39.10 (Oct. 1976), pp. 1014–1022. DOI: 10.1136/jnnp.39.10.1014.

[159] Can Ozan Tan. "Defining the characteristic relationship between arterial pressure and cerebral flow". In: *Journal of Applied Physiology* 113.8 (Oct. 15, 2012).

Publisher: American Physiological Society, pp. 1194–1200. DOI: 10.1152/japplphysiol.00783.2012.

[160] Donald D. Heistad and Hermes A. Kontos. "Cerebral Circulation". In: *Comprehensive Physiology*. _eprint: https://onlinelibrary.wiley.com/doi/pdf/10.1002/cphy.cp020305. John Wiley & Sons, Ltd, 2011, pp. 137–182. DOI: 10.1002/cphy.cp020305.

[161] William M. Armstead. "Cerebral Blood Flow Autoregulation and Dysautoregulation". In: *Anesthesiology clinics* 34.3 (Sept. 2016), pp. 465–477. DOI: 10.1016/j.anclin.2016.04.002.

[162] Daan L. K. de Jong et al. "Lack of linear correlation between dynamic and steady-state cerebral autoregulation". In: *The Journal of Physiology* 595.16 (Aug. 15, 2017), pp. 5623–5636. DOI: 10.1113/JP274304.

[163] Patrice Brassard et al. "Evidence for hysteresis in the cerebral pressure-flow relationship in healthy men". In: *American Journal of Physiology-Heart and Circulatory Physiology* 312.4 (Apr. 2017). Publisher: American Physiological Society, H701–H704. DOI: 10.1152/ajpheart.00790.2016.

[164] Lawrence Labrecque et al. "Dynamic cerebral autoregulation and cerebrovascular carbon dioxide reactivity in middle and posterior cerebral arteries in young endurance-trained women". In: *Journal of Applied Physiology* 130.6 (June 2021). Publisher: American Physiological Society, pp. 1724–1735. DOI: 10.1152/japplphysiol.00963.2020.

[165] Ronney B. Panerai et al. "Directional sensitivity of dynamic cerebral autoregulation in squat-stand maneuvers". In: *American Journal of Physiology-Regulatory, Integrative and Comparative Physiology* 315.4 (Oct. 2018). Publisher: American Physiological Society, R730–R740. DOI: 10.1152/ajpregu.00010.2018.

[166] Yu-Chieh Tzeng et al. "Cerebrovascular Regulation During Transient Hypotension and Hypertension in Humans". In: *Hypertension* 56.2 (Aug. 2010). Publisher: American Heart Association, pp. 268–273. DOI: 10.1161/HYPERTENSIONAHA.110.152066.

[167] Lingzhong Meng. "Regulation of Cerebral Autoregulation by Carbon Dioxide". In: *Anesthesiology* (2015), p. 10.

[168] Jasper Verbree et al. "Assessment of middle cerebral artery diameter during hypocapnia and hypercapnia in humans using ultra-high-field MRI". In: *Journal of Applied Physiology* 117.10 (Nov. 15, 2014). Publisher: American Physiological Society, pp. 1084–1089. DOI: 10.1152/japplphysiol.00651.2014.

[169] Nicole S. Coverdale et al. "Cerebral blood flow velocity underestimates cerebral blood flow during modest hypercapnia and hypocapnia". In: *Journal of Applied Physiology* 117.10 (Nov. 15, 2014). Publisher: American Physiological Society, pp. 1090–1096. DOI: 10.1152/japplphysiol.00285.2014.

[170] G. P. Molhoek et al. "Evaluation of the Penàz servo-plethysmo-manometer for the continuous, non-invasive measurement of finger blood pressure". In: *Basic Research in Cardiology* 79.5 (Sept. 1, 1984), pp. 598–609. DOI: 10.1007/BF01910489.

[171] Takuya Kurazumi et al. "Short-Term Volume Loading Effects on Estimated Intracranial Pressure in Human Volunteers". In: *Aerospace Medicine and Human Performance* 93.4 (Apr. 1, 2022), pp. 347–353. DOI: 10.3357/AMHP.6004.2022.

[172] Riccardo Pernice et al. "Spectral decomposition of cerebrovascular and cardiovascular interactions in patients prone to postural syncope and healthy controls". In: *Autonomic Neuroscience* 242 (Nov. 1, 2022), p. 103021. DOI: 10.1016/j.autneu.2022.103021.

[173] Vlasta Bari. "Exploring metrics for the characterization of the cerebral autoregulation during head-up tilt and propofol general anesthesia". In: *Autonomic Neuroscience* 242 (Nov. 1, 2022). Publisher: Elsevier, p. 103011. DOI: 10.1016/j.autneu.2022.103011.

[174] Alexander J. Rosenberg et al. "The impact of acute central hypovolemia on cerebral hemodynamics: does sex matter?" In: *Journal of Applied Physiology* 130.6 (June 2021). Publisher: American Physiological Society, pp. 1786–1797. DOI: 10.1152/japplphysiol.00499.2020.

[175] Andrew D. Robertson, Ismina Papadhima, and Heather Edgell. "Sex differences in the autonomic and cerebrovascular responses to upright tilt". In: *Autonomic Neuroscience* 229 (Dec. 1, 2020), p. 102742. DOI: 10.1016/j.autneu.2020.102742.

[176] Wim J. Stok et al. "Slow sinusoidal tilt movements demonstrate the contribution to orthostatic tolerance of cerebrospinal fluid movement to and from the spinal dural space". In: *Physiological Reports* 7.4 (2019). _eprint: https://onlinelibrary.wiley.com/doi/pdf/10.14814/phy2.14001, e14001. DOI: 10.14814/phy2.14001.

[177] Taylor Elyse Schlotman et al. "Differentiating compensatory mechanisms associated with low tolerance to central hypovolemia in women". In: *American Journal of Physiology-Heart and Circulatory Physiology* 316.3 (Mar. 2019). Publisher: American Physiological Society, H609–H616. DOI: 10.1152/ajpheart.00420.2018.

[178] Hisao Yoshida et al. "Relative contributions of systemic hemodynamic variables to cerebral autoregulation during orthostatic stress". In: *Journal of Applied Physiology* 124.2 (Feb. 2018). Publisher: American Physiological Society, pp. 321–329. DOI: 10.1152/japplphysiol.00700.2017.

[179] Noud van Helmond et al. "Effect of acute hypoxemia on cerebral blood flow velocity control during lower body negative pressure". In: *Physiological Reports* 6.4 (2018). _eprint: https://onlinelibrary.wiley.com/doi/pdf/10.14814/phy2.13594, e13594. DOI: 10.14814/phy2.13594.

[180] Jan W. van der Scheer et al. "A comparison of static and dynamic cerebral autoregulation during mild whole-body cold stress in individuals with and without cervical spinal cord injury: a pilot study". In: *Spinal Cord* 56.5 (May 2018). Number: 5 Publisher: Nature Publishing Group, pp. 469–477. DOI: 10.1038/s41393-017-0021-7.

[181] Anne-Sophie G. T. Bronzwaer et al. "Aging modifies the effect of cardiac output on middle cerebral artery blood flow velocity". In: *Physiological Reports* 5.17 (2017). _eprint: https://onlinelibrary.wiley.com/doi/pdf/10.14814/phy2.13361, e13361. DOI: 10.14814/phy2.13361.

[182] A. Lund et al. "Muscle oxygen saturation increases during head-up tilt-induced (pre)syncope". In: *Acta Physiologica* 221.1 (2017). _eprint: https://onlinelibrary.wiley.com/doi/pdf/10.1111/apha.12863, pp. 74–80. DOI: 10.1111/apha.12863.

[183] Anne-Sophie G. T. Bronzwaer et al. "The cerebrovascular response to lower-body negative pressure vs. head-up tilt". In: *Journal of Applied Physiology* 122.4 (Apr. 2017). Publisher: American Physiological Society, pp. 877–883. DOI: 10.1152/japplphysiol.00797.2016.

[184] Yojiro Ogawa et al. "The relationship between widespread changes in gravity and cerebral blood flow". In: *Environmental Health and Preventive Medicine* 21.4 (July 2016), pp. 186–192. DOI: 10.1007/s12199-016-0513-7.

[185] Victoria L. Kay and Caroline A. Rickards. "The role of cerebral oxygenation and regional cerebral blood flow on tolerance to central hypovolemia". In: *American Journal of Physiology-Regulatory, Integrative and Comparative Physiology* 310.4 (Feb. 15, 2016). Publisher: American Physiological Society, R375–R383. DOI: 10.1152/ajpregu.00367.2015.

[186] Caroline A. Rickards et al. "Cerebral blood velocity regulation during progressive blood loss compared with lower body negative pressure in humans". In: *Journal of Applied Physiology* 119.6 (Sept. 15, 2015), pp. 677–685. DOI: 10.1152/japplphysiol.00127.2015.

[187] Blake G. Perry et al. "The effect of hypercapnia on static cerebral autoregulation". In: *Physiological Reports* 2.6 (2014). _eprint: https://onlinelibrary.wiley.com/doi/pdf/10.14814/phy2.12059, e12059. DOI: 10.14814/phy2.12059.

[188] Andrew T. Del Pozzi et al. "Blunted cerebral blood flow velocity in response to a nitric oxide donor in postural tachycardia syndrome". In: *American Journal of Physiology - Heart and Circulatory Physiology* 307.3 (Aug. 1, 2014), H397–H404. DOI: 10.1152/ajpheart.00194.2014.

[189] Brett H. Shaw et al. "The effect of orthostatic stress type on cardiovascular control". In: *Blood Pressure Monitoring* 19.6 (Dec. 2014), pp. 327–338. DOI: 10.1097/MBP.0000000000000067.

[190] Nia C S Lewis et al. "Impact of hypocapnia and cerebral perfusion on orthostatic tolerance". In: *The Journal of Physiology* 592 (Pt 23 Dec. 1, 2014), pp. 5203–5219. DOI: 10.1113/jphysiol.2014.280586.

[191] Blake G. Perry et al. "Middle cerebral artery blood flow velocity in response to lower body positive pressure". In: *Clinical Physiology and Functional Imaging* 33.6 (2013). _eprint: https://onlinelibrary.wiley.com/doi/pdf/10.1111/cpf.12046, pp. 483–488. DOI: 10.1111/cpf.12046.

[192] Zachary J. Schlader et al. "Acute volume expansion attenuates hyperthermia-induced reductions in cerebral perfusion during simulated hemorrhage". In: *Journal of Applied Physiology* 114.12 (June 15, 2013), pp. 1730–1735. DOI: 10.1152/japplphysiol.00079.2013.

[193] Song Guo et al. "The effect of sodium nitroprusside on cerebral hemodynamics and headache in healthy subjects". In: *Cephalalgia* 33.5 (Apr. 1, 2013). Publisher: SAGE Publications Ltd STM, pp. 301–307. DOI: 10.1177/0333102412475239.

[194] Gregory S. H. Chan et al. "Contribution of arterial Windkessel in low-frequency cerebral hemodynamics during transient changes in blood pressure". In: *Journal of Applied Physiology* 110.4 (Apr. 2011). Publisher: American Physiological Society, pp. 917–925. DOI: 10.1152/japplphysiol.01407.2010.

[195] Yojiro Ogawa et al. "The Different Effects of Midazolam and Propofol Sedation on Dynamic Cerebral Autoregulation". In: *Anesthesia & Analgesia* 111.5 (Nov. 2010), pp. 1279–1284. DOI: 10.1213/ANE.0b013e3181f42fc0.

[196] Patrice Brassard et al. "Phenylephrine decreases frontal lobe oxygenation at rest but not during moderately intense exercise". In: *J Appl Physiol* 108 (2010), p. 7.

[197] Raihan Hussain et al. "Vasodilatory effect of adenosine triphosphate does not change cerebral blood flow: a PET study with 15O-water". In: *Annals of Nuclear Medicine* 23.8 (Oct. 2009), pp. 717–723. DOI: 10.1007/s12149-009-0294-9.

[198] Timothy J McCulloch, Tillman W Boesel, and Arthur M Lam. "The Effect of Hypocapnia on the Autoregulation of Cerebral Blood Flow During Administration of Isoflurane". In: *ANESTH ANALG* (2005), p. 5.

[199] Shahar Lavi et al. "Role of Nitric Oxide in the Regulation of Cerebral Blood Flow in Humans". In: *Circulation* 107.14 (Apr. 15, 2003). Publisher: American Heart Association, pp. 1901–1905. DOI: 10.1161/01.CIR.0000057973.99140.5A.

[200] Lisbeth Hjorth Lassen, Helle Klingenberg Iversen, and Jes Olesen. "A dose–response study of nitric oxide synthase inhibition in different vascular beds in man". In: *European Journal of Clinical Pharmacology* 59.7 (Oct. 1, 2003), pp. 499–505. DOI: 10.1007/s00228-003-0662-7.

[201] Timothy J. McCulloch, Elizabeth Visco, and Arthur M. Lam. "Graded Hypercapnia and Cerebral Autoregulation during Sevoflurane or Propofol Anesthesia". In: *Anesthesiology* 93.5 (Nov. 1, 2000), pp. 1205–1209. DOI: 10.1097/00000542-200011000-00012.

[202] Y. Kawai et al. "Cerebral blood flow velocity in humans exposed to 24 h of head-down tilt". In: *Journal of Applied Physiology* (June 1, 1993). DOI: 10.1152/jappl.1993.74.6.3046.

[203] David R. Jobes et al. "Effects of Morphine–Nitrous Oxide Anesthesia on Cerebral Autoregulation". In: *Anesthesiology* 42.1 (Jan. 1, 1975), pp. 30–34. DOI: 10.1097/00000542-197501000-00006.

[204] Lawrence Labrecque et al. "Diminished dynamic cerebral autoregulatory capacity with forced oscillations in mean arterial pressure with elevated cardiorespiratory fitness". In: *Physiological Reports* 5.21 (2017). _eprint: https://onlinelibrary.wiley.com/doi/pdf/10.14814/phy2.13486, e13486. DOI: 10.14814/phy2.13486.

[205] Jonathan D. Smirl et al. "Methodological comparison of active- and passive-driven oscillations in blood pressure; implications for the assessment of cerebral pressure-flow relationships". In: *Journal of Applied Physiology* 119.5 (Sept. 1, 2015), pp. 487–501. DOI: 10.1152/japplphysiol.00264.2015.

[206] Jill N. Barnes. "Sex Specific Factors Regulating Pressure and Flow". In: *Experimental physiology* 102.11 (Nov. 1, 2017), pp. 1385–1392. DOI: 10.1113/EP086531.

[207] L Wollner et al. "Failure of cerebral autoregulation as a cause of brain dysfunction in the elderly." In: *British Medical Journal* 1.6171 (Apr. 28, 1979), pp. 1117–1118.

[208] Andrew D. Robertson, Heather Edgell, and Richard L. Hughson. "Assessing cerebrovascular autoregulation from critical closing pressure and resistance area product during upright posture in aging and hypertension". In: *American Journal of Physiology-Heart and Circulatory Physiology* 307.2 (July 15, 2014). Publisher: American Physiological Society, H124–H133. DOI: 10.1152/ajpheart.00086.2014.

[209] Dieter Conen et al. "Short- and Long-Term Cerebrovascular Effects of Nitrendipine in Hypertensive Patients". In: *Journal of Cardiovascular Pharmacology* 12 (1988), S64.

[210] S Strandgaard. "Autoregulation of cerebral blood flow in hypertensive patients. The modifying influence of prolonged antihypertensive treatment on the tolerance to acute, drug-induced hypotension." In: *Circulation* 53.4 (Apr. 1976). Publisher: American Heart Association, pp. 720–727. DOI: 10.1161/01.CIR.53.4.720.

[211] Vera Novak et al. "Multimodal pressure-flow method to assess dynamics of cerebral autoregulation in stroke and hypertension". In: *BioMedical Engineering OnLine* 3 (Oct. 25, 2004), p. 39. DOI: 10.1186/1475-925X-3-39.

[212] Penelope J. Eames et al. "The systemic haemodynamic and cerebral autoregulatory effects of bendrofluazide in the subacute post-stroke period". In: *Journal of Hypertension* 22.10 (Oct. 2004), p. 2017.

[213] D. Georgiadis et al. "Cerebral Autoregulation Under Moderate Hypothermia in Patients With Acute Stroke". In: *Stroke* 33.12 (Dec. 2002). Publisher: American Heart Association, pp. 3026–3029. DOI: 10.1161/01.STR.0000038423.35569.93.

[214] Stefan Schwarz et al. "Effects of Induced Hypertension on Intracranial Pressure and Flow Velocities of the Middle Cerebral Arteries in Patients With Large Hemispheric Stroke". In: *Stroke* 33.4 (Apr. 2002). Publisher: American Heart Association, pp. 998–1004. DOI: 10.1161/01.STR.0000014584.17714.2E.

[215] Yasuomi Ouchi et al. "Postural Effects on Brain Hemodynamics in Unilateral Cerebral Artery Occlusive Disease: A Positron Emission Tomography Study". In: *Journal of Cerebral Blood Flow & Metabolism* 21.9 (Sept. 1, 2001). Publisher: SAGE Publications Ltd STM, pp. 1058–1066. DOI: 10.1097/00004647-200109000-00003.

[216] T S Olsen et al. "Blood flow and vascular reactivity in collaterally perfused brain tissue. Evidence of an ischemic penumbra in patients with acute stroke." In: *Stroke* 14.3 (May 1983). Publisher: American Heart Association, pp. 332–341. DOI: 10.1161/01.STR.14.3.332.

[217] Martyn Ezra et al. "Phase dynamics of cerebral blood flow in subarachnoid haemorrhage in response to sodium nitrite infusion". In: *Nitric Oxide* 106 (Jan. 1, 2021), pp. 55–65. DOI: 10.1016/j.niox.2020.10.004.

[218] Michael N. Diringer et al. "Effect of high-dose simvastatin on cerebral blood flow and static autoregulation in subarachnoid hemorrhage". In: *Neurocritical care* 25.1 (Aug. 2016), pp. 56–63. DOI: 10.1007/s12028-015-0233-7.

[219] Bronwen Gould et al. "Autoregulation of Cerebral Blood Flow is Preserved in Primary Intracerebral Hemorrhage". In: *Stroke* 44.6 (June 2013). Publisher: American Heart Association, pp. 1726–1728. DOI: 10.1161/STROKEAHA.113.001306.

[220] E. M. Manno et al. "Effects of Induced Hypertension on Transcranial Doppler Ultrasound Velocities in Patients After Subarachnoid Hemorrhage". In: *Stroke* 29.2 (Feb. 1998). Publisher: American Heart Association, pp. 422–428. DOI: 10.1161/01.STR.29.2.422.

[221] J. Paul Muizelaar and Donald P. Becker. "Induced hypertension for the treatment of cerebral ischemia after subarachnoid hemorrhage. Direct effect on cerebral blood flow". In: *Surgical Neurology* 25.4 (Apr. 1, 1986), pp. 317–325. DOI: 10.1016/0090-3019(86)90205-3.

[222] John D. Pickard et al. "Prediction of late ischemic complications after cerebral aneurysm surgery by the intraoperative measurement of cerebral blood flow". In: *Journal of Neurosurgery* 53.3 (Sept. 1980), pp. 305–308. DOI: 10.3171/jns.1980.53.3.0305.

[223] Madelijn H. Oudegeest-Sander et al. "Assessment of dynamic cerebral autoregulation and cerebrovascular CO2 reactivity in ageing by measurements of cerebral blood flow and cortical oxygenation". In: *Experimental Physiology* 99.3 (2014). _eprint: https://onlinelibrary.wiley.com/doi/pdf/10.1113/expphysiol.2013.076455, pp. 586–598. DOI: 10.1113/expphysiol.2013.076455.

[224] James P. Fisher et al. "Regulation of middle cerebral artery blood velocity during dynamic exercise in humans: influence of aging". In: *Journal of Applied Physiology* 105.1 (July 2008). Publisher: American Physiological Society, pp. 266–273. DOI: 10.1152/japplphysiol.00118.2008.

[225] Farzaneh A. Sorond et al. "Regional Cerebral Autoregulation during Orthostatic Stress: Age-Related Differences". In: *The journals of gerontology. Series A, Biological sciences and medical sciences* 60.11 (Nov. 2005), pp. 1484–1487.

[226] Rogier V. Immink et al. "Dynamic Cerebral Autoregulation in Acute Lacunar and Middle Cerebral Artery Territory Ischemic Stroke". In: *Stroke* 36.12 (Dec. 2005). Publisher: American Heart Association, pp. 2595–2600. DOI: 10.1161/01.STR.0000189624.06836.03.

[227] J. Gierthmühlen et al. "Dynamic cerebral autoregulation in stroke patients with a central sympathetic deficit". In: *Acta Neurologica Scandinavica* 123.5 (2011). _eprint: https://onlinelibrary.wiley.com/doi/pdf/10.1111/j.1600-0404.2010.01424.x, pp. 332–338. DOI: 10.1111/j.1600-0404.2010.01424.x.

[228] Karol P. Budohoski et al. "Clinical relevance of cerebral autoregulation following subarachnoid haemorrhage". In: *Nature Reviews Neurology* 9.3 (Mar. 2013). Number: 3 Publisher: Nature Publishing Group, pp. 152–163. DOI: 10.1038/nrneurol.2013.11.

[229] Elke Muench et al. "Effects of positive end-expiratory pressure on regional cerebral blood flow, intracranial pressure, and brain tissue oxygenation*". In: *Critical Care Medicine* 33.10 (Oct. 2005), p. 2367. DOI: 10.1097/01.CCM.0000181732.37319.DF.

[230] William J. Powers et al. "Autoregulation after ischaemic stroke". In: *Journal of hypertension* 27.11 (Nov. 2009), pp. 2218–2222. DOI: 10.1097/HJH.0b013e328330a9a7.

[231] George M. Hoffman, Nancy S. Ghanayem, and James S. Tweddell. "Noninvasive assessment of cardiac output". In: *Seminars in Thoracic and Cardiovascular Surgery: Pediatric Cardiac Surgery Annual* 8.1 (Jan. 1, 2005), pp. 12–21. DOI: 10.1053/j.pcsu.2005.01.005.

[232] A. A. Birch et al. "Assessment of Autoregulation by Means of Periodic Changes in Blood Pressure". In: *Stroke* 26.5 (May 1995). Publisher: American Heart Association, pp. 834–837. DOI: 10.1161/01.STR.26.5.834.

[233] Rune Aaslid et al. "Asymmetric Dynamic Cerebral Autoregulatory Response to Cyclic Stimuli". In: *Stroke* 38.5 (May 2007), pp. 1465–1469. DOI: 10.1161/STROKEAHA.106.473462.

[234] Bernhard Schmidt, Marek Czosnyka, and Jürgen Klingelhöfer. "Asymmetry of cerebral autoregulation does not correspond to asymmetry of cerebrovascular pressure reactivity". In: *Perspectives in Medicine*. New Trends in Neurosonology and Cerebral Hemodynamics – an Update 1.1 (Sept. 1, 2012), pp. 285–289. DOI: 10.1016/j.permed.2012.02.026.

[235] Priscila A. Cassaglia, Robert I. Griffiths, and Adrian M. Walker. "Sympathetic nerve activity in the superior cervical ganglia increases in response to imposed increases in arterial pressure". In: *American Journal of Physiology-Regulatory, Integrative and Comparative Physiology* 294.4 (Apr. 2008). Publisher: American Physiological Society, R1255–R1261. DOI: 10.1152/ajpregu.00332.2007.

[236] Ronney B Panerai et al. "Directional sensitivity of dynamic cerebral autoregulation during spontaneous fluctuations in arterial blood pressure at rest". In: *Journal of Cerebral Blood Flow & Metabolism* 43.4 (Apr. 2023), pp. 552–564. DOI: 10.1177/0271678X221142527.

[237] Maximilian Wiesmann, Amanda J Kiliaan, and Jurgen AHR Claassen. "Vascular aspects of cognitive impairment and dementia". In: *Journal of Cerebral Blood Flow & Metabolism* 33.11 (Nov. 2013), pp. 1696–1706. DOI: 10.1038/jcbfm.2013.159.

[238] Kurt Krejcy et al. "Characterization of angiotensin-II effects on cerebral and ocular circulation by noninvasive methods". In: *British Journal of Clinical Pharmacology* 43.5 (May 1997), pp. 501–508. DOI: 10.1046/j.1365-2125.1997.00585.x.

[239] Ronney B Panerai. "Assessment of cerebral pressure autoregulation in humans - a review of measurement methods". In: *Physiological Measurement* 19.3 (Aug. 1, 1998), pp. 305–338. DOI: 10.1088/0967-3334/19/3/001.

[240] K. F. Lindegaard et al. "Variations in middle cerebral artery blood flow investigated with noninvasive transcranial blood velocity measurements". In: *Stroke* 18.6 (1987), pp. 1025–1030. DOI: 10.1161/01.str.18.6.1025.

[241] G. Greisen et al. "Cerebral blood flow in the newborn infant: comparison of Doppler ultrasound and 133xenon clearance". In: *The Journal of Pediatrics* 104.3 (Mar. 1984), pp. 411–418. DOI: 10.1016/s0022-3476(84)81108-7.

[242] C. C. Bishop et al. "Transcranial Doppler measurement of middle cerebral artery blood flow velocity: a validation study". In: *Stroke* 17.5 (1986), pp. 913–915. DOI: 10.1161/01.str.17.5.913.

[243] Farzaneh Sorond et al. "BRAIN BLOOD FLOW AND VELOCITY: CORRELATIONS BETWEEN MAGNETIC RESONANCE IMAGING AND TRANSCRANIAL DOPPLER". In: *Journal of ultrasound in medicine : official journal of the American Institute of Ultrasound in Medicine* 29.7 (July 2010), pp. 1017–1022.

[244] C. K. Willie et al. "Utility of transcranial Doppler ultrasound for the integrative assessment of cerebrovascular function". In: *Journal of Neuroscience Methods* 196.2 (Mar. 30, 2011), pp. 221–237. DOI: 10.1016/j.jneumeth.2011.01.011.

[245] Ronney B. Panerai, Thompson G. Robinson, and Jatinder S. Minhas. "The upper frequency limit of dynamic cerebral autoregulation". In: *The Journal of Physiology* 597.24 (Dec. 2019), pp. 5821–5833. DOI: 10.1113/JP278710.

[246] Richard B. Buxton et al. "Modeling the hemodynamic response to brain activation". In: *NeuroImage* 23 (Jan. 2004), S220–S233. DOI: 10.1016/j.neuroimage.2004.07.013.

[247] Michèle Koenigsberger et al. "Ca2+ Dynamics in a Population of Smooth Muscle Cells: Modeling the Recruitment and Synchronization". In: *Biophysical Journal* 87.1 (July 1, 2004), pp. 92–104. DOI: 10.1529/biophysj.103.037853.

[248] J. D. Stockand and S. C. Sansom. "Mechanism of activation by cGMP-dependent protein kinase of large Ca(2+)-activated K+ channels in mesangial cells". In: *American Journal of Physiology-Cell Physiology* 271.5 (Nov. 1, 1996). Publisher:

American Physiological Society, pp. C1669–C1677. DOI: 10.1152/ajpcell.1996.271.5.C1669.

[249] Sepideh Sadaghiani, Kâmil Uğurbil, and Kâmil Uludağ. "Neural activity-induced modulation of BOLD poststimulus undershoot independent of the positive signal". In: *Magnetic Resonance Imaging*. Proceedings of the International School on Magnetic Resonance and Brain Function 27.8 (Oct. 1, 2009), pp. 1030–1038. DOI: 10.1016/j.mri.2009.04.003.

[250] Ying Zheng et al. "A dynamic model of neurovascular coupling: implications for blood vessel dilation and constriction". In: *NeuroImage* 52.3 (Sept. 2010), pp. 1135–1147. DOI: 10.1016/j.neuroimage.2010.01.102.

[251] J G McCarron et al. "Myogenic contraction by modulation of voltage-dependent calcium currents in isolated rat cerebral arteries." In: *The Journal of Physiology* 498 (Pt 2 Jan. 15, 1997), pp. 371–379.

[252] Michael T. Kirber et al. "Both membrane stretch and fatty acids directly activate large conductance Ca2+-activated K+ channels in vascular smooth muscle cells". In: *FEBS Letters* 297.1 (Feb. 3, 1992), pp. 24–28. DOI: 10.1016/0014-5793(92)80319-C.

[253] M. T. Nelson et al. "Calcium channels, potassium channels, and voltage dependence of arterial smooth muscle tone". In: *American Journal of Physiology-Cell Physiology* 259.1 (July 1, 1990), pp. C3–C18. DOI: 10.1152/ajpcell.1990.259.1.C3.

[254] U. Lindauer et al. "Nitric oxide: a modulator, but not a mediator, of neurovascular coupling in rat somatosensory cortex". In: *The American Journal of Physiology* 277.2 (Aug. 1999), H799–811. DOI: 10.1152/ajpheart.1999.277.2.H799.

[255] Sean J. Mulligan and Brian A. MacVicar. "Calcium transients in astrocyte endfeet cause cerebrovascular constrictions". In: *Nature* 431.7005 (Sept. 2004). Number: 7005 Publisher: Nature Publishing Group, pp. 195–199. DOI: 10.1038/nature02827.

[256] Francesca Campolongo, Jessica Cariboni, and Andrea Saltelli. "An effective screening design for sensitivity analysis of large models". In: *Environmental Modelling* (2007), p. 10.

[257] Kevin Murphy, Ashley D. Harris, and Richard G. Wise. "Robustly measuring vascular reactivity differences with breath-hold: normalising stimulus-evoked and resting state BOLD fMRI data". In: *NeuroImage* 54.1 (Jan. 1, 2011), pp. 369–379. DOI: 10.1016/j.neuroimage.2010.07.059.

[258] Catherine N. Hall et al. "Capillary pericytes regulate cerebral blood flow in health and disease". In: *Nature* 508.7494 (Apr. 3, 2014), pp. 55–60. DOI: 10.1038/nature13165.

[259] Yi Yang and Gary A. Rosenberg. "Blood–Brain Barrier Breakdown in Acute and Chronic Cerebrovascular Disease". In: *Stroke* 42.11 (Nov. 2011). Publisher: American Heart Association, pp. 3323–3328. DOI: 10.1161/STROKEAHA.110.608257.

[260] Per-Olof Grände and Bertil Romner. "Osmotherapy in Brain Edema: A Questionable Therapy". In: *Journal of Neurosurgical Anesthesiology* 24.4 (Oct. 2012), p. 407. DOI: 10.1097/01.ana.0000419730.29492.8b.

[261] Lisa L. Larive et al. "Introducing hypertonic saline for cerebral edema". In: *Neurocritical Care* 1.4 (Dec. 1, 2004), pp. 435–440. DOI: 10.1385/NCC:1:4:435.

[262] Xi Chen, Tamás I. Józsa, and Stephen J. Payne. "Computational modelling of cerebral oedema and osmotherapy following ischaemic stroke". In: *Computers in Biology and Medicine* 151 (Dec. 1, 2022), p. 106226. DOI: 10.1016/j.compbiomed.2022.106226.

[263] T. I. Józsa et al. "A porous circulation model of the human brain for *in silico* clinical trials in ischaemic stroke". In: *Interface Focus* 11.1 (Feb. 6, 2021), p. 20190127. DOI: 10.1098/rsfs.2019.0127.

[264] Wahbi K. El-Bouri and Stephen J. Payne. "Multi-scale homogenization of blood flow in 3-dimensional human cerebral microvascular networks". In: *Journal of Theoretical Biology* 380 (Sept. 7, 2015), pp. 40–47. DOI: 10.1016/j.jtbi.2015.05.011.

[265] Wahbi K. El-Bouri and Stephen J. Payne. "Investigating the effects of a penetrating vessel occlusion with a multi-scale microvasculature model of the human cerebral cortex". In: *NeuroImage* 172 (May 15, 2018), pp. 94–106. DOI: 10.1016/j.neuroimage.2018.01.049.

[266] P A Fraser, A D Dallas, and S Davies. "Measurement of filtration coefficient in single cerebral microvessels of the frog." In: *The Journal of Physiology* 423.1 (1990). _eprint: https://onlinelibrary.wiley.com/doi/pdf/10.1113/jphysiol.1990.sp018026, pp. 343–361. DOI: 10.1113/jphysiol.1990.sp018026.

[267] Yoji Hakamata et al. "Long-term High-Colloid Oncotic Therapy for Ischemic Brain Edema in Gerbils". In: *Stroke* 26.11 (Nov. 1995). Publisher: American Heart Association, pp. 2149–2153. DOI: 10.1161/01.STR.26.11.2149.

[268] H. M. Duvernoy, S. Delon, and J. L. Vannson. "Cortical blood vessels of the human brain". In: *Brain Research Bulletin* 7.5 (Nov. 1, 1981), pp. 519–579. DOI: 10.1016/0361-9230(81)90007-1.

[269] Amy F. Smith et al. "Brain Capillary Networks Across Species: A few Simple Organizational Requirements Are Sufficient to Reproduce Both Structure and Function". In: *Frontiers in Physiology* 10 (Mar. 26, 2019). Publisher: Frontiers. DOI: 10.3389/fphys.2019.00233.

[270] Shen-Wei Su, Mark Catherall, and Stephen Payne. "The Influence of Network Structure on the Transport of Blood in the Human Cerebral Microvasculature". In: *Microcirculation* 19.2 (2012). _eprint: https://onlinelibrary.wiley.com/doi/pdf/10.1111/j.1549-8719.2011.00148.x, pp. 175–187. DOI: 10.1111/j.1549-8719.2011.00148.x.

[271] B. Tully and Y. Ventikos. "Cerebral water transport using multiple-network poroelastic theory: application to normal pressure hydrocephalus". In: *Journal of Fluid Mechanics* 667 (Jan. 2011), pp. 188–215. DOI: 10.1017/S0022112010004428.

[272] Lena Claesson-Welsh. "Vascular permeability—the essentials". In: *Upsala Journal of Medical Sciences* 120.3 (Aug. 2015), pp. 135–143. DOI: 10.3109/03009734.2015.1064501.

[273] Anders Logg, Kent-Andre Mardal, and Garth Wells. *Automated Solution of Differential Equations by the Finite Element Method: The FEniCS Book*. Google-Books-ID: ASWN_VRr1NQC. Springer Science & Business Media, Feb. 24, 2012. 723 pp.

[274] Anders Logg and Garth N. Wells. "DOLFIN: Automated finite element computing". In: *ACM Transactions on Mathematical Software* 37.2 (Apr. 23, 2010), 20:1–20:28. DOI: 10.1145/1731022.1731030.

[275] T. I. Józsa et al. "On the Sensitivity Analysis of Porous Finite Element Models for Cerebral Perfusion Estimation". In: *Annals of Biomedical Engineering* 49.12 (Dec. 1, 2021), pp. 3647–3665. DOI: 10.1007/s10439-021-02808-w.